(2)

SECURITY CLASSIFICATION OF THIS PAGE

REPORT DOCUMENTATION PAGE

1a. REPORT SECURITY CLASSIFICATION: UNCLASSIFIED	1b. RESTRICTIVE MARKINGS
2a. SECURITY CLASSIFICATION AUTHORITY: UNCLASSIFIED — ELECTE OCT 0 5 1988	3. DISTRIBUTION/AVAILABILITY OF REPORT: Approved for public release; distribution unlimited.
2b. DECLASSIFICATION/DOWNGRADING SCHEDULE	
4. PERFORMING ORGANIZATION REPORT NUMBER(S): H C2	5. MONITORING ORGANIZATION REPORT NUMBER(S): AFOSR-TR-88-0971
6a. NAME OF PERFORMING ORGANIZATION: Stanford University	6b. OFFICE SYMBOL (If applicable):
6c. ADDRESS (City, State and ZIP Code): Dept of Applied Physics & Eng Stanford, CA 94305-0215	7a. NAME OF MONITORING ORGANIZATION: AFOSR/NE 7b. ADDRESS (City, State and ZIP Code): Bldg 410 Bolling AFB DC 20332
8a. NAME OF FUNDING/SPONSORING ORGANIZATION: AFOSR/NE	8b. OFFICE SYMBOL (If applicable): NE
8c. ADDRESS (City, State and ZIP Code): Bldg 410 Bolling AFB DC 20332-6448	9. PROCUREMENT INSTRUMENT IDENTIFICATION NUMBER: F49620-88-C-0002

10. SOURCE OF FUNDING NOS.

PROGRAM ELEMENT NO.	PROJECT NO.	TASK NO.	WORK UNIT NO.
61102 F	D812	B1	

11. TITLE (Include Security Classification): Detectors of Infrarred Radiation Based on High T(c) Superconducting YBCO Films

12. PERSONAL AUTHOR(S): Geballe

13a. TYPE OF REPORT	13b. TIME COVERED	14. DATE OF REPORT (Yr., Mo., Day)	15. PAGE COUNT
Annual Report	FROM 01 Dec 87 TO 23 Feb 88		

16. SUPPLEMENTARY NOTATION

17. COSATI CODES			18. SUBJECT TERMS (Continue on reverse if necessary and identify by block number)
FIELD	GROUP	SUB. GR.	

AD-A199 820

19. ABSTRACT (Continue on reverse if necessary and identify by block number)

We achieved control over the orientation and microstructure of the thin films of $YBa_2Cu_3O_{7-\delta}$ (YBCO). We elucidated the optical properties of YBCO, including the penetration depth (which turned out to be rather small) and the optical anisotropy (which is rather large). We have observed photo-induced signals (i.e. changes in resistivity) of YBCO films in superconducting state as well as in the normal state-- upon illumination with short pulsed IR radiation generated by the Stanford free-electron laser.

20. DISTRIBUTION/AVAILABILITY OF ABSTRACT	21. ABSTRACT SECURITY CLASSIFICATION
UNCLASSIFIED/UNLIMITED ☐ SAME AS RPT. ☐ OTIC USERS ☐	

22a. NAME OF RESPONSIBLE INDIVIDUAL	22b. TELEPHONE NUMBER (Include Area Code)	22c. OFFICE SYMBOL
WEINSTOCK	(202) 767-4933	NE

DD FORM 1473, 83 APR — EDITION OF 1 JAN 73 IS OBSOLETE.

88 10 5 142

SECURITY CLASSIFICATION OF THIS PAGE

SUMMARY OF WORK AT STANFORD IR DETECTOR PROGRAM, APRIL 7 - JUNE 30, 1988

1. The major results of research related to this program obtained before April 1, 1988 have been already described in our previous progress report of April 4, 1988 and hence will be summarized very briefly here. First, we achieved control over the orientation and microstructure of the thin films of $YBa_2Cu_3O_{7-x}$ (YBCO). Second, we elucidated the optical properties of YBCO, including the penetration depth (which turned out to be rather small) and the optical anisotropy (which is rather large). Third, we have observed photo-induced signals (i.e. changes in resistivity) of YBCO films - in superconducting state as well as in the normal state -- upon illumination with short-pulsed IR radiation generated by the Stanford free-electron laser.

2. On the other hand, we have also identified certain obstacles hampering the ultimate successful construction of competitive IR detectors based on high-T_c superconductors. First, sample-to-sample variations in the optical properties of YBCO thin films have been found to be rather large. One of the reasons underlying these variations is the ease with which oxygen diffuses into and out of the YBCO films. Second, the best (epitaxial) superconducting YBCO films are grown on the SrT_iO_3 substrates, which may be disadvantageous for certain (e.g. bolometric) modes of operation. Third, we had concluded that the most useful frequency range may lay outside the detecting range of the instrumentation available to us at that time.

3. Hence, we have focused our efforts onto these open problems. In the first place, we have been investigating the newly-discovered high-T_c superconducting materials based on Bi rather than Y. The compound $Bi_2Sr_2CaCu_2O_8$ (BSCCO) was found to have T_c=84 K, slightly lower than YBCO but still high enough for useful applications. We found BSCCO to be much less surface-sensitive and, in particular, its optical properties are much less sample dependent than those of YBCO. Otherwise, their IR/visible/UV reflectance and transmittance spectra are quite similar (Figure 1 a, b, c), in particular to the $Y_2Ba_4Cu_8O_{20-x}$ phase discovered in our group recently [1,2]; indeed, the BSCCO and the "2-4-8" phase show substantial structural similarities. The Bi compound appears somewhat

more anisotropic in both the optical (Figure 2) and the transport properties. Actually, the same is true for its mechanical properties: BSCCO is easily cleaved along the crystal ab plane. Freshly cleaved surfaces are of highest optical quality, which is maintained over many days of exposure to air.

We have also synthesized other Bi-based superconducting compounds, but so far it has not been possible to obtain single-phase samples of the "three-layered" $Ba_2Sr_2Ca_2Cu_3O_{10}$ compound which has T_c>100 K.

4. As compared to our earlier studies of YBCO, we have extended our investigations of BSCCO to samples of several forms--sintered pellets, thin films, single crystals and fibers. We have grown thin BCSCO films on SrT_iO_3 substrates(3); they showed zero resistance at T_c=84 K and critical currents $j_c=10^5$Å/cm^2. Single crystals and fibers have also been grown successfully(4). These are of potential interest for bolometric mode of operation; the study of this issue is underway. We have determined the anisotropy of the infrared reflectance by utilizing these single crystal specimens, Figure 2. (The films are epitaxially oriented with the ab planes parallel to the substrate, and hence their spectra are comparable to those from the ab face of the crystal.)

5. To overcome our instrumental limitations, we have acquired two new top-of-the-line spectrometers -- a Digilab FTS-40V Fourier-transform vacuum-FIR spectrometer, and a Perkin-Elmer λ-9 double-beam double-monochrometer NIR/visible/UV spectrophotometer. Thus we are now able to study optical properties over a broad spectral range from ~6 ev down to a few meV. With the λ-9 spectrometer we have acquired an integrating sphere detector to measure the diffuse reflectance, which is important for thin-film studies. (For example, the spectrum in Figure 3 actually shows a rise in reflectance in the high-frequency side which is real and which is in agreement with electron-energy-loss studies, but which is usually lost with the usual specular-reflectance-only configurations.) The technical difficulty that we had faced was that both instruments are constructed for studies of samples much larger than our thin film or single crystal specimens. To resolve this, we have constructed a home-made beam condenser, for the λ-9 instrument, with which the spectrum in Figure 3

was obtained. The construction of a similar accessory for the FTS-40V machine is underway.

6. Finally, intensive work has been continued, and substantial advances made, in the construction of in-situ-growth facilities in our group. Noise measurements have been made using films prepared at the Stanford facility by M. R. Beasley's group in collaboration with John Clarke's group at UC Berkeley. The noise is found to increase markedly as the quality of the films deteriorates. Further experiments with P. L. Richards group at Berkeley are underway.

7. Raman effect measurements[5] (see Figures 4a, b) (with Varian) and ellipsometric measurements[6] (with Bellcore) etc., give further diagnostic information as to film quality and further understanding of the basic processes going on in the films.

---

[1]"Ordered-defect Structure in Epitaxial $YBa_2Cu_3O_{7-x}$ Thin Films," A. Marshall, R. W. Barton, K. Char, A. Kapitulnik, B. Oh, R. H. Hammond, S. S. Laderman, Phys. Rev. B 37, (16), 1 June 1988.

[2]"Properties of Y-Ba-Cu-O Thin Films with Ordered Defect Structure: $Y_2Ba_4Cu_8O_{20-x}$," K. Char, M. Lee, R. W. Barton, A. F. Marshall, I. Bozovic, R. H. Hammond, M R. Beasley, T. H. Geballe, A. Kapitulnik and S. S. Laderman, Phys. Rev. B, Rapid Communications, 38 (1), 1 July 1988.

[3]"Two-dimensional Superstructure in the A-B Plane of $Bi_2(Ca,Sr)_3Cu_2O_{8+\delta}$ Thin Films," A. F. Marshall, B. Oh, S. Spielman, M. Lee, C. B. Eom, R. W. Barton, R. H. Hammond, A. Kapitulnik, M. R. Beasley and T. H. Geballe; submitted to Appl. Phys. Lett. 3-8-88.

[4]"Superconducting Bi-Ca-Sr-Cu-O Fibers Grown by the Laser-Heated Pedestal Growth Method," R. S. Feigelson, D. Gazit, D. K. Fork, T. H. Geballe, Science, Vol. 240, Pages 1581-1704, 17 June 1988.

[5]"Resonance Effects in Raman Scattering in $YBa_2Cu_3O_7$," D. Kirillov, I. Bozovic, K. Char, and A. Kapitulnik, submitted to Phys. Rev. B. Rapid Communications.

[6]"Optical Anisotropy of $YBa_2Cu_3O_{7-x}$," I. Bozovic, K. Char, S. J. B. Yoo, A. Kapitulnik, M. R. Beasley, T. H. Geballe, Z. Z. Wang, S. Hagen, N. P. Ong, D. E. Aspnes, and M. K. Kelly, Phys. Rev. B. Rapid Communications 38 (1988) in press.

MID-IR REFLECTANCE OF A GOOD C-AXIS ORIENTED YBCO FILM

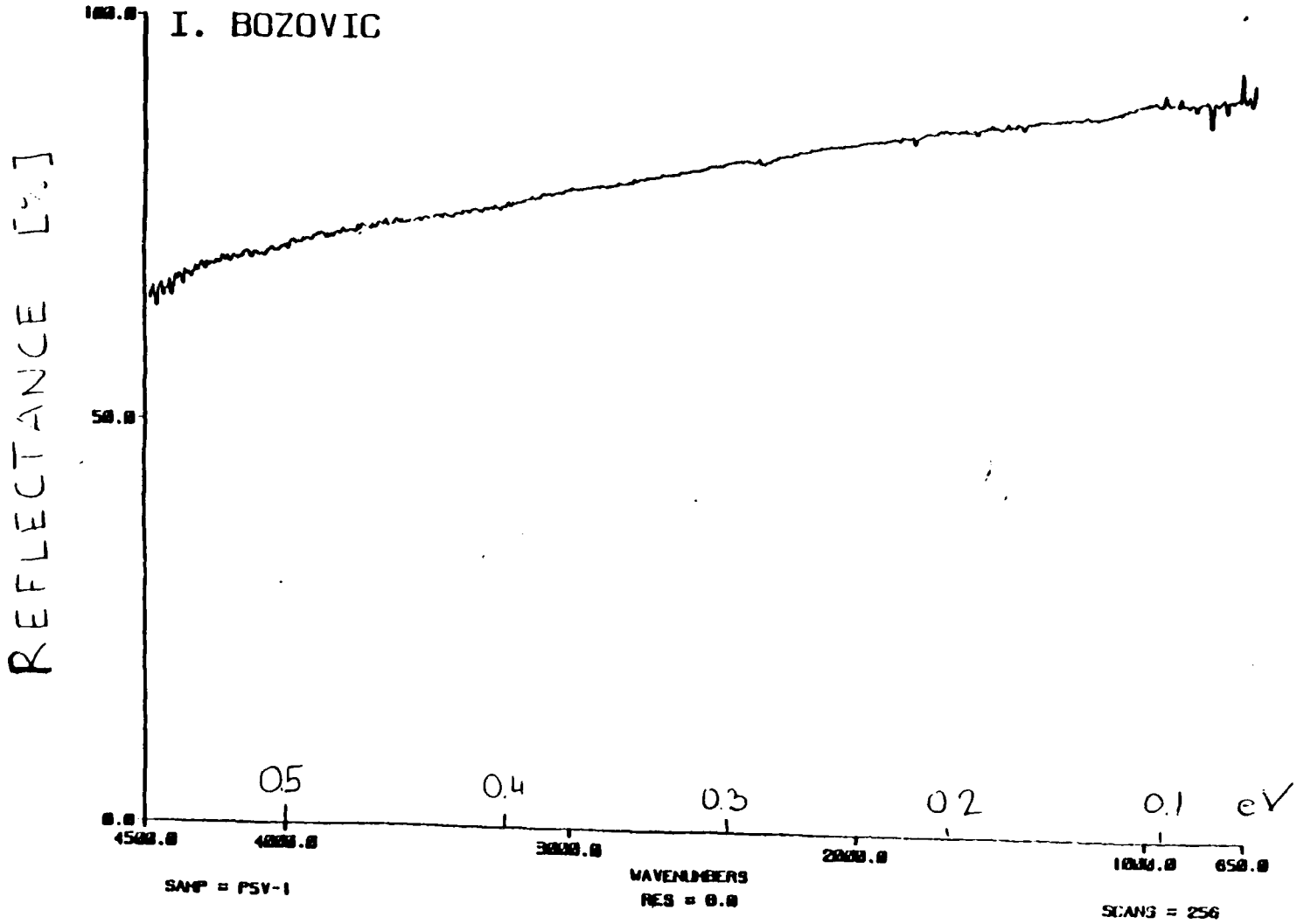

mid-IR reflectance from a cleaved surface (ab face) of a large ($10 \times 5\ mm^2$) single crystal of $Ba_2Sr_2CaCu_2O_8$

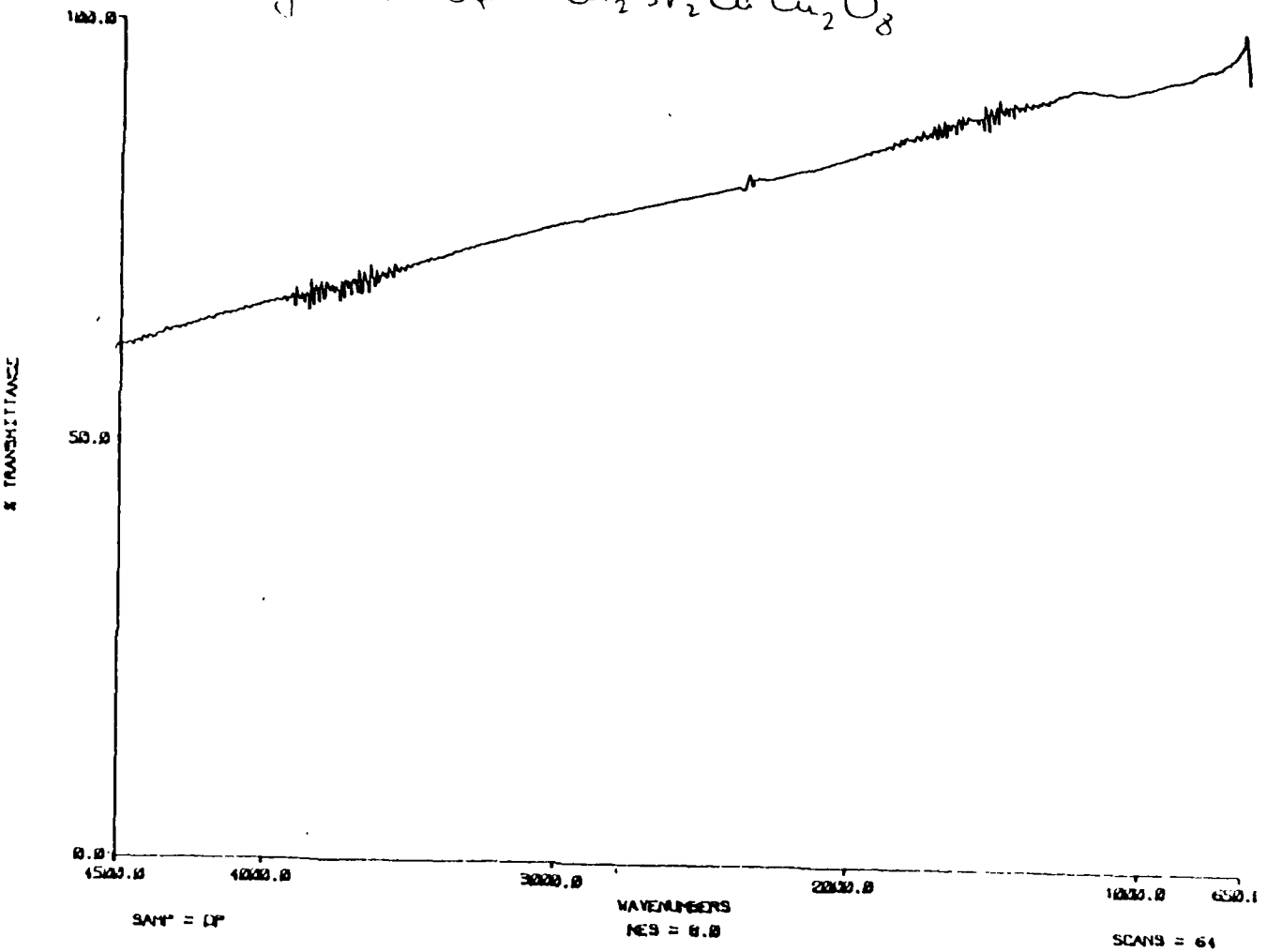

mid-IR reflectance from a single-crystal fiber of $Ba_2Sr_2CaCu_2O_8$ (from ab face). Practically indistinguishable from Fig. , illustrating sample-to-sample stability of optical properties of this material.

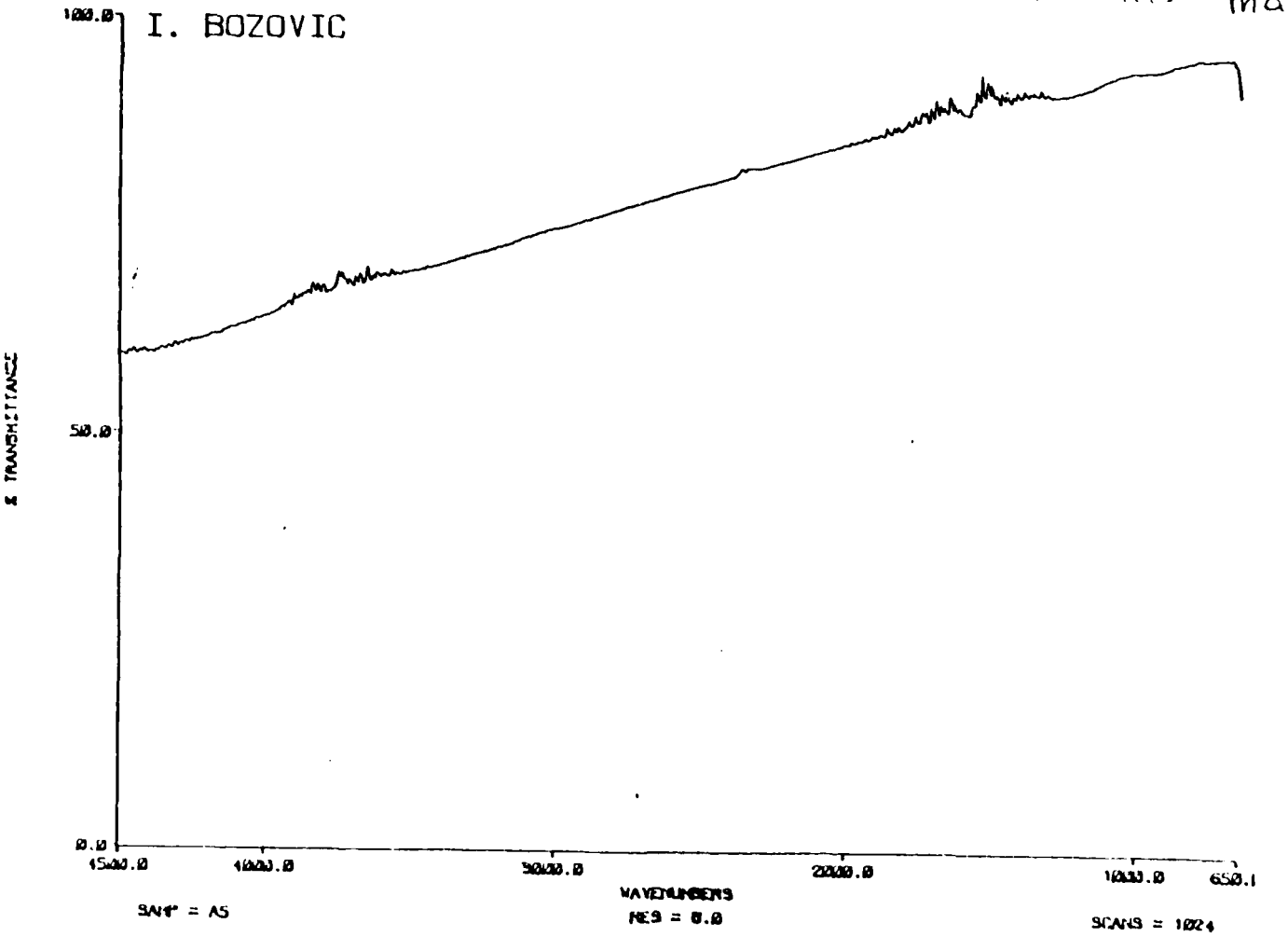

The infrared reflectance spectra from a single-crystal fiber of $Ba_2Sr_2CaCu_2O_8$, showing a huge anisotropy

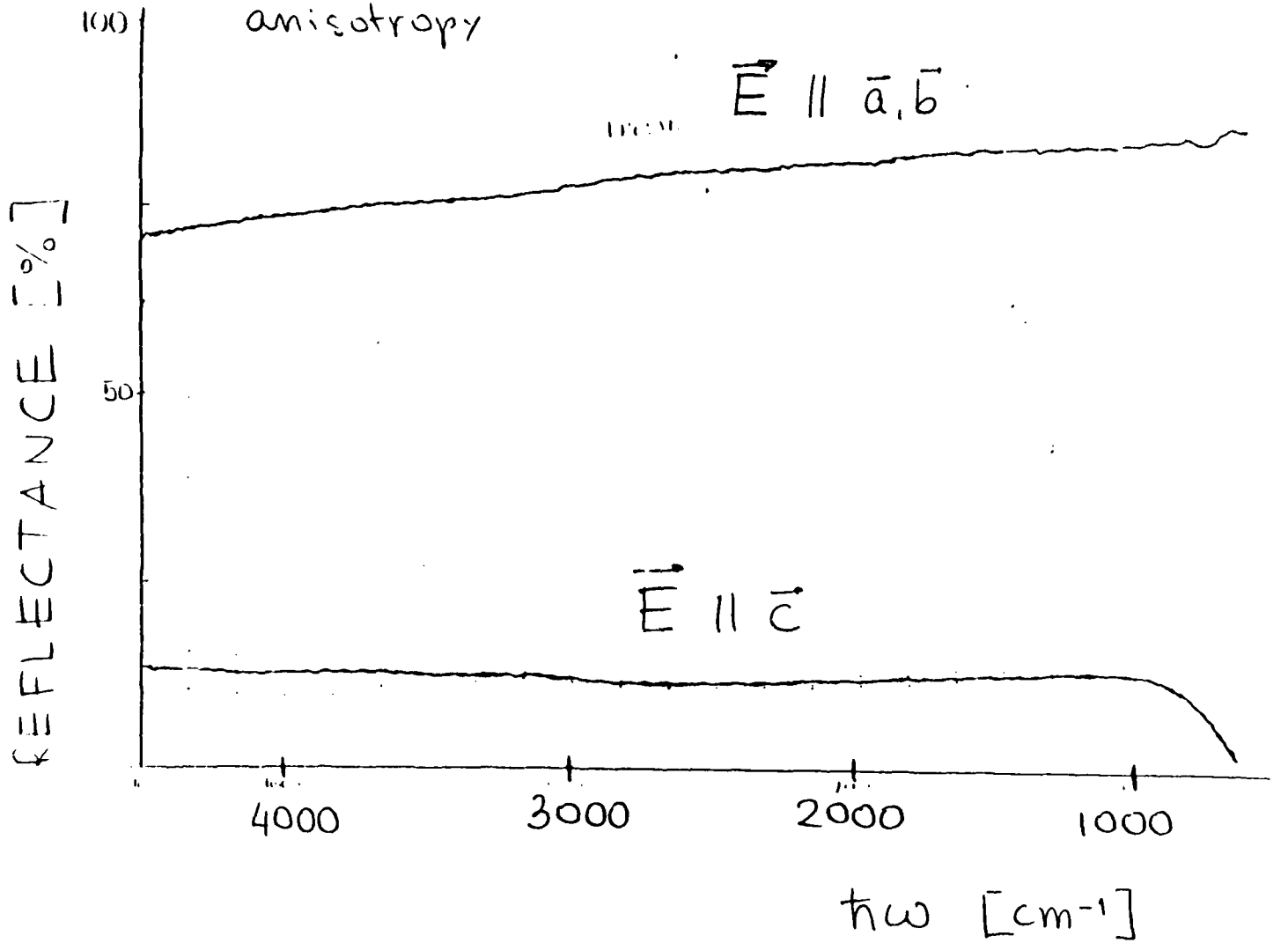

Fig. 2

NIR/visible/UV reflectance spectrum of a $Ba_2Sr_2CaCu_2O_8$ single crystal (ab face)

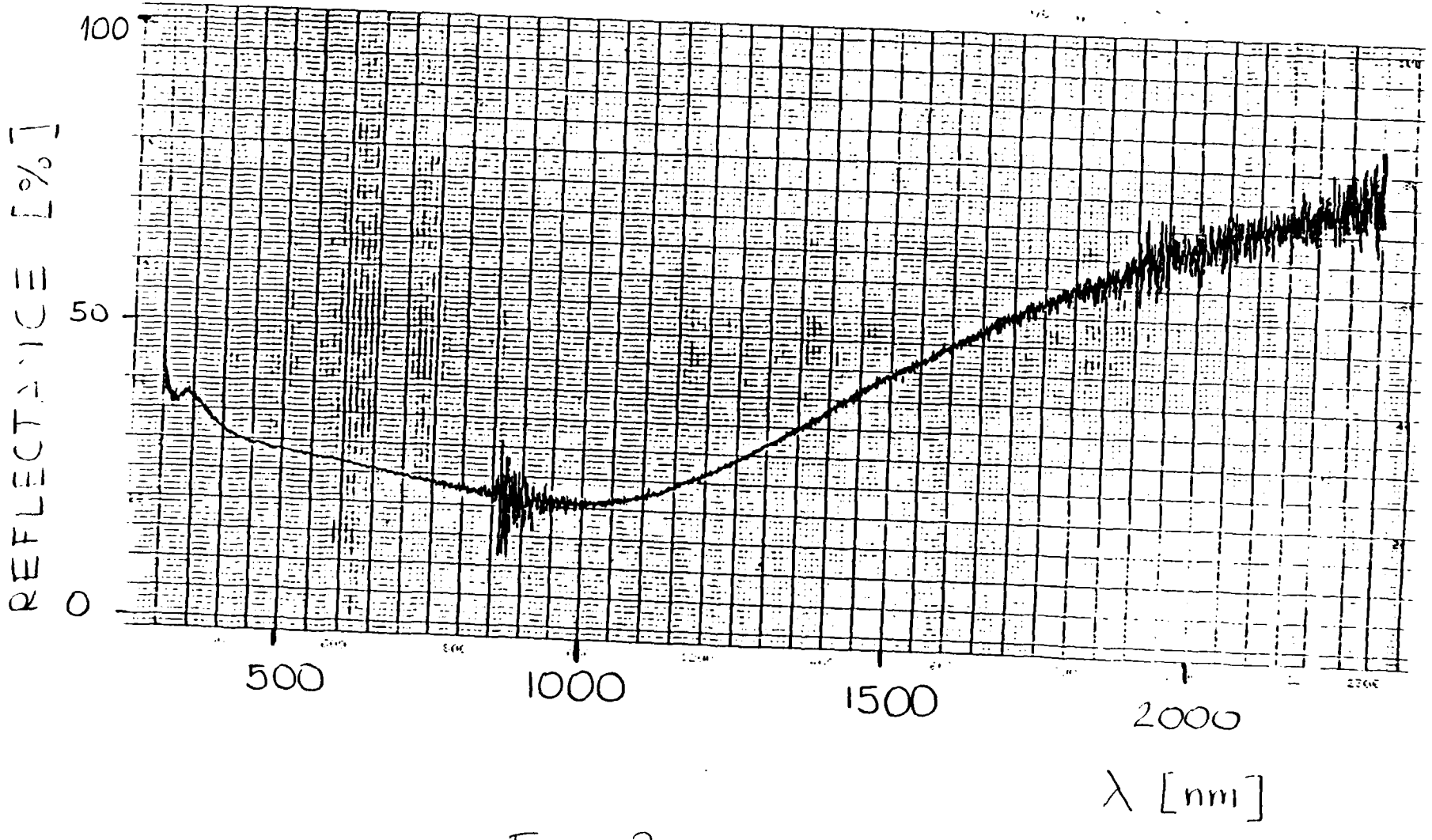

Fig. 3

Raman spectrum of a $Ba_2Sr_2CaCu_2O_8$ single crystal (from ab face)

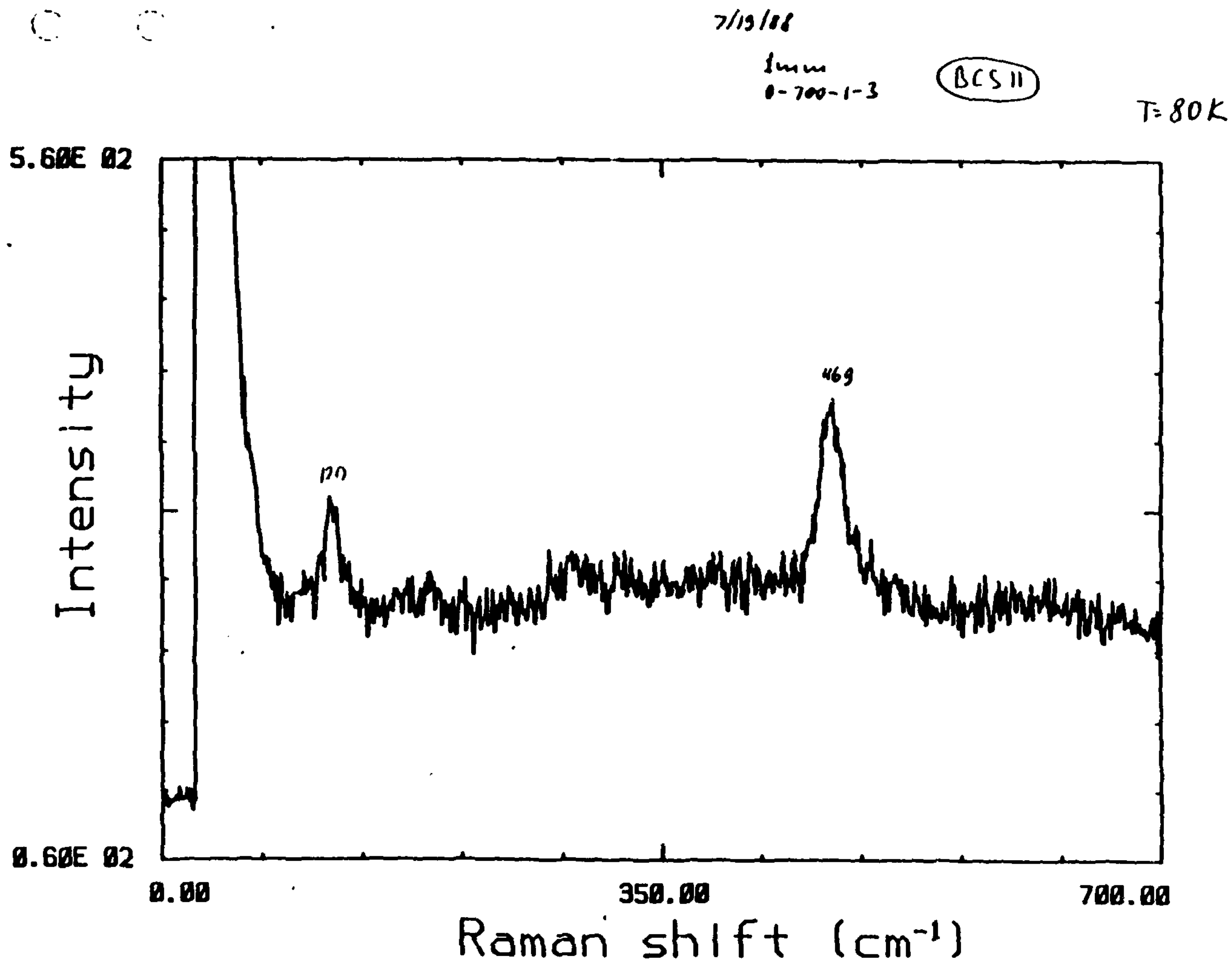

Fig. 4a

Raman spectrum of a $Ba_2Sr_2CaCu_2O_8$ single crystal, at T = 12 K. The superconducting gap is seen to open below $\hbar\omega = 300\ cm^{-1}$.

7/19/88
1mm 800mW+filter
0-700-1-3
DCS10
T = 12K

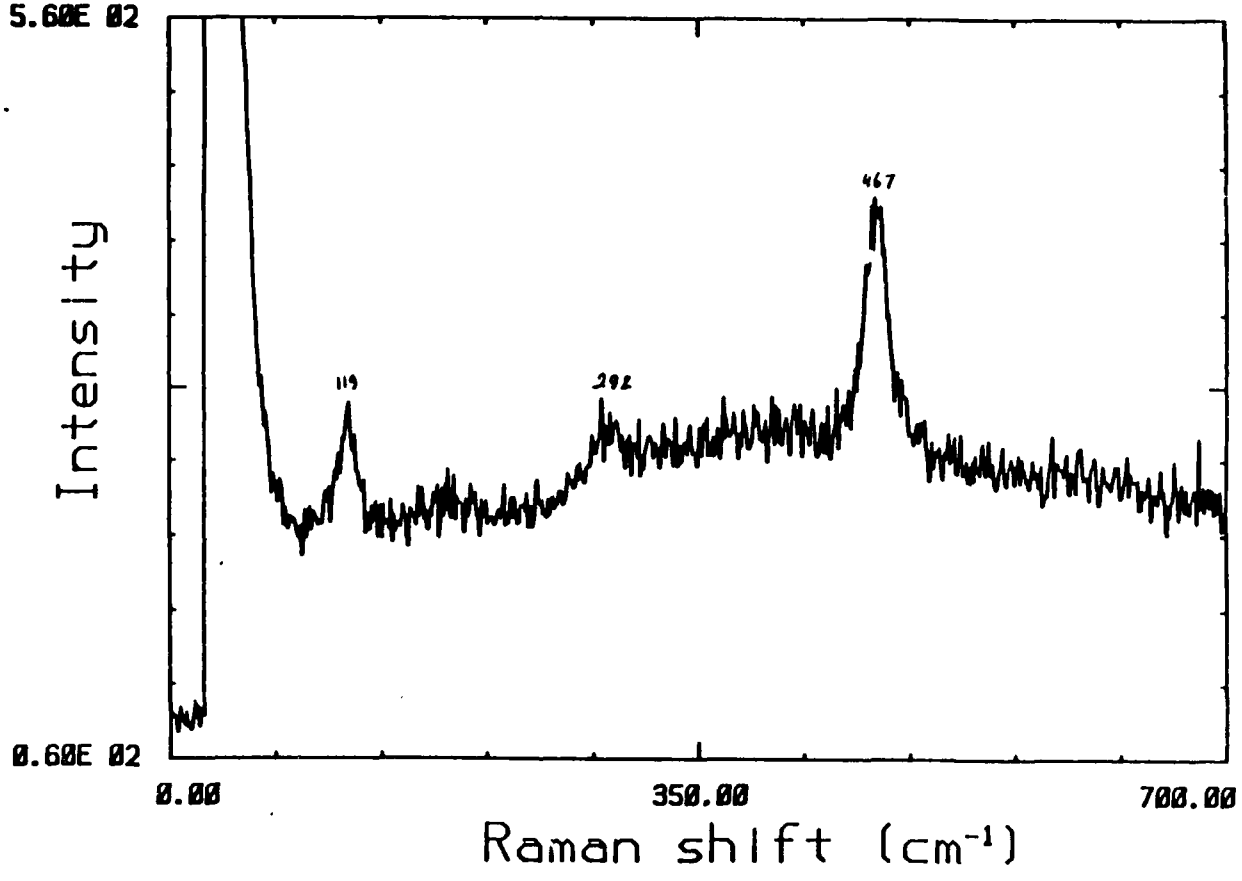

SUMMARY OF WORK AT STANFORD ON IR DETECTOR PROGRAM

1. During the initial phase of this work (which is still in progress), we have been able to gain control of the orientation and microstructure of the thin films of $YBa_2Cu_3O_{7-x}$ (YBCO) laid down by both electron-beam metal sources and planar magnetron sputtering sources[1]. The resulting electrical and optical properties are so diverse that it seems clear that there will also be a vast difference in the infrared detector figure of merit in the devices fabricated from different films. We believe that the most viable approach is first to prepare a number of films with well differentiated properties and then to compare their photoconducting properties. We are well along the first stage. Our principal results are the following ones.

A. The optical response (reflectance and transmittance) of YBCO is rather featureless and almost flat[2] in the mid-IR spectral range [see Figs. 1 and 2]. This is quite favorable from the viewpoint of detector applications; one could expect a flat spectral response. In fact, $T(\omega)$ and $R(\omega)$ do not change much throughout the visible, either, see Fig.6; ellipsometry (done in collaboration with D. Aspnes at Belcorre) does show some broad and mild features at about 2.7 and 4.7 eV, see Fig.7.

B. The optical penetration depth is less than 1000 Å in the mid-IR region. It decreases at lower frequencies due to the free-carrier absorption; it also decreases at higher photon energies due to increasing absorption of as yet unidentified origin [Interband transition(s)? Holstein processes?]. Hence, for a good responsivity, one needs

rather thin YBCO films, say 1000 Å thick, or less. This result is in varriance with estimates which suggested 1-10 μm as the optimum thickness, on the basis of what we now believe were erroneous estimates of the transmittance due to multiple reflections in granular samples (embedded in KBr) , being understood as transmission through the bulk[3]. This also illustrates well the necessity of studying the material in detail first.

C. Finally, we have observed large sample-to-sample variations in reflectance of YBCO films [see Figs. 3A - 3D] , despite the fact that they showed comparable transport properties. Hence, it has been necessary to first understand the causes of these variations, and than to learn to control the growth process in such a way as to ensure reproducible behavior.

2. So far, we were able to trace two major sources of the mentioned sample-to-sample variations. The first is formation of the "junk" overlayer; YBCO is a "line" compound - i.e. it forms at nearly exact stoichiometry composition. As it grows epitaxially on the (001) face of SrTiO3 substrate, it expels the foreign phases (which are likely to form due to small off-stoichiometry variations in composition) to the film surface. In Fig. 4, we compare the reflectance spectrum of an YBCO film with the spectra of the same film after two successive ion-milling runs. In each run, the first 800Å were removed with the argon-ion beam, at the lowest voltage possible and at almost the grazing angle of incidence. The last 200Å were removed with the oxygen-ion beam; thus one avoids formation of an oxygen-depleted overlayer. High

metallic reflectance is obtained [Fig. 4] matching and even surpassing that from specular (001) faces of the best available YBCO single crystals. We have obtained independent and consistent confirmation of these conclusions from our ellipsometric studies on ion-milled YBCO films. In addition to removal of the impurity phases, the surface density is found to increase, as evidenced by increase of the dielectric function - in some cases surpassing the single-crystal values. High-temperature oxygen annealing may well be producing some surface roughness in single-crystal samples, too.

The second major source of sample-to-sample variations in the optical properties in the mid-IR region are differences in grain orientation, because of the huge anisotropy of YBCO in this spectral range. This is illustrated in Fig. 5, displaying the reflectance spectra taken from a side of an YBCO single crystal, with the polarization paralle' and perpendicular, respectively, to the CuO_2 layers[4]. The anisotropy decreases as the phonon energy is increased to the visible and virtually diminishes above ~2eV or so [see Figs. 6 and 7].

3. Thus we have identified three basic requirements for an YBCO film to be suitable for optical applications: it has to be thinner than 1000Å ; the grain orientation has to be controlled and the surface has to be cleaned. Indeed, we have succeeded in growing very good superconducting YBCO fillms (T_c = 91K with 1-2K wide transitions; $j_c > 1.2 \times 10^7$ A/cm^2 at 4.2 K), ~ 500Å thick and well-oriented (up to 90%), with the c-axis or the a-axis perpendicular to the substrate[1].

4. In parallel to the above work and in analogy to some earlier studies[3] on thin superconducting granular films of Nb/BN and $BaPb_{0.7}Bi_{0.3}O_3$, we have attempted to observe an increase in resistivity of thin $YBa_2Cu_3O_{7-x}$ (YBCO) films exposed to infrared (IR) radiation. The films were kept in liquid nitrogen, i.e. bellow the measured T_c (zero-resistance). The 1 μm thick YBCO films were grown on the $SrTiO_3$ substrates. Silver paint was utilized to make the contacts. The Stanford free-electron laser (FEL) was utilized as a tunable source of intense, short-pulsed, monochromatic IR radiation. In Fig.8. we show the temporal dependence of the photo-induced resistivity jump. The FEL pulses of 300 fsec duration are repeated at 36 GHz rate, and they come in trains of 1000 pulses each; the wavelength employed was 3.2 μm. The bias voltage was 15 V.

Hence, the IR-photodetecting capability of thin superconducting YBCO films has been demonstrated, in principle.

However, we have found the above result unsatisfactory in two respects: first, the response was much slower than what was expected, and second, the responsivity was rather low. As for the first problem, a simple calculation (now that the thermal conductivity of YBCO is known) shows that the absorbed energy was more than enough to heat the sample into the normal state, i.e. what is shown in Fig.8 is largely a thermal effect. Hence one has to decrease the incoming beam energy; however, that requires the second problem, that of low responsivity, to be solved first - the signal becomes too weak. This will most likely require an optimization of the orientation and microstructure of the superconducting film as we are presently doing.

5. Our preliminary experiments with very thin (500 Å) YBCO films encountered problems due to large and uncontrollable variations of the FEL beam intensity. We are looking now for more stable and controllable short-pulse IR sources. Also, in immediate future we intend to extend our experiments into the far-IR spectral region. Except for some early work[6] done in collaboration with the Emory University group, our spectroscopical studies were limited to mid-IR/visible/UV region. However, for the specific needs of this project we have acquired recently a Digilab FTS-40V Fourier-transform vacuum-FIR spectrometer; we are equipped now to cover a broad spectral range from 6 eV down to 1-2 meV. Finally, good superconducting films of the 2-4-8 YBCO phase, as well as of the Bi-Sr-Ca-Cu-O phases, have been grown succesfully in our group, and we plan to extend our investigations to these high-T_c *materials, too.*

References

1. A, Kapitulnik, in Proc. Int. Conf. on High-Temperature Superconductors, Interlaken, 1988 [Physica C, to be published];
K. Char et al., preprint. (enclosed)

2. I. Bozovic et al., Phys. Rev. Lett. **59**,2219 (1987). (enclosed)

3. Z. Schlesinger et al., Phys. Rev. B **35**, 5334 (1987).
M. Stavola et al., ibid, **36**, 850 (1987).

4. I. Bozovic et al., preprint (enclosed).

5. Y. Enomoto and J. Noda, Jap. J. Appl. Phys. **26** S3, 37 (1987);
K. Weiser et al., J. Appl. Phys. **52**, 4888 (1981);
M. Leung et al., preprint.

6. I. Bozovic et al., Phys. Rev. B **36**, 4000 (1987). (enclosed)

MID-IR REFLECTANCE OF A GOOD C-AXIS ORIENTED YBCO FILM

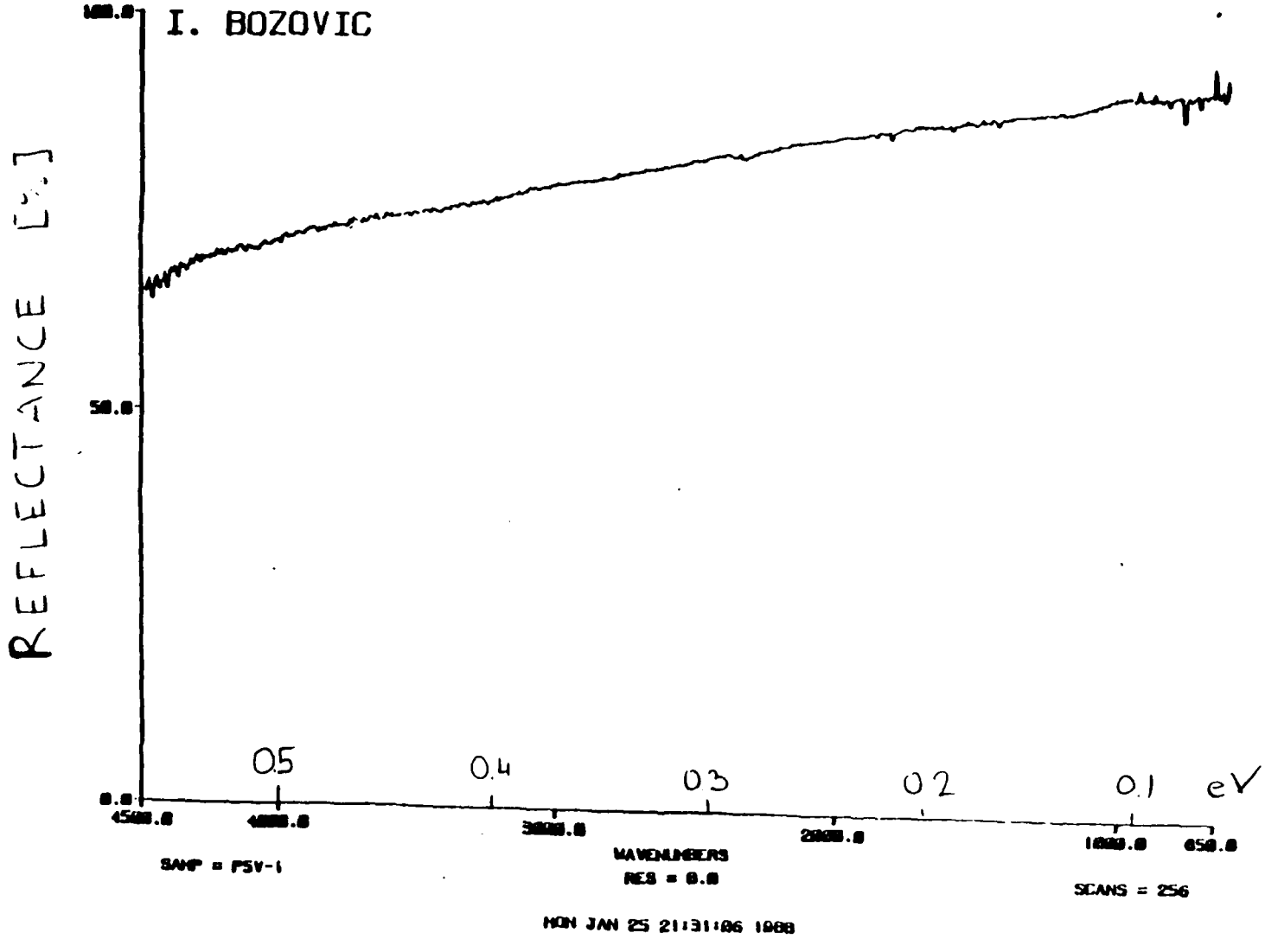

I. Bozovic
Stanford U.

MID-IR TRANSMITTANCE OF AN YBC
FILM ON $SrTiO_3$ ORIENTATION
IS ROUGHLY 50% C-AXIS, 50%
a-axis PERPENDICULAR TO THE
SUBSTRATE. FILM THICKNESS ≈ 1200 Å

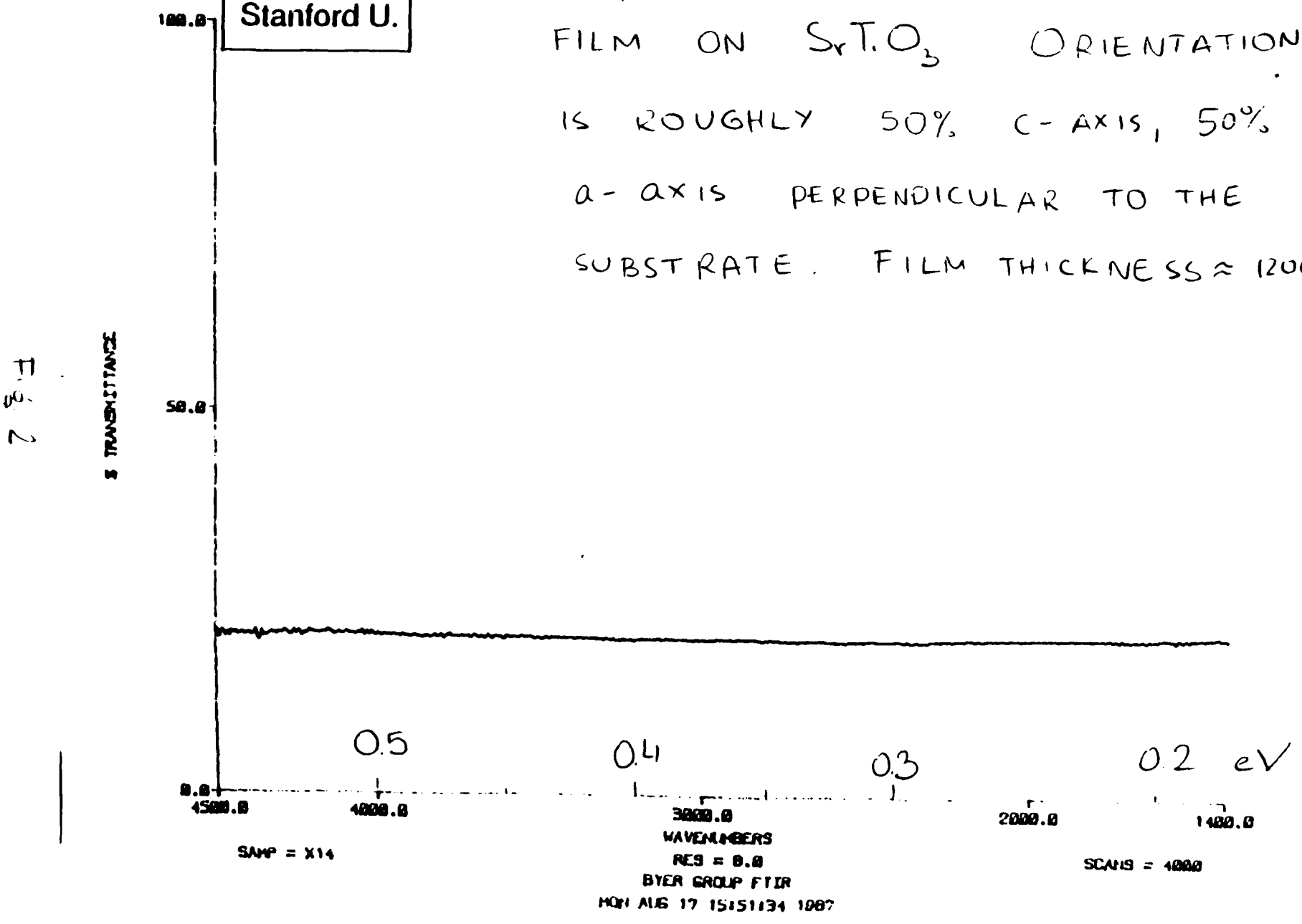

MID-IR REFLECTANCE OF FOUR YBCO FILMS FROM THE SAME BATCH, ALL WITH WELL-BEHAVED HIGH T_c TRANSITION TEMPERATURES AS MEASURED BY DC RESISTANCE.

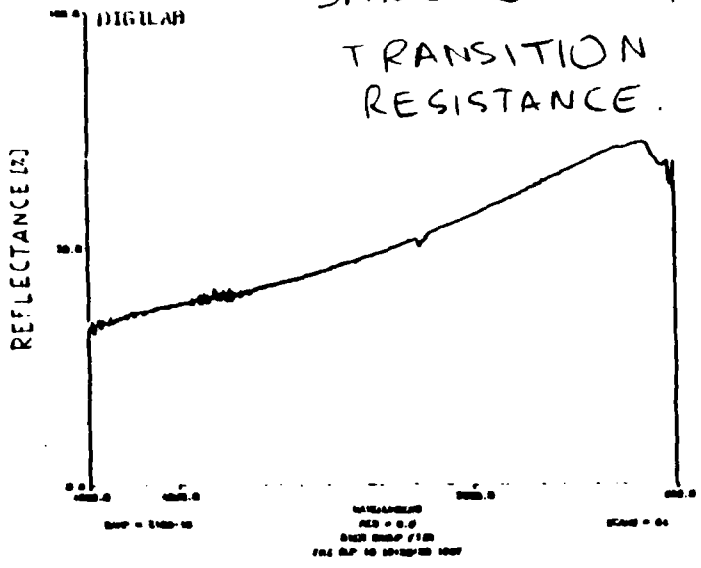

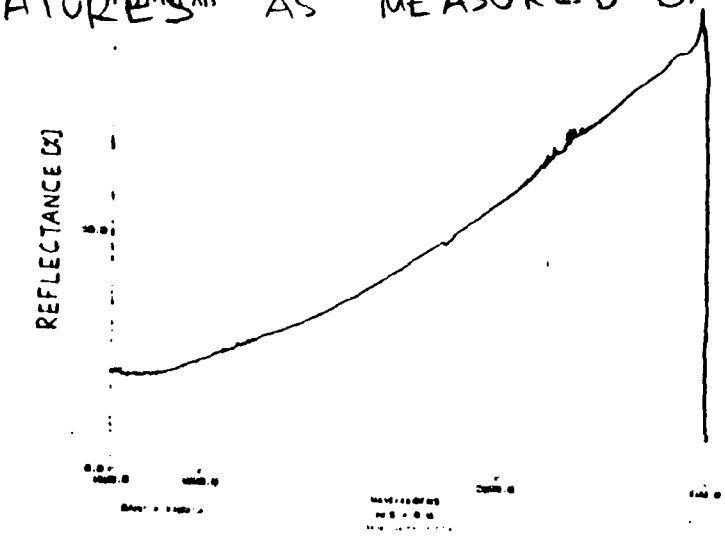

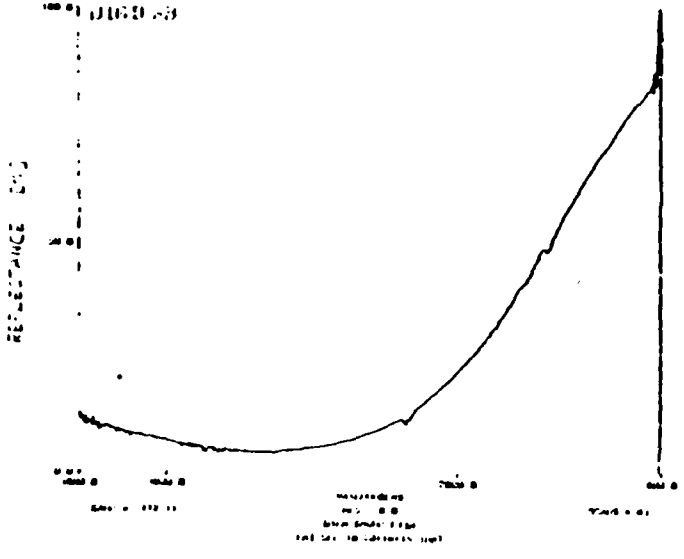

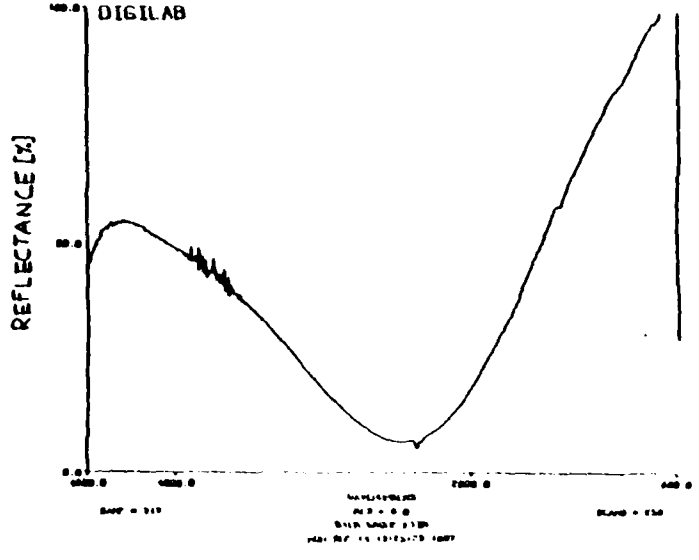

THIS ILLUSTRATES HOW MUCH VARIATIONS IN REFLECTANCE DO

THE EFFECTS OF CLEANING THE SURFACE OF AN YBCO FILM (c-axis oriented) ON ITS MID-IR REFLECTANCE

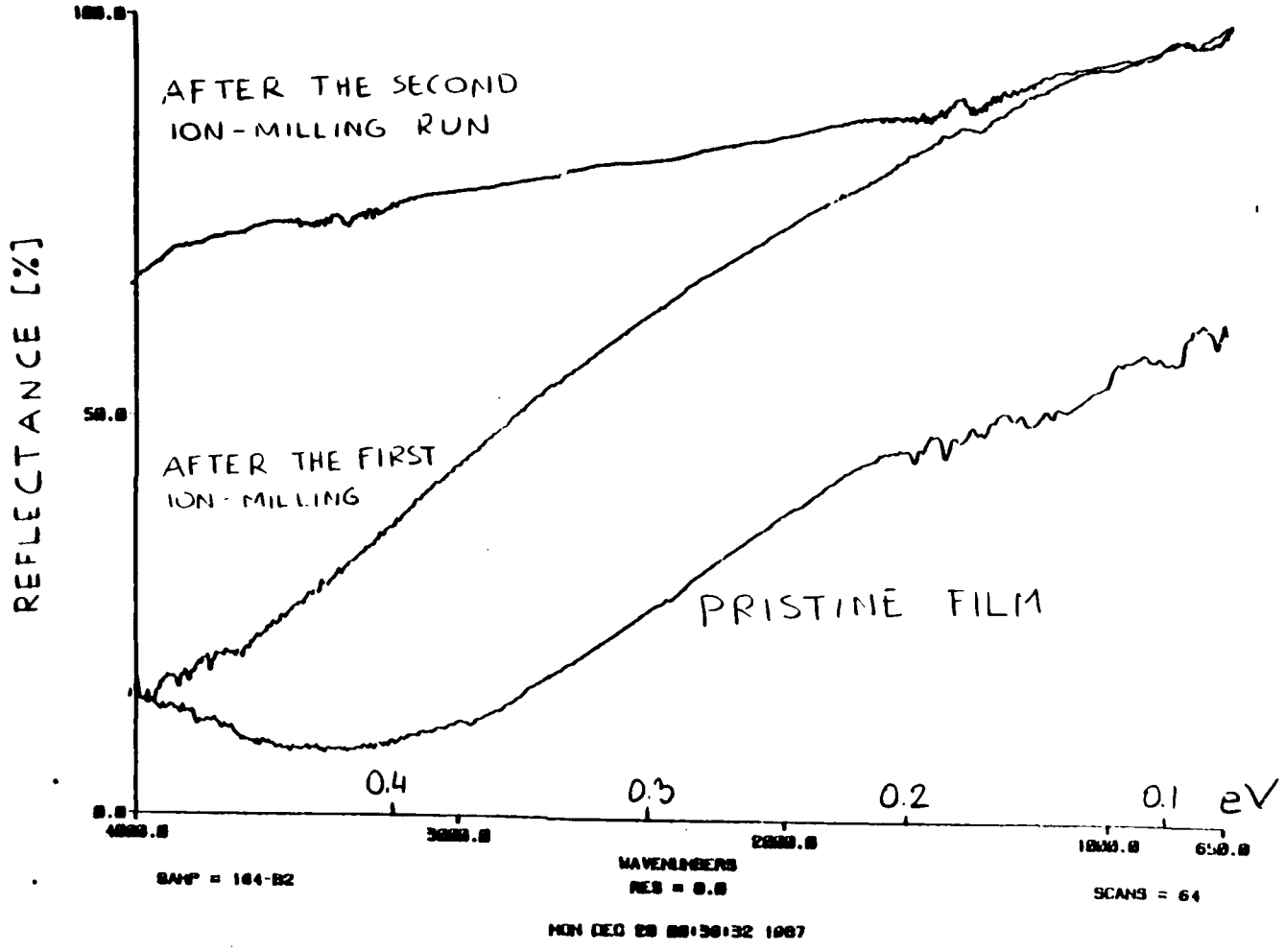

As-grown films can have non-superconducting non-metallic phases on their surfaces, which can be removed by ion-milling.

ANISOTROPY OF YBCO SINGLE CRYSTAL AS DETERMINED BY IR REFLECTANCE.

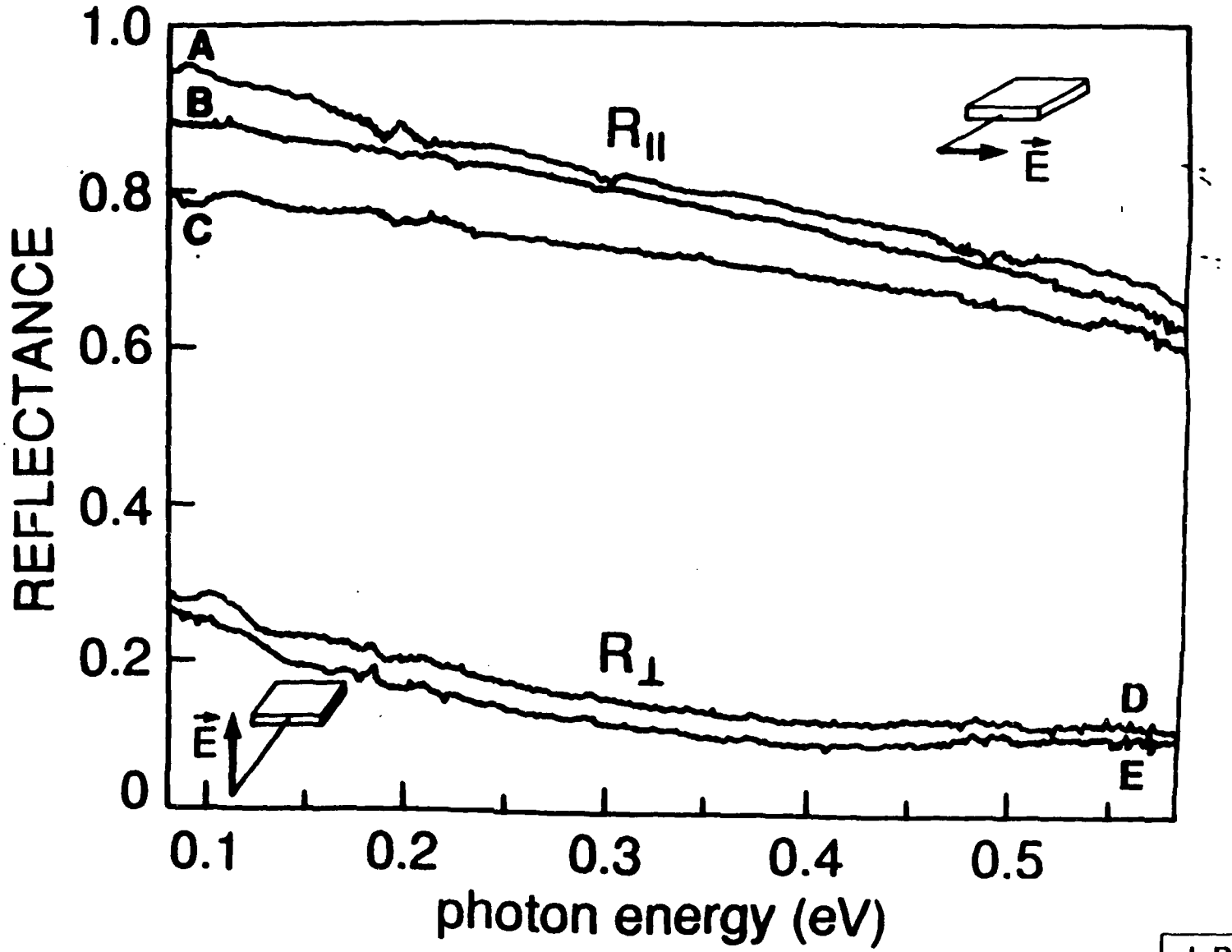

I. Bozovic
Stanford U.

The film orientation is important in determining the optical properties. We have learned how to control the orientation.

ANISOTROPY OF YBCO THIN FILMS AS DETERMINED BY IR/VISIBLE TRANSMITTANCE

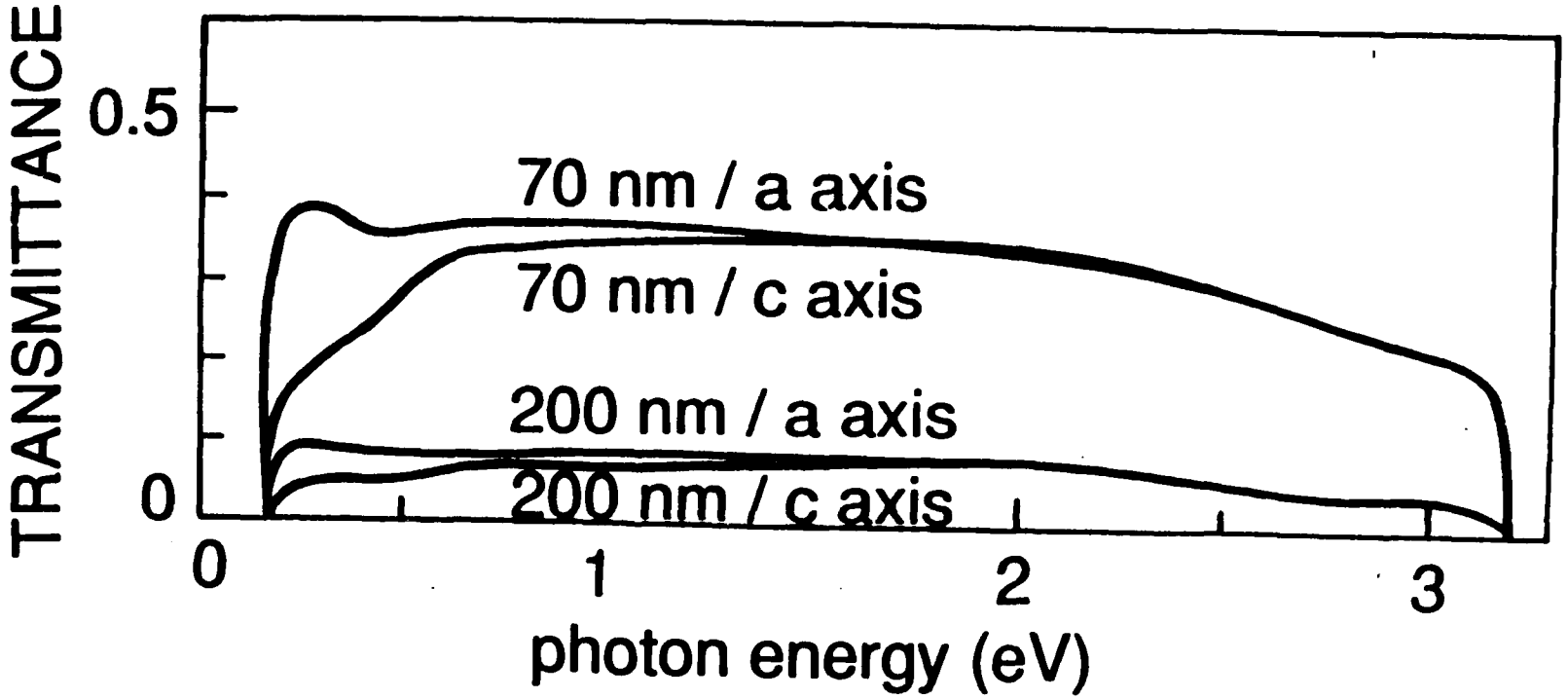

Fig. 6

AS DETERMINED BY ELLIPSOMETRY.

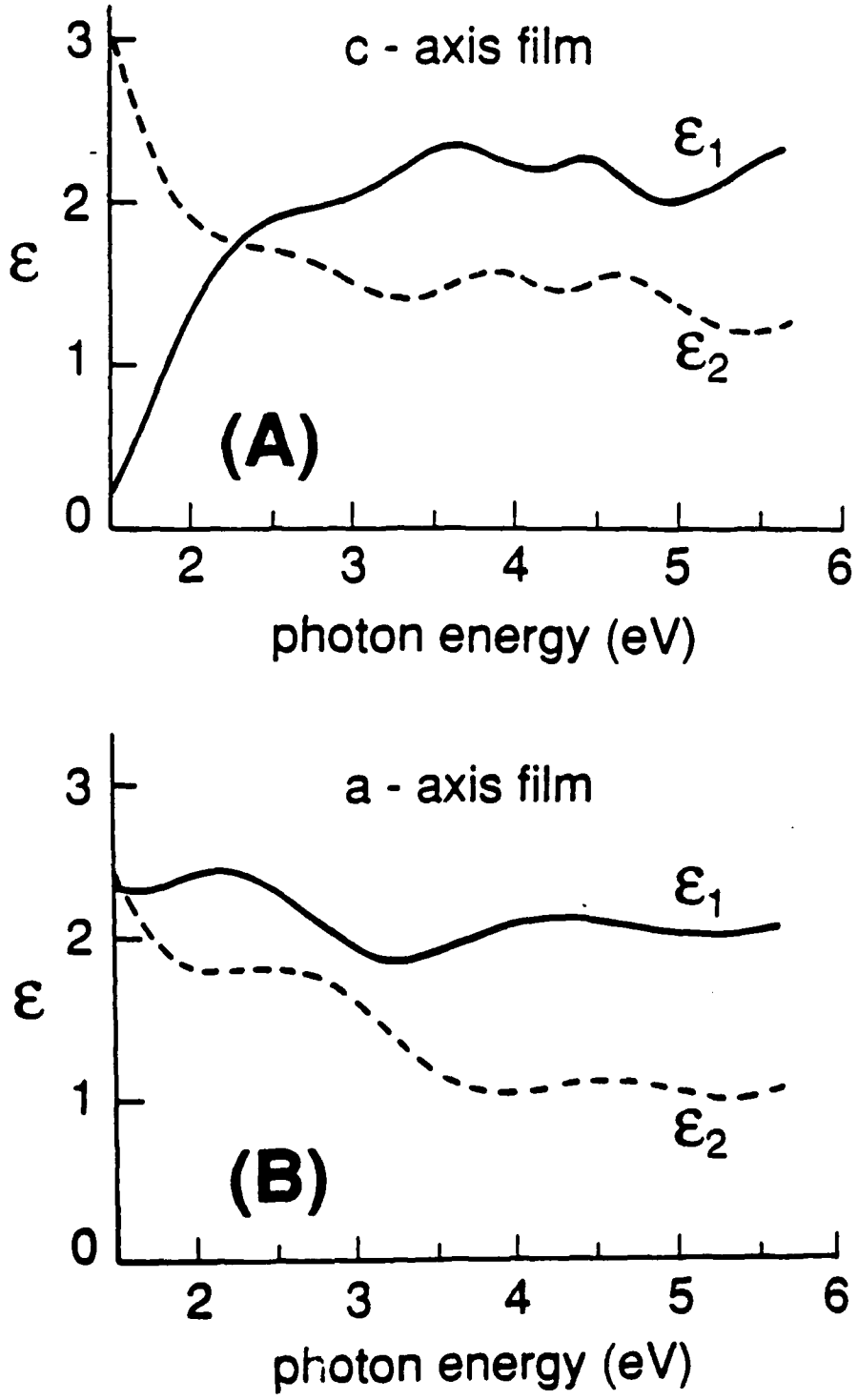

Fig. 7

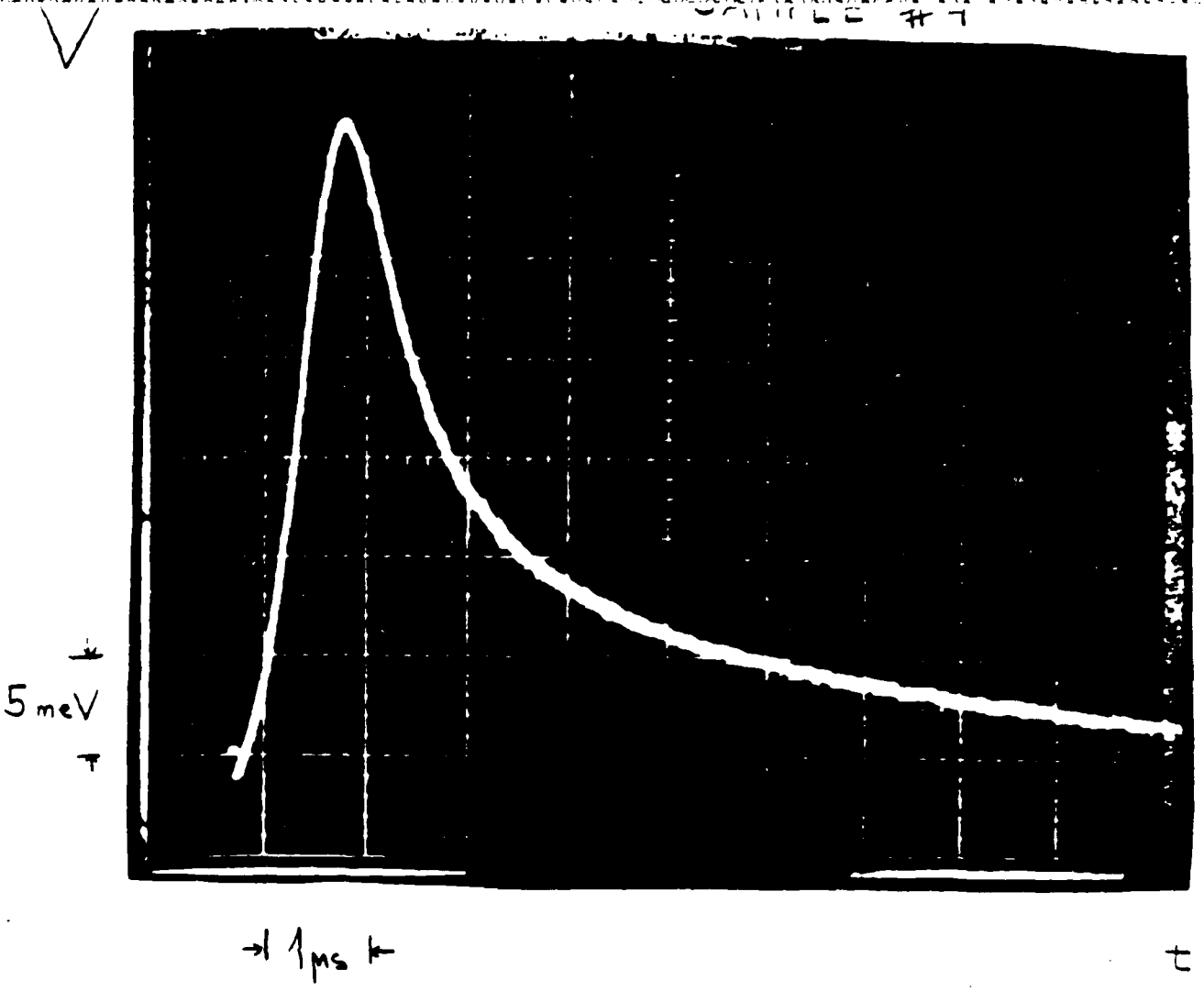

BIAS : 15 V T = 77 K

Fig. 8

A JUMP IN RESISTIVITY OF AN YBCO FILM INDUCED UPON IRRADIATING IT BY AN FEL PULSE.

AN ORDERED DEFECT STRUCTURE IN EPITAXIAL $Y_1Ba_2Cu_3O_{7-x}$ THIN FILMS

submitted Phys Rev. B

A. F. Marshall, R. W. Barton, K. Char, A. Kapitulnik,
B. Oh, and R. H. Hammond
Center for Materials Research, Stanford University,
Stanford, CA 94305 and

S. S. Laderman
Circuit Technology R&D, Hewlett Packard Company
3500 Deer Creek Road
Palo Alto, CA 94304

ABSTRACT

An ordered defect structure in superconducting Y-Ba-Cu-O thin films has been characterized by both x-ray diffraction and transmission electron micrsoscopy. The defect structure, which is observed growing epitaxially within the grains of normal $YBa_2Cu_3O_{7-x}$ structure, has the diffraction characteristics of a distinct phase whose volume fraction can be correlated with changes in film composition. The diffraction characteristics are consistent with an orthorhombic unit cell ($a \equiv b = 3.86$ Å, $c = 27.19$ Å) with space group Ammm. These are the characteristics to be expected from a structure in which extra copper-oxygen layers create fault planes, which are inserted at every unit cell in the parent $YBa_2Cu_3O_{7-x}$ structure. The composition expected for the pure phase is $Y_2Ba_4Cu_8O_{20-x}$. Preliminary transport measurements on films containing this extra phase are characterized by lower normal state resistances and a lower Hall constant.

I. Introduction

While the pseudo-ternary phase diagram for the high-T_c superconductor $YBa_2Cu_3O_{7-x}$ has been generally estabilished [1,2], finer details of the phase equilibria near this composition are still of great interest. Several research groups have recently reported observations of defect structures in the $YBa_2Cu_3O_{7-x}$ phase and have attempted to correlate these with the presence of various superconducting transport properties[3-7]

Transmission electron microscopy (TEM) studies by several researchers[4,8,9] have reported c-axis defects in the $YBa_2Cu_3O_{7-x}$ phase which locally expand the c-axis spacing by 16%. Zandbergen[8], using image calculations of high resolution TEM images, modelled this expansion as the insertion of an extra CuO planes between barium layers in the normal $YBa_2Cu_3O_{7-x}$ structure. Narayan et al[3], as well as others[10,11], reported an apparently new phase with a lattice fringe spacing uniformly expanded by the same amount (c=13.55 A). This phase appeared in small volume fractions growing epitaxially on the parent $YBa_2Cu_3O_{7-x}$ phase[3,11]. Narayan et al, however, have not to our knowledge reported high resolution images or a diffraction analysis of their new phase. All of the above observations have been carried out on bulk or "powdered" specimens. The appearance of structural defects in these studies has been attributed by some to a decomposition of the sample surface[8,12,13], and by others to to an artifact of the TEM sample preparation process (specifically ion milling)[14-16].

In this paper we present observations of an ordered defect structure in thin film samples of $YBa_2Cu_3O_{7-x}$. An important aspect of our results is the correlation

between TEM and X-ray diffraction patterns, clearly demonstrating the existence of such a structure independent of the TEM specimen preparation method. Further, we show that this structure can exist in large volume fractions of the films, its appearance correlated to variations in film composition instead of annealing or atmospheric condition. We show evidence that at high concentrations the ordered defects can form a distinct crystallographic phase with a unit cell parameter of 27.2 Å. From preliminary transport measurments we associate the presence of this phase with lower normal state resistivities and a lower Hall constant. Finally, our results show this phase to be consistent with an extension of the Zandbergen model, specifically, an ordered array of extra Cu-O planes.

II. Experimental Methods:

The films reported on here were made by reactive magnetron sputtering and by electron beam evaporation onto (100) $SrTiO_3$ substrates. Details of each of these techniques have been reported previously [17,18]. A distinctive characteristic of each of these deposition processes is the use of separate metal sources pointed at sample holders that contain long arrays of samples. In this manner a continuous set of film compositions is obtained in one run. It has therefore been possible to make good correlations of both sample properties and microstructures with composition. When expressed as a ratio of metal atoms, for example, the variations in copper concentration within a 6 mm by 6 mm sample were typically within one atomic percent absolute, while copper concentrations across two rows of 10 samples each were as much as 8 percent. A typical sample employed in this study had nominal metal ratios of $Y_{18}Ba_{29}Cu_{53}$. Thicknesses were either 1800 or 4000 Å.

All of the samples as removed from deposition chambers were found to be highly disordered by x-ray diffraction. The samples then underwent similar annealing procedures, resulting in crystallization and oxidation of the Y-Ba-Cu-O superconducting phase(s). Given the similarities of the post-annealing process, we have not been surprised to find that films deposited by different techniques (e-beam or sputtering) have resulted in similar microstructures. The usual annealing procedure includes 6 hours at 650 C , followed by one hour at 750 C , followed by one hour at 850 C, followed by a slow furnace cool, all under flowing O_2.

Procedures for characterizing epitaxial films in a four-circle x-ray diffractometer have also been described previously[17]. The films are generally polycrystalline, though restricted to a limited number of orientations on the $SrTiO_3$ substrate. The c-axis of the $YBa_2Cu_3O_{7-x}$ structure is usually found in a mixture of 90 degree orientations, either normal to the substrate or parallel to one of the $SrTiO_3$ crystal axes in the plane of the film. In the symmetrical or Bragg-Brentano geometry only those peaks originating from a* or c* axes are detected. In order to detect peaks with mixed Miller indices it is necessary to rotate the sample about one of the axes in the film plane.

We often distinguish between films with either a- or c-axis orientation, referring to that crystalline axis which appears predominately in the normal direction. We have not yet made quantitative distinctions between a- or b-axis orientations[17]; in this paper "a-axis" refers to either orientation It is known that the $YBa_2Cu_3O_{7-x}$ structure is heavily twinned[4,12], causing a large amount of coincidence between a and b axes.

Planar sections of both a-and c-axis oriented films were thinned for TEM studies by grinding, dimpling and ion milling from the substrate side until perforation. The surface of the film was also ion milled slightly so as to examine the interior of the film. Ion milling was carried out in a liquid N_2 cold stage and with low ion beam conditions (5kV, 0.3 mamp gun current) so as to minimize potential heating and ion bombardment damage to the specimen. TEM analysis was carried out on a Philips 400ST equipped with an EDAX 9100 energy dispersive spectrometer. High resolution images were obtained on a Philips 430ST.

III . Results

A. Structural Properties

Figure 1 is an x-ray diffraction pattern of a c-axis oriented sputtered film (sample A). Typical substrate and $YBa_2Cu_3O_{7-x}$ peaks are seen. Extra peaks, marked by asterisks are observed, all of which can be indexed according to a c-axis spacing of 13.6 Å (00l) or 27.2 Å (00l, l=2n). The larger unit cell is consistent with a superlattice structure seven times the length of the fundamental perovskite unit cell. The intensity of these extra peaks indicates a volume fraction of the new structure comparable to the total oriented volume of the normal $YBa_2Cu_3O_{7-x}$ phase. Variations in the x-ray intensities and widths of these peaks have been observed to correlate to variations in sample composition, the intensities generally increasing in samples prepared with simultaneous excesses of yttrium and copper. Samples reported on here contained typically 3 excess atomic percent of each element.

A number of films made by both deposition techniques and with predominantly either a- and c-axis orientation were examined in TEM. The data shown here originated from one sputtered film (sample A) and one evaporated film (sample B). Each film was Cu- and Y-rich relative to the $YBa_2Cu_3O_{7-x}$ composition. A-axis grains in each film showed characteristic defect regions such as are typified in Figure 2. This TEM micrograph shows c-axis fringes in two perpendicular $YBa_2Cu_3O_{7-x}$ grains. The region of defects runs along the length of each grain, the individual faults lying parallel to (001) planes in $YBa_2Cu_3O_{7-x}$. The defect regions shown here are representative of those observed in many other samples as well as in at least one bulk specimen. They tend to occur within grains rather than at grain boundaries, parallel to (001) planes, and energy dispersive microanalysis indicates that they are somewhat Cu-rich. Defect regions are generally unstable under the electron beam. Degradation or amorphization of the lattice tends to occur more quickly during observation of these regions than it does in the normal $YBa_2Cu_3O_{7-x}$ material.

In addition to the defects shown in Fig. 2, a significant number of small, randomly oriented second phase particles were observed in the TEM. Microanalysis of these particles revealed them to be Y-rich, with a composition approximating that of the Y_2BaCuO_5 phase.

A high resolution image of a defect region from a different grain of sample B is shown in Figure 3. The left side of this micrograph shows normal $YBa_2Cu_3O_{7-x}$ material with characteristic 11.7 Å c-axis fringe spacing. The right side shows defects, appearing as local expansions of the unit cell. The expansion is approximately 16% of the c-lattice parameter. The defects occur at a density of one per unit cell. If one refers to the high resolution image calculations reported by

others[5,8,9,19,20] then one can assign the specific position of the local lattice expansion to an area between adjacent barium-oxygen layers. The defects in Figure 3 are therefore similar to those observed by Zandbergen et. al.[8], except that they are occuring at a much higher density. In observations over many different grains and in several different samples we have observed considerable variations in ordering: from structures with isolated defects, to structures with defects in every other or every third unit cell, to the densely packed and well ordered structures shown in Figure 3.

Microdiffraction patterns of similar well-ordered defect regions occurring within [100] and [110] oriented $YBa_2Cu_3O_{7-x}$ grains are shown in Figure 4. The first two patterns are from sample A, the third from sample B. Because defects occur epitaxially in narrow bands within grains of the $YBa_2Cu_3O_{7-x}$ material, controlled tilting experiments on particular regions have not yet been possible. Each of the patterns shown in Figure 4, however, shows marked deviations from the normal superlattice/sublattice symmetries observed in neighboring $YBa_2Cu_3O_{7-x}$ material (cf. references 13,15,19). For example, normal $YBa_2Cu_3O_{7-x}$, [100] diffraction patterns are characterized by a square perovskite sublattice and a superlattice, occuring in the c* rows, indicative of the tripled (11.7 Å) unit cell. The new phase, as represented in Figure 4, is characterized by either a smearing or a complete absence of intensity in the vicinity of the first c* subcell reflection (what would be (003) in $YBa_2Cu_3O_{7-x}$). The second c* subcell reflection (formerly (006) now appears as the seventh spot in the row. A similar seven-fold superlattice periodicity can be observed between sublattice spots labeled 017 and 01(-7) in Figure 4a. The d-spacings between spots in c* rows correspond to multiples of 13.6 Å, in agreement with the extra peaks observed in x-ray diffraction.

Systematic extinctions in the diffraction patterns of this new phase can also be observed by comparing the patterns obtained within defect regions to those in neighboring $YBa_2Cu_3O_{7-x}$ material. When moving the beam between neighboring regions it is observed that the spacings between reciprocal lattice rows remains the same, while the arrangement of spots within a row varies. Figures 4a and 4c, for example, show reflections along the c*-axis which are offset by 1/2 in alternating rows. This suggests a true periodicity for the material of 27.2 instead of 13.6 Å. A consistent interpretation of the three patterns can be obtained by assigning them to the zone axes [100], [010], and [110] respectively. All special conditions for the reflections can then be described by the single formula: k + l = 2n. These conditions are characteristic of side-centered unit cells. The diffraction spots in Figure 4 have been indexed accordingly.

Summarizing our interpretations of Figure 4, we find an orthorhombic unit cell with a single formula for special conditions: k + l = 2n. This symmetry is consistent with of each of four space groups: A222, Amm2, Cmm2, and Ammm.

Using the systematic extinctions observed in Figure 4 as a guide, we have been able to identify further x-ray peaks from the new phase by tilting a sputtered sample (A', similar to that shown in Figure 1) away from its symmetrical axis on the four-circle x-ray diffractometer. A listing of observed peak positions and approximate intensities is given in Table I for identification purposes. The peaks listed here were then used to refine the dimensions of the unit cell, giving: $a \equiv b = 3.86 \pm 0.02$ Å and $c = 27.19 \pm 0.07$ Å. The peaks observed in samples A and A' (Figure 1) are relatively broad and assymetrical, perhaps because the faults in defect regions are not completely ordered. This resulted in relatively large error

bars from the cell refinement. Subsequently, we have synthesized samples with significantly narrower peak widths, yielding the same c-axis lattice parameter to an accuracy of 0.03 Å. As another consequence of the observed peak broadening, and the fact that oriented grains in our thin films appear randomly aligned with respect to a 90 degree rotation about the c-axis, we have been unable as yet to make accurate distinctions between a and b-axis lattice parameters.

B. Transport Properties:

Preliminary measurements of transport properties in these films have been obtained. A more in-depth study of superconducting and normal state properties is still in progress. All of the films reported on here are 90 K superconductors, the superconductivity being most likely due to the presence of significant fractions of $YBa_2Cu_3O_{7-x}$. No resistive anomolies between 90 and 300 K have been observed. Films with significant volume fractions of the new phase are primarily distinguished by lower normal state resistivities. The resistivity observed in one mixed phase sample is 100 micro-ohm centimeters at 100 K. While this resistivity is not particularly low (subsequent films of $YBa_2Cu_3O_{7-x}$ at different thicknesses have been observed in the range of 80 micro-ohm centimeters), when compared to samples prepared at the 1:2:3 composition in the same runs (ρ = 300 micro-ohm centimeters at 100 K) resistivities in mixed phase samples are lower. Additionally, one mixed phase sample was observed to have an anomolously low Hall coefficient: + 7.4 x 10^{-6} microohm-cm/gauss compared to + 2.0 x 10^{-5} microohm-cm/gauss for $YBa_2Cu_3O_{7-x}$. The lower Hall coefficient suggests the existence of higher carrier concentrations in mixed phase samples (as high as 10^{22} cm^{-3}). Measurements are underway on recently prepared samples which contain higher volume fractions of the new phase.

IV. Discussion:

A. Structural model:

Our real space images and diffraction patterns demonstrate the existence of an ordered array of c-axis stacking faults. A structural model for a new phase based on these stacking faults will now be considered.

Considering first the diffraction data alone, one can try to fit the new unit cell dimensions and symmetries to models in which either extra Y planes, extra Ba-O planes, or extra Cu-O planes have been inserted into the normal $YBa_2Cu_3O_{7-x}$ structure. In each case one might look for the presence of two counterbalancing fault planes per unit cell. With the addition of two extra planes then, of average thickness 1/6 C_{123}, one would expect a resultant c-axis dimension of:

$$C_{new} = C_{123} \times 2 \times 1\frac{1}{6}$$

yielding C = 27.255 Å. This agrees within experimental error to the c-parameter refined from Table I. Differences from this value may be attributable to relaxed thicknesses in the two stacking faults.

Chemical precedents for the structure of stacking faults can be derived from model compounds such as La_2CuO_4 [21] or $SrCuO_2$ [22,23]. In the former compound, extra Ba or La atoms are accomodated in a perovskite structure by the formation of a body-centered unit cell. $SrCuO_2$ appears to be more relevant to the present case, however, since it demonstrates that extra planes of copper atoms can lead to the formation of a side-centered unit cell, in agreement with our diffraction results.

Zandbergen et al.[8] proposed a model for isolated c-axis defects in $YBa_2Cu_3O_{7-x}$ based upon high-resolution TEM images. They showed that their images, similar to ours, can be modeled with the insertion an extra Cu-O plane between adjacent Ba-O layers. Besides the appropriate expansion of the lattice by 16%, this also results in a lattice shift across the defect by 1/2 [010]. The insertion of one such plane in every unit cell would produce a side-centered, 27.2 Å phase, consistent with our diffraction results. This model also accounts for the excess copper concentration observed in our defect regions. (Extra yttrium concentrations, present in our thin film samples, have been observed as incoherent precipitates, probably the Y_2BaCuO_5 phase.)

The space group for this new phase, based upon the Zandbergen defect model, would be Ammm. A schematic of the structure is shown in Figure 5. The composition would be $Y_2Ba_4Cu_8O_{20-x}$. Since neither our real space images nor our diffraction data are very sensitive toward oxygen concentrations, we are unable to comment at this time on the existence or non-existence of Cu-O chains in the either of the copper-oxygen layers. Some evidence for plane or chain structure might arise in the future from measured differences between a and b lattice parameters. We note that, in a study of the compound $SrCuO_2$ [23] where two CuO planes were found to exist between SrO layers, a chain structure in the layers was reported. An interpretation of transport properties however, as presented below, may argue against the existence of chains.

Based on the observation that Cu-O stacking faults exist as isolated entities as well as in ordered arrays, it is reasonable to conclude that a range of solid solutions exists between the limits of $YBa_2Cu_3O_{7-x}$ and $Y_2Ba_4Cu_8O_{20-x}$, at least in

metastable equilibrium. While such a metastable equilibrium might be restricted to materials in thin film form, it would be interesting to look for greater quantities of this phase in bulk materials.

B. Transport Properties

The question of oxygen stoichiometry and placement in $Y_2Ba_4Cu_8O_{20-x}$, which cannot yet be determined from our data, will certainly be important to the study of electronic transport properties. It might be expected that, if the ratio of extra oxygen atoms to extra copper atoms were greater than one to one, then the resulting material would be doped, i.e. it would have a greater concentration of holes. This might explain the observation of lower Hall constants in materials containing the second phase. Adding extra oxygens in this ratio to extra coppers, however, argues against the existence of Cu-O chains in the additional layers. Certainly we expect the chemical environment of the coppers to be different in this new material, where two CuO_x layers now exist side by side. The differences between $Y_2Ba_4Cu_8O_{20-x}$ and $YBa_2Cu_3O_{7-x}$ may allow for significant comparisons of transport properties in the CuO_x layers of different types.

V. Conclusions

Based on images as well as diffraction patterns we conclude that ordered arrays of stacking faults can form a distinct phase in the Y-Ba-Cu-O system near the $YBa_2Cu_3O_{7-x}$ composition. In many regions the ordering of the faults is nearly complete, giving unique electron diffraction symmetries. X-ray diffraction indicates that the new phase exists in volume fractions comparable to that of its parent: $YBa_2Cu_3O_{7-x}$. Both composition and diffraction information support a

model based on extra Cu-O planes, identified as $Y_2Ba_4Cu_8O_{20-x}$. The existence of the new phase may be associated with unusual transport properties in the films such as low normal state resistivities and higher carrier concentrations.

VI. Acknowledgments

The authors would like to thank Doug Keith and Bill Holmes for their help in the sputtering lab. We also thank Helen Kirby, Bob Smith, Rosemarie Koch and Kim Nelson for their help with x-ray diffraction and TEM sample preparation. Professors John Bravman, Malcolm Beasley, and Theodore Geballe provided support and a critical reading of the manuscript. One of us (A.K.) acknowledges an Alfred P. Sloan Fellowship. This work was supported by the NSF-MRL Program thruough the Center for Materials Research at Stanford University and by AFOSR under contract #F49620-88-C-0004.

REFERENCES

1. G. Wang, S.J. Hwu, S.N. Song, J.B. Ketterson, L.D. Marks, K.R. Poeppelmeier, and T.O. Mason, Adv. Ceram. Mater. **2**, 313 (1987).

2. K.G. Frase, E.G. Liniger, D.R. Clarke, J. Am. Ceramic Soc. **70**, C204 (1987).

3. J. Narayan, V.N. Shukla, S.J. Lukasiewicz, N. Biunno, R. Singh, A.F. Schreiner, and S.J. Pennycook, Appl. Phys. Lett. **51**, 940 (1987).

4. B. Domenges, M. Hervieu, C. Michel, and B. Raveau, Europhys. Lett. **4**, 211 (1987).

5. Abbas Ourmazd, J.A. Rentshler, J.C.H. Spence, M. O'Keeffe, R.J. Graham, D.W. Johnson Jr., and W.W. Rhodes, Nature **327**, 308 (1987).

6. X. Zeng, X. Jiang, H. Qi, D. Pang, N. Zhu, and Z. Zhang, Appl. Phys. Lett. **51**, 31 (1987).

7. M.M. Fang, V.G. Kogan, D.K. Finnemore, J.R. Clem, L.S. Chumbly, and D.E. Farrell, Phys. Rev. B, to be published.

8. H. W. Zandbergen, R. Gronsky and G. Thomas, Phys. Stat. Solidi, to be published.

9. Y. Matsui, E. Takayama-Muromachi, A. Ono, S. Horiuchi, and K. Kato, Japanese J. of Applied Physics **26**, L777 (1987)

10. D.J. Eaglesham, C.J. Humphreys, N. McN. Alford, W.J. Clegg, M.A. Harmer, and J.D. Birchall, Appl. Phys. Lett. **51**, 457 (1987).

11. M.P.A Viegers, D.M. deLeeuw, C.A.H.A. Mutsaers, H.A.M. van Hal, H.C.A. Smoorenburg, J.H.T. Hengst, J.W.C. deVries, and P.C. Zalm, J. Mater. Res. **2**, 743 (1987).

12. R. Beyers, G. Lim, E.M. Engler, V.Y. Lee, M.L. Ramirez, R.J. Savoy, R.D. Jacowitz, T.M. Shaw, K.G. Frase, E.G. Liniger, D.R. Clarke, S. LaPlaca, R. Boehme, C.C. Tsuei, S.I. Park, M.W. Shafer, W.J. Gallagher, and G.V. Chandrashenkhar, Proc. Materials Research Society, Anaheim, 1987, D.U. Gubser M. Schluter eds. (Materials Research Society, Pittsburgh, Pa, 1987).

13. B.G. Hyde, J.G. Thompson, R.L. Withers, J.G. Fitsgerald, A.M. StewartD.J.M. Bevan, J.S. Anderson, J. Bitmead and M.S. Paterson, Nature **327**, 402 (1987).

14. R.F. Cook, T.M. Shaw and P.R. Duncombe, Adv. Ceram. Mat. **2**, 606 (1987).

15. M. Sarikaya, B.L. Thiel, I.A. Aksay, W.J. Weber, and W.S. Frydrych, J. Mater. Res. **2**, 736 (1987).

16. S. Nakahara, G.J. Fisanick, M.F. Yan, R.B. van Dover, and T. Boone, J Crystal Growth, to be published.

17. B. Oh, M. Naito, S. Arnason, P. Rosenthal, R. Barton, M.R. Beasley, T.H. Geballe, R.H. Hammond, and A. Kapitulnik, Appl. Phys. Lett. **51**, 852 (1987).

18. K. Char, A.D. Kent, A Kapitulnik, M.R. Beasley, and T.H. Geballe, Appl. Phys. Lett. **51**, 1370 (1987).

19. E.A. Hewat, M. Dupuy, A. Bourret, J.J. Caponi, and M. Marezio, Nature **327**, 400 (1987).

20. M. Hervieu, B. Domenges, C. Michel, J. Provost, and B. Raveau, J. Sol. State Chem., to be published.

21. S. Uchida, H. Takagi, K. Kitazawa, and S. Tanaka, Jpn. J. Appl. Phys. **26**, L1 (1987).

22. C.L. Teske and H. Mueller-Buschbaum, Z. Anorg. Allg. Chem. **379**, 234 (1970).

23. H. Mueller-Buschbaum and H. Mattausch, Z. Anorg. Allg. Chem. **377**, 144 (1970).

Table I:

X-ray diffraction peaks of the new phase observed in sample A', indexed according to an A-centered unit cell (consistent with Figure 4). The refined cell parameters are: $a \cong b = 3.86$ +/- 0.02 Å and $c = 27.19$ +/- 0.07 Å. An independant x-ray determination of extinctions was not possible in this sample because of interference from peaks of the substrate and of the $YBa_2Cu_3O_{7-x}$.

hkl	d, exp. Å	Intensity
002	13.22	s
004	6.66	s
006	4.52	w
008	3.41	w
104	3.35	vs
106	2.90	s
0010	2.74	s
108	2.56	vs
0012	2.28	vs
0016	1.69	s
1113	1.66	w
1115	1.52	vs

FIGURE CAPTIONS:

Figure 1:
X-ray diffraction pattern of a "mixed phase" sample (sample A). The strongest peaks are due to $SrTiO_3$ (001) and (002), the others are due to 00l peaks of either the $YBa_2Cu_3O_{7-x}$ structure or the new phase. Peaks from the new phase are marked by asterisks and correspond to multiples of a 13.6 Å spacing.

Figure 2:
A-axis grains of $YBa_2Cu_3O_{7-x}$ (sample B) at 90 degrees to each other. Defect regions several hundred angstroms in width are observed along the (001) planes within the grains.

Figure 3:
A high resolution image of the grain in Figure 2 shows the normal $YBa_2Cu_3O_{7-x}$ structure on the left and the defect region on the right. The strong white fringes at 11.7 Å of the normal structure are the Cu-O planes between the Ba-O planes. These regions are expanded in the defect region indicating insertion of extra planes. Occasional "good" interfaces (arrows) also are seen in this region.

Figure 4:
Microdiffraction patterns from defect regions appearing within [100] (a and b) and [110] (c) $YBa_2Cu_3O_{7-x}$ grains. Figures a and b are from two different grains of Sample A, Figure c is from sample B. The symmetry shown in each pattern is distinct and yet related by epitaxy to that of the neighboring $YBa_2Cu_3O_{7-x}$ material. A consistent indexing of the spots can be obtained by assigning the zone axis of the patterns to [100], [010] and [110] respectively.

Figure 5:
Schematic structure of the new phase $Y_2Ba_4Cu_8O_{20-x}$ with space group Ammm. For reasons of clarity, oxygen atoms have been ommitted.

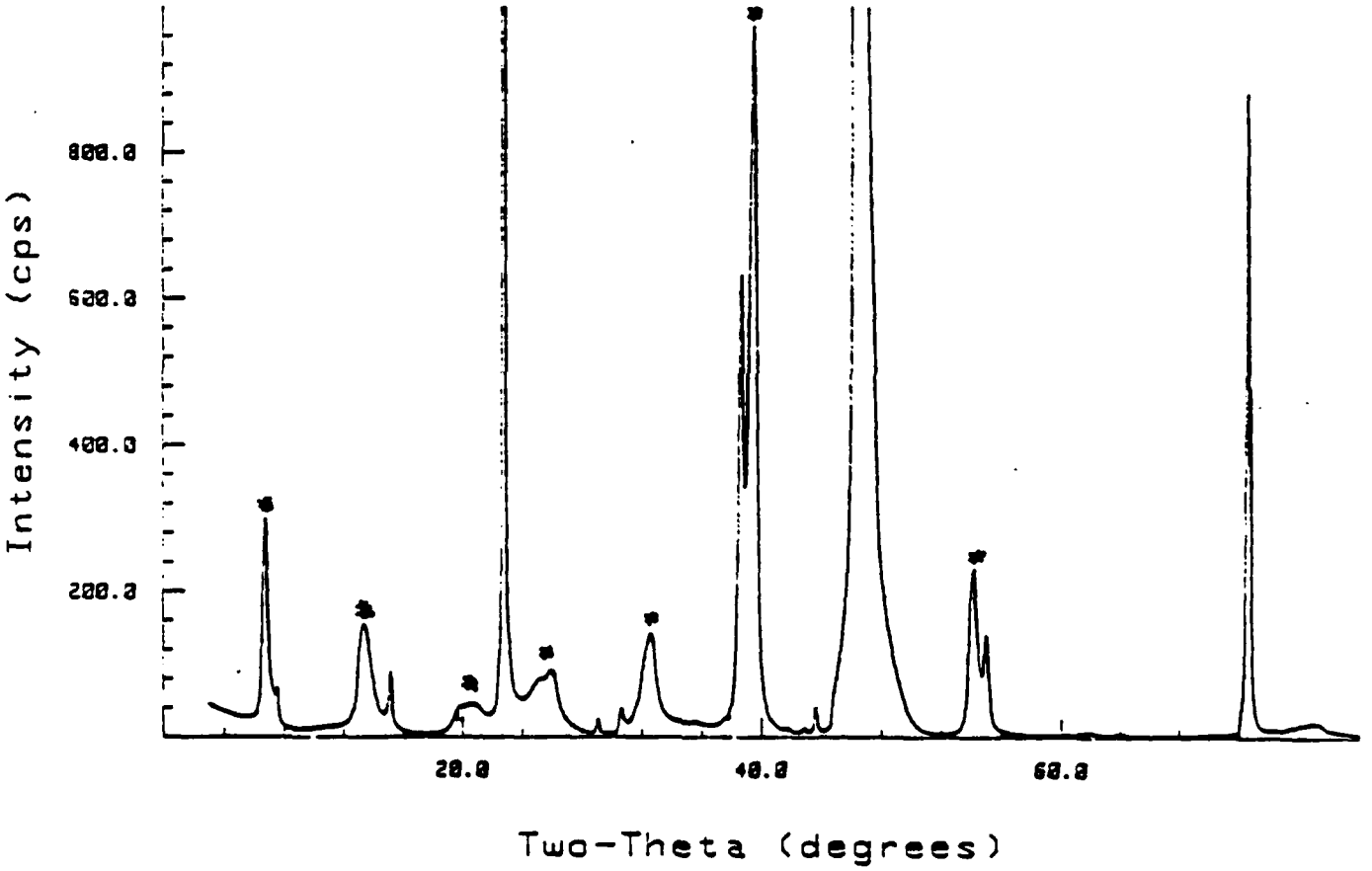
800.0
600.0
400.0
200.0
Intensity (cps)
20.0
40.0
60.0
Two-Theta (degrees)

Fig. 1


100 nm

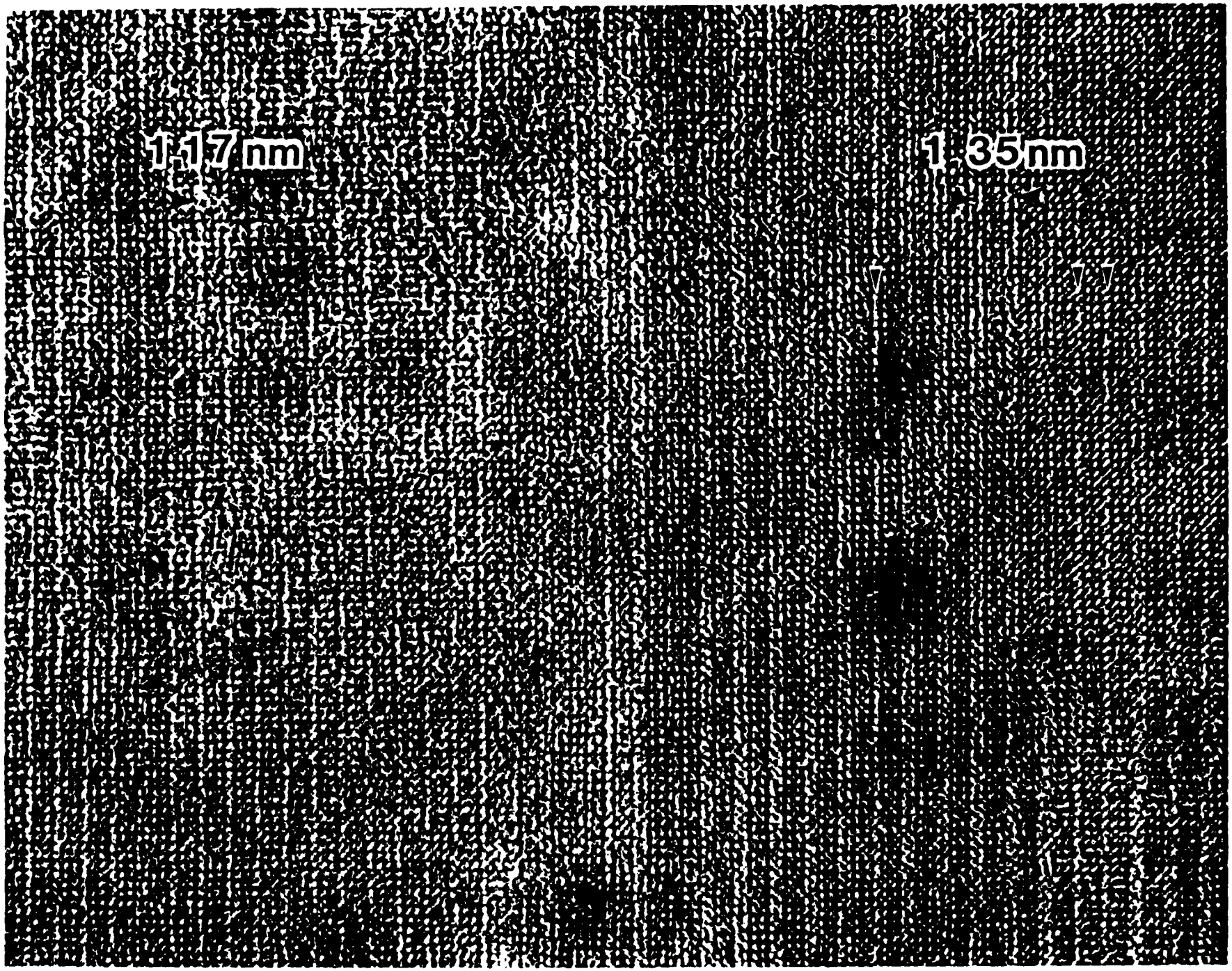
1.17 nm
1.35nm

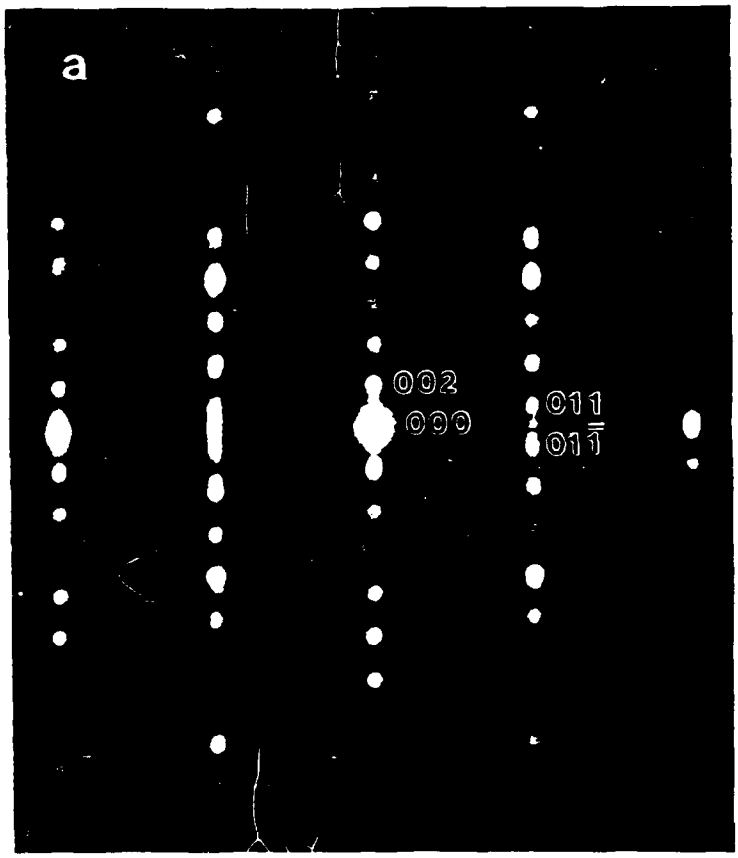
a
002
000
011
01$\bar{1}$

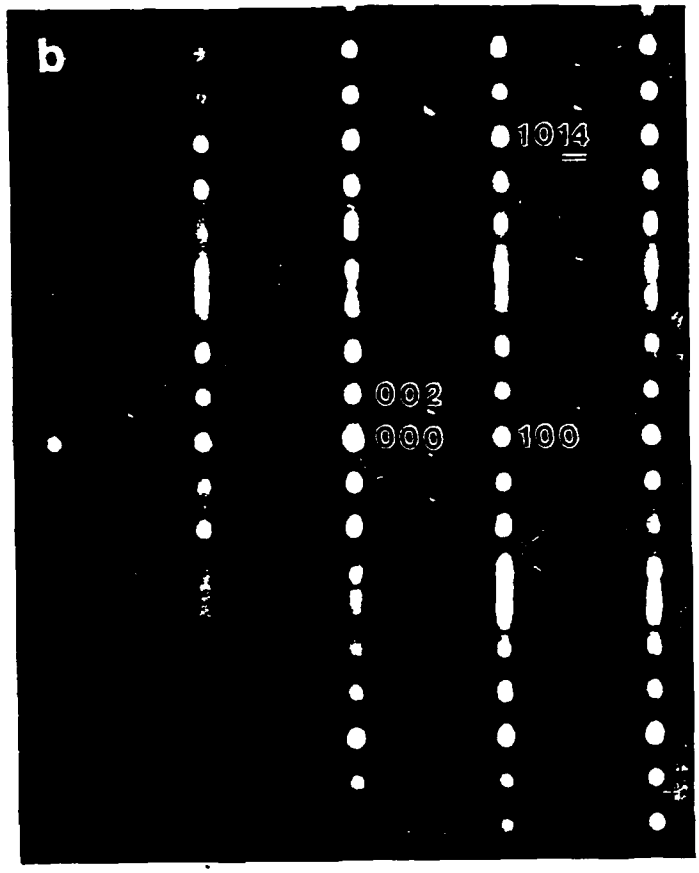
b
10$\bar{1}$4
002
000
100

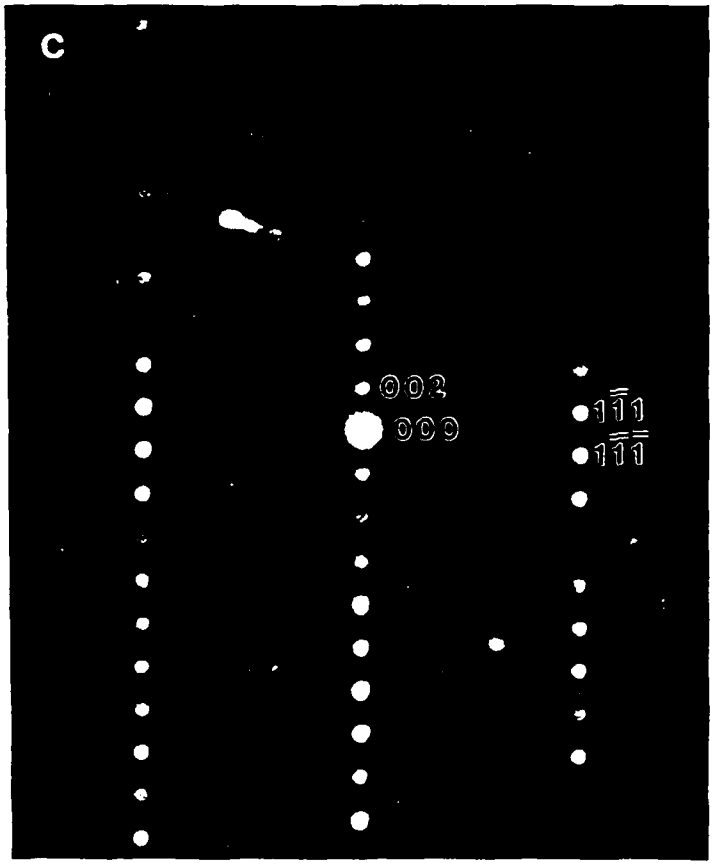
c
002
000
11$\bar{1}$1
111$\bar{1}$

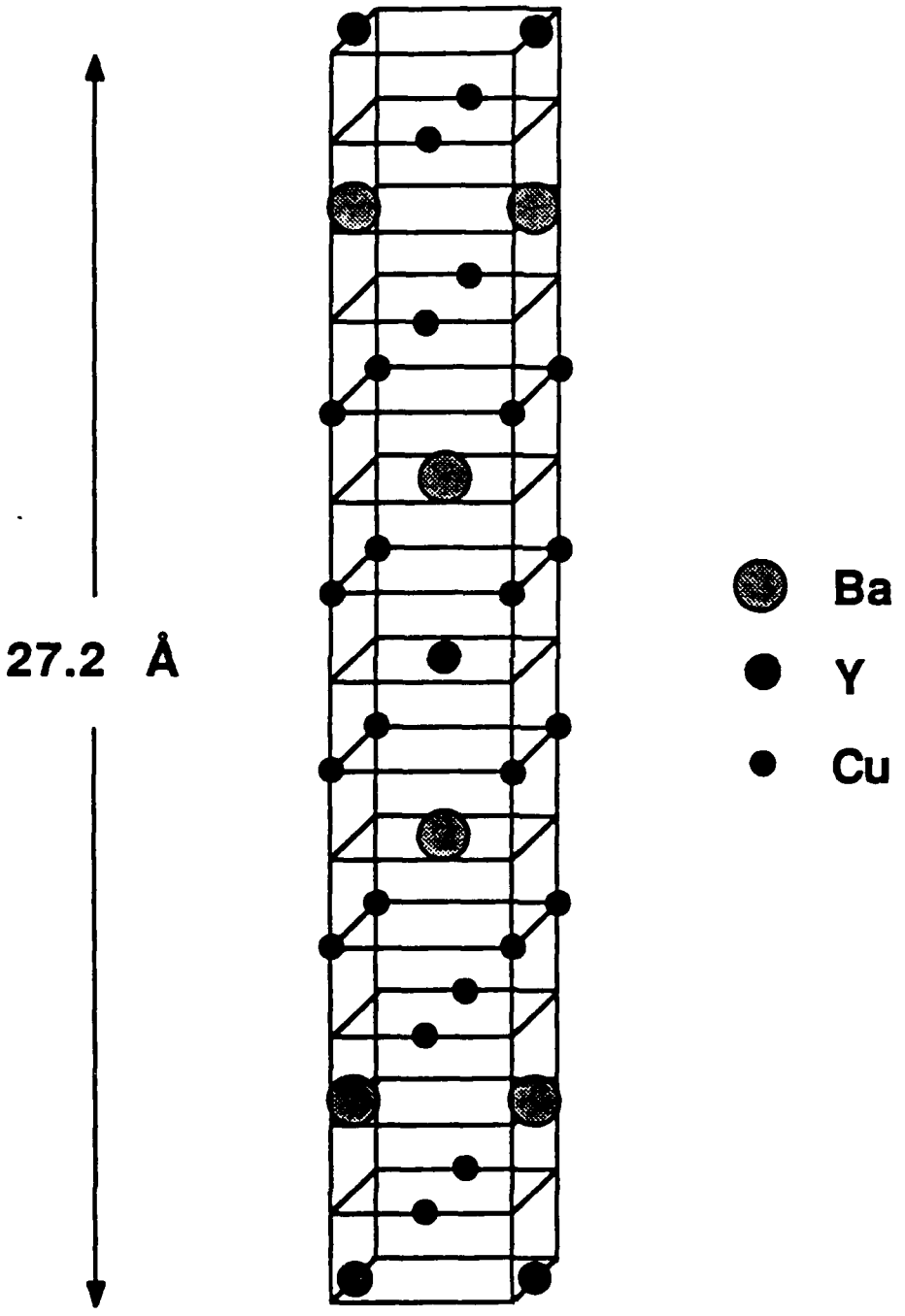
27.2 Å
Ba
Y
Cu

Submitted to Appl. Phys. Lett
3/8/88

Two-dimensional Superstructure in the A-B Plane of $Bi_2(Ca,Sr)_3Cu_2O_{8+\delta}$ Thin Films

A.F. Marshall, B. Oh, S. Spielman, Mark Lee, C.B. Eom, R.W. Barton, R.H. Hammond, A. Kapitulnik, M.R. Beasley and T.H. Geballe

Department of Applied Physics and Center for Materials Research
Stanford University
Stanford, CA 94305

Abstract

Thin films of Bi-Ca-Sr-Cu-O showing superconductivity above 100 K have been made by electron beam evaporation with post oxygen annealing. The major superconducting phase ($Bi_2[Ca,Sr]_3Cu_2O_{8+\delta}$, $T_c \sim 85$ K) is oriented epitaxially with the (100) $SrTiO_3$ substrate. In addition to the one dimensional incommensurate superstructure along the b-axis, which is characteristic of this phase, we have observed by transmission electron microscopy a two-dimensional incommensurate superstructure in the a-b plane with a differen periodicity and a different orientation relationship to the subcell.

Recently, Maeda et. al. [1] reported the existence of superconductivity above 100 degrees K in samples made from the Bi-Sr-Ca-Cu-O system. This work has been reproduced in other laboratories [2-5] and a superconducting phase at 85 K has been identified with the approximate composition $Bi_2(Sr,Ca)_3Cu_2O_{8+\delta}$, ("232"). Many groups have reported the existence of two superconducting phases based on observations of significant magnetic flux exclusions and sharp drops in resistivity at 110 K. To our knowledge, however, the 110 K phase has not been isolated. The composition and crystal structure differences between the 85 and 110 K phases are likely to be very subtle. For example, Tarascon et al [4] reported that while high temperature heat treatments on the "232" phase could enhance the magnitude of the 110 K transition, no significant changes in the x-ray diffraction patterns were observed.

This paper reports the succesful synthesis and initial structure-property analyses of Bi-Sr-Ca-Cu-O thin films. Transitions at both 110 K and 80 K have been observed, even in samples which appear from x-ray diffraction to be of a single "232" phase and of nearly a single epitaxial orientation. In a transmission electron microscope (TEM) study of the "232" phase from a multiphase sample, however, we have observed variations in superstructure order within the single parent phase. Large areas of the material show incommensurate order along the b-axis, as reported by Shaw et al [6]. In addition we observe a two-dimensional incommensurate

superstructure in the a-b plane with both a different periodicity and a different orientation relationship to the parent phase.

The films were deposited by electron beam co-evaporation with three metal sources: Bi, Cu and Ca/Sr onto (100) $SrTiO_3$ substrates. The substrate was held at ambient temperature during deposition. Initial depositions were made at a nominal composition 1:1:1:2 (Bi:Ca:Sr:Cu) resulting in multiphase films. Subsequent depositions near the 4:3:3:4 composition have produced almost single phase material with superconducting transitions similar to that of the multiphase film. During deposition oxygen gas was introduced through a stainless steel tube directed to the substrates; oxygen partial pressure was ~4×10^{-6} Torr. Samples with composition 1:1:1:2 were post-annealed at 650 C for 1 hr, 750 C for 1 hr and 850 C for 1 hr in sequence under oxygen flow; samples of composition 4:3:3:4 were post annealed at 850 C for 6 hrs under oxygen flow. The transition temperature seems not to depend on the cooling rate: samples quenched from high temperature give almost the same results as those cooled slowly.

X-ray diffraction of the films in both the normal (Bragg-Brentano) and asymetric geometries confirms the presence of the $Bi_2(Ca,Sr)_3Cu_2O_{8+\delta}$ phase ($a = b = 5.4$ Å, $c = 30.78$ Å). Samples made at the 4:3:3:4 composition show no evidence of second phases and only one peak ($d = 2.7$ Å) in the normal scan which cannot be indexed as either c-axis "232" or $SrTiO_3$. The

2.7 Å peak in this scan might represent an a-axis-normal orientation of the superconducting phase (index (200)); its intensity is less than 1% of the neighboring c-axis (00$\underline{10}$) peak. In off-stoichiometry films, including the 1:1:1:2 sample reported on below, we have observed three additional phases. Preliminary analyses using x-rays and electron microprobe indicate that these are: A) CuO, B) a plate-like epitaxial phase with c-axis diffraction at multiples of 12.26 Å (While containing all five elements, this phase is bismuth rich relative to "232" as was reported by (3)), and finally C) a randomly oriented needle-like phase with characteristic 6.50 Å spacing and approximate composition $(Ca,Sr)_{1.2}Cu_2O_x$.

The resistivity vs. temperature data for two samples with the 1:1:1:2 and 4:3:3:4 compositions are shown in Fig. 1. The resistivity was measured by the four-point probe method. Both films show a significant drop near 110 K and a sharp full transition at 75 K for the multiphase sample and 80 K for the single phase sample. In these films the grains are believed to extend through the thickness; this implies two-dimensional percolation and a suppression of the 110 K signal as compared with bulk samples [7]. While we have observed similar superconducting transitions in samples made from several different compositions, we have also noted that annealing temperatures of at least 850 C are necessary in order to produce a 110 K signal. Additionally, prolonged anneals at temperatures in excess of 880 C have been observed to result in a decomposition of the film (generally resulting in the three additional phases noted above). The observation of

both 80 and 110 K transitions in single phase films supports the proposition that the structures responsible for the two transitions are closely related.

TEM results presented here were obtained from film A of Figure 1. Analysis of the single phase films is currently being carried out. TEM shows that there is a significant amount of in-plane orientation of the "232" phase with the a and b axes of the structure aligned with the [110] directions of the substrate. Because our TEM specimens thus far have been planar sections we cannot directly image the layering along the c-axis. However, convergent beam patterns, which give access to the third dimension of reciprocal space, confirm that the layer periodicity is ~31 Å (Figure 2). We find that the superperiod along the b-axis is consistently shorter than the commensurate 27 Å spacing reported by some [2,3]. This incommensuration also occurs in bulk specimens made in our laboratories; the periodicity is of the same order as that reported by Shaw et al. [6], 25.8 Å, and has not been observed to vary significantly with composition or annealing treatment.

Analysis of the convergent beam pattern shown in Figure 2 indicates a point group mm2. This is based on rather subtle variations in the patterns of diffuse intensity in the non-zero order discs showing a single mirror rather than two perpendicular mirrors in the [001] projection. Others have suggested the point groups mmm [2,10], or 4mm or 4/mmm [4]. While these other point groups may be applicable to the subcell, our convergent

beam patterns may reflect the loss of a mirror plane due to the b-axis superstructure.

In additional to the one dimensional superstructure along the b-axis we have also observed a two-dimensional superstructure in the [001] orientation. The two types of patterns are compared in Figure 3, a and b. The two-dimensional superstructure exhibits a significantly larger periodicity, approximately 36 Å as compared with 26 Å in the one-dimensional b-axis ordering, and is rotated between four and five degrees with respect to the substructure. This results in a pattern with apparent four-fold symmetry but with a loss of mirror planes parallel to the four-fold axis. Convergent beam patterns show that the 30.7 Å periodicity along the c-axis remains; however, we have been unable to obtain convergent beam patterns of sufficient quality to determine if the structure is truly tetragonal. Regions of the film showing the two-dimensional superstructure have the same sublattice orientation as adjacent one-dimensional regions and there is no clear boundary between the two. However there are sometimes regions between the two that appear to be transitional as shown in Figure 3c. We have also observed the two-dimensional ordering at least once in bulk specimens showing superconductivity above 100 K. No obvious difference in composition was found between one and two dimensional regions using semi-quantitative x-ray microanalysis.

High-resolution images of the one and two dimensional superstructures in the a-b plane are shown in Figure 4. The superstructure fringes appear diffuse with no sharp boundaries; the rotation of the two-dimensional superstructure with respect to the 2.7 Å subcell fringes is evident in Fig. 4b. The true periodicity of the superstructure is twice that of the image. Shaw et al. [6] have shown that the b-axis ordering as seen in the [100] direction occurs along Bi_2O_2 layers and is "out-of-phase" in alternating Bi_2O_2 layers; this gives the appearance of one-half the period when viewed in the [001] direction.

The one and two dimensional superstructures in the a-b plane appear to be due to the same structural modulation both because of their similar diffraction and imaging characteristics, and because they occur intimately intermixed in the same "grain" of the subcell structure with no clear boundary between them. However, the nature of this modulation, even in the more commonly observed one-dimensional structure, has not yet been determined. The appearance of strong satellites about subcell reflections, the intensity of which falls off rapidly with distance from the subcell reflections, is characteristic of several types of modulated structures, including composition modulations (e.g. spinodals), periodic shear or antiphase boundary structures, and, in some cases, charge density waves [8]. The rotation of such superstructures with respect to the subcell has been observed in shear structures [8] and charge density waves [9]. The lack of sharply defined interfaces in the real space image suggests a compositional

modulation or charge density wave rather than a crystallographic shear or displacement. However, the discontinuity of the modulation along the c-axis and localized distortion of the superstructure as observed in the b-c plane by Shaw et al. [6] may allow for diffuse imaging of such a structure.

It will be a challenge to model the structural origin of various observed superstructures in $Bi_2(Ca,Sr)_3Cu_2O_{8+\delta}$,, and to establish their relationship, if any, to the existence of 110 K superconductivity. We are currently looking for correlations between the density of these phases and the existence of sharp resistivity drops at 110 K.

Acknowledgments:

The authors would like to thank Kim Nelson for TEM specimen preparation, Chris Zercher for microprobe analysis and Rosemarie Koch for optical microscopy. We would also like to acknowledge the Stanford/Varian MBE group, Eric Hellman, Darrell Schlom and Jim Eckstein, for sharing with u analysis of their Bi-Ca-Sr-Cu-O thin films. One A.K. acknowledges an Alfred P. Sloan Fellowship. This work was supported by the NSF-MRL Program through the Center for Materials Research at Stanford University and by AFOSR under contract #F49620-88-C-0004.

References:

1) H. Maeda, Y. Tanaka, M. Fukutomi and T. Asano, to be published, Jpn. J. Appl. Phys. Lett., **27** (1988).

2) M.A. Subramanian,j C.C. Torardi, J.C. Calabrese, J. Gopalakrishnan, K.J. Morrissey, T.R. Askew, R.B. Flippen, U. Chowdhry and A.W. Sleight, Science, in press.

3) R.M. Hazen, C.T. Prewitt, R.J. Angel, N.L. Ross, L.W. Finger, C.G. Hadidiacos, D.R. Veblen, P.J. Heaney, P.H. Hor, R.L. Meng, Y.Y. Sun, Y.Q. Wang, Y.Y. Xue, Z.J. Huang, L. Gao, J. Bechtold and C.W. Chu, Phys. Rev. Lett., submitted, (1988).

4) J. M. Tarascon, Y. Le Page, P. Barboux, B.G. Bagley, L.H. Greene, W.R. McKinnon, *G. W. Hull, M. Giroud and D.M. Hwang, preprint* (1988).

5) S.A. Sunshine, T. Siegrist, L.F. Schneemeyer, D.W. Murphy, R.J. Cava, B. Batlogg, R.B. van Dover, R.M. Fleming, S.H. Glarum, S. Nakahara, R. Farrow, J.J. Krajewski, S.M. Zahurak, J.V. Waszczak, J.H. Marshall, P. Marsh, L.W. Rupp, Jr. and W.F. Peck, preprint (1988).

6) T.M. Shaw, S.A. Shivashankar, S.J. LaPlaca, J.J. Cuomo, T.R. McGuire, R. A. Roy, K.H. Kelleher and D.S. Yee, preprint (1988).

7) Recall that, for zero resistance in 3-dimensional percolation, only 15% of the appropriate phase is required, while in two dimensions 50 % would be required.

8) See, for example, the review article by S. Amelinckx in "Modulated Structures -- 1979", J.M. Cowley et al., editors, AIP Conference Proceedings No. 53, p. 102 (1979).

9) J.A.Wilson, F.J. Di Salvo and S. Mahajan, Phys. Rev. Lett. 32, 882 (1974).

10) D.R. Veblen, P.J. Heaney, R.J. Angel, L.W. Finger, R.M. Hazen, C.T. Prewitt, N.L. Ross, C.W. Chu, P.H. Hor and R.L. Mang, Nature, submitted (1988).

Figure Captions:

1) Resistivity vs. temperature for two films of nominal composition 1:1:1:2 (A) and 4:3:3:4 (B). Both show a drop in resistivity of similar magnitude at 110 K and zero resistance at 75 K (A) and 80 K (B).

2) Convergent beam diffraction pattern of the "232" structure in the [001] orientation. The first Laue ring (arrow) corresponds to a periodicity along the c-axis of ~31 Å. The symmetry of the center disc and of the whole pattern are observed to be 2mm and m (marked) respectively. This corresponds to a point group 2mm.

3) Microdiffraction patterns of the "232" phase in the [001] orientation showing a) one dimensional ordering along the b-axis, b) two dimensional ordering in the a-b plane which is rotated with respect to the subcell by approximately five degrees and c) a transitional region between the two.

4) High resolution images of the (a) one and (b) two dimensional superstructures in the a-b plane of the "232" structure. The periodicity observed is half that of the true superstructure (see text). The rotation of the 18 Å fringes with respect to the 2.7 Å fringes of Figure 4b can be clearly seen by sighting along the fringes close to the plane of the page.

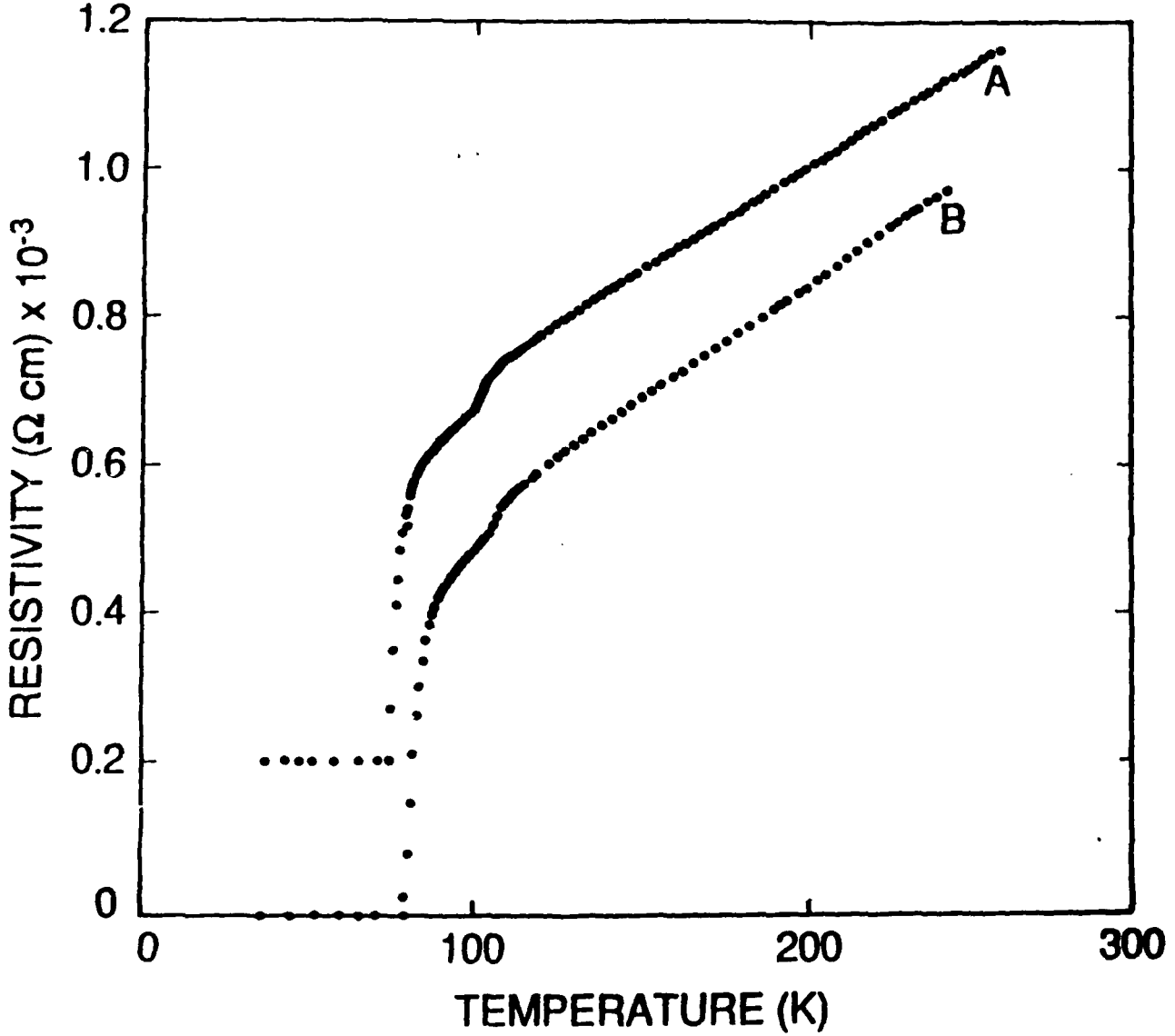
1.2
1.0
0.8
0.6
0.4
0.2
0
RESISTIVITY (Ω cm) x 10-3
A
B
0
100
200
300
TEMPERATURE (K)

5793-2

Fig 2

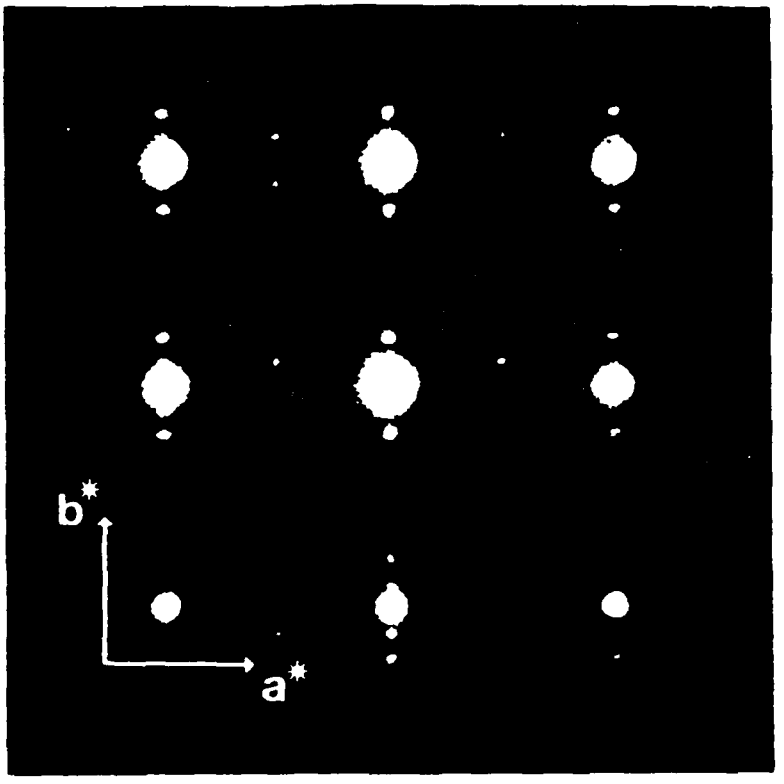
b*
a*

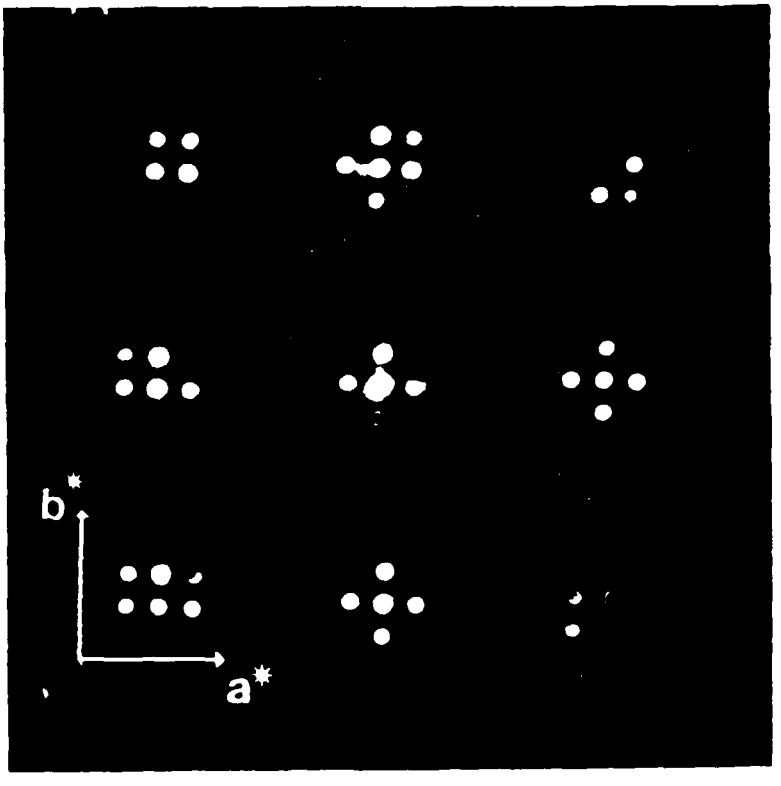
b*
a*

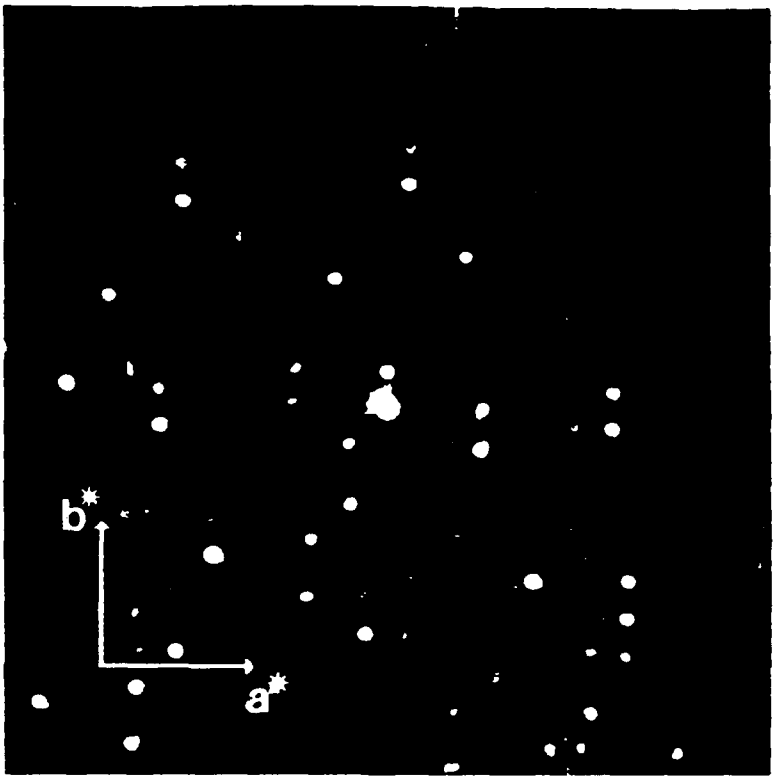

3c

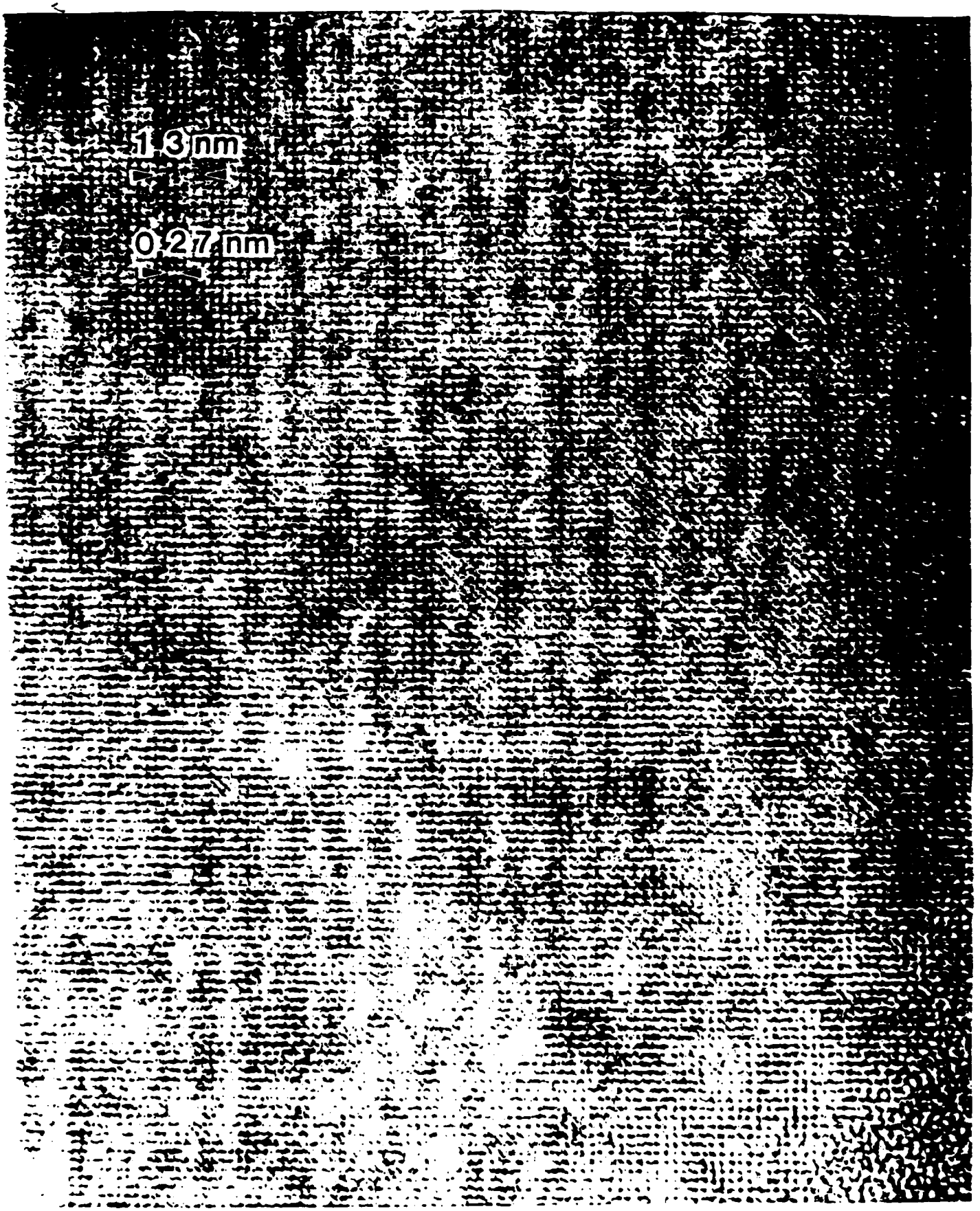
1.3 nm
0.27 nm

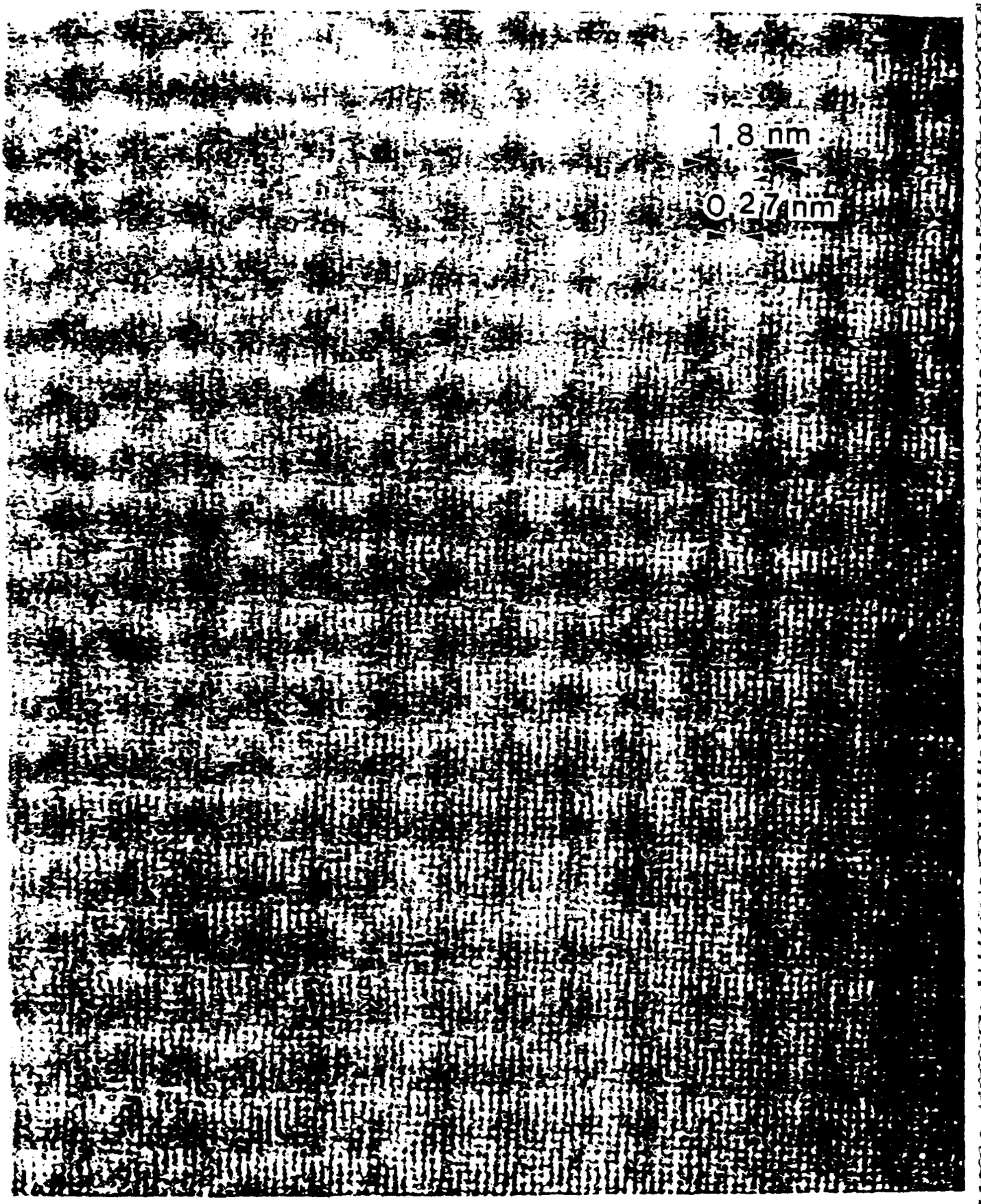
1.8 nm
0.27 nm

PHYSICAL REVIEW B VOLUME 38, NUMBER 1 1 JULY 1988

Properties of Y-Ba-Cu-O thin films with ordered defect structure: $Y_2Ba_4Cu_8O_{20-x}$

K. Char, Mark Lee, R. W. Barton, A. F. Marshall, I. Bozovic, R. H. Hammond, M. R. Beasley, T. H. Geballe, and A. Kapitulnik

Department of Applied Physics, Stanford University, Stanford, California 94305

S. S. Laderman

Circuit Technology R&D, Hewlett Packard Company, 3500 Deer Creek Road, Palo Alto, California 94304

(Received 26 February 1988)

Properties of both unfaulted and faulted *c*-axis-oriented $Y_2Ba_4Cu_8O_{20-x}$ thin films are reported. Their superconducting transition temperatures are 81 and 93 K, respectively. This implies that the precise ordering of copper-oxygen layers in $YBa_2Cu_3O_{7-x}$ is not crucial for the high T_c. $Y_2Ba_4Cu_8O_{20-x}$ exhibits lower resistivity and lower Hall coefficient than $YBa_2Cu_3O_{7-x}$. The extra copper-oxygen layers seem to play an important role in the normal state.

Recently, we presented an analysis, using both x-ray and electron diffraction, of an ordered defect structure in epitaxial films of Y-Ba-Cu-O.[1] We determined that significant volume fractions of a film could be characterized by a *c*-axis parameter which is expanded by the width of one atomic layer from the normal $YBa_2Cu_3O_{7-x}$ (1:2:3) structure.[2] Using a model originally proposed by Zandbergen *et al.*[3] for isolated defects in bulk materials, we proposed the existence of an ordered defect structure in which an extra copper-oxygen layer appears in every unit cell of the parent 1:2:3 material (see the inset in Fig. 1). The composition of this structure would be $Y_2Ba_4Cu_8O_{20-x}$ (2:4:8). In this paper, we report additional evidence for the 2:4:8 model as well as the synthesis of films in which the new material appears as nearly a single phase with a high degree of ordering perfection. Upon changes in growth and postannealing conditions, samples could be made either as 1:2:3, or 2:4:8, or more commonly, as faulted structures that mix the two. We report normal-state and superconducting properties for the new phase as well as its structurally faulted variations. We find that the new phase is characterized by significant changes in the normal-state transport properties when compared to the 1:2:3 compound, while its critical temperature is decreased by only 10 K. Our interpretations of the observed properties are discussed in terms of the proposed 2:4:8 structure.

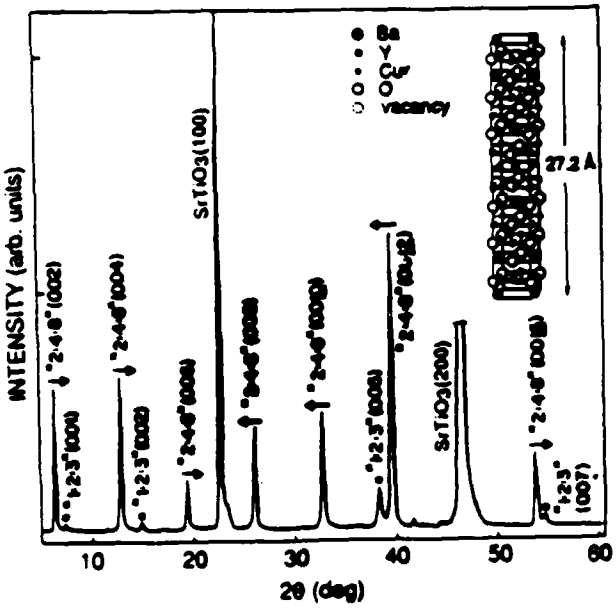

FIG. 1. X-ray diffraction data of a *c*-axis-oriented 2:4:8 sample. Peaks marked with an asterisk belong to the 1:2:3 phase of the sample. Each arrow on the 2:4:8 peaks denotes the direction it moves when the stacking faults appear. Inset shows a unit cell of 2:4:8 structure.

Samples were prepared by both electron-beam evaporation and reactive magnetron sputtering. Detailed descriptions of the deposition techniques were published elsewhere.[4,5] BaF_2 was used as the Ba source in the evaporation,[6] and a Ba metal target was used in the sputtering. Microprobe analysis showed no fluorine in the samples made with BaF_2 after a wet O_2 anneal. In order to achieve the well-ordered new phase, the films had to be rich in Cu with slightly Y-rich composition ($Y_{15}Ba_{28}Cu_{57}$) according to the microprobe. Films made with Ba metal have properties consistent with those of films made with BaF_2. For transport measurements, samples were patterned into 0.4-mm-wide and 2-mm-long strips by regular photolithographic techniques. Low-resistance contacts were made using silver evaporated on the pads. The x-ray diffraction data in this paper were obtained using a four-circle x-ray diffractometer in a symmetrical scattering geometry (diffraction vectors normal to the film). Despite a clear interest in determining oxygen concentrations in the new structure, we have not yet found a reliable analytical method which is applicable to thin films.

Figure 1 shows x-ray diffraction data of an oriented 2:4:8 sample (curve A in Fig. 3) with *c* axis perpendicular to the $SrTiO_3$ (100) substrate. As indicated in the figure, each major peak can be assigned to either the substrate, *c*-axis-oriented 1:2:3, or *c*-axis-oriented phase having a

lattice parameter of 27.19 Å with odd-order reflections missing. We note that, relative to a film made up almost entirely of 1:2:3, the intensity of the 1:2:3 is about 8%. Furthermore, each peak of the 27.19 Å phase is sharp and falls at a scattering vector whose magnitude is an integer multiple of $2\pi/27.19$ Å^{-1} within our experimental precision of ± 0.003 Å^{-1}. For the remainder of this paper, we refer to samples which satisfy this criterion as "well ordered" or "unfaulted," in contrast to the "faulted" structure described next.

As reported earlier,[1] we also observed diffraction patterns having broad peaks close to, but not precisely aligned with, the well-ordered positions. Figure 2 shows diffraction and resistivity data for (a) a well-ordered sample and (b) the same sample after further annealing. After a further anneal the peaks shifted. We interpret these results to imply that the well-ordered structure is not stable at higher temperatures. This may be a reason why our films made with BaF_2 have a more well-ordered material since they were annealed at lower temperatures and for less time. We believe that the peak shifts are due to layering disorder in the structure. Support for this interpretation is found by considering the diffraction patterns expected for layered structures with random faults.[7] As random faults are introduced, diffraction peaks broaden and shift. The magnitude and direction of the shift depend on the details of the model. A simple relevant model is the case of stacking monoatomic layers with two possible interlayer distances: 11.7 and 13.6 Å. These spacings reproduce the observed sets of well-ordered peak positions. Taking the 13.6 Å spacing as the norm and introducing 11.7 Å spacings as faults, the peak shifts are found to oscillate with scattering angle with the same direction as our observations. The amplitude of the shifts increase with an increasing density of faults. These considerations lead us to refer to material showing such oscillatory peak shifts as "faulted." More complete calculations taking into account the multicomponent nature of our films are underway. We have also found that upon further anneal, a Bragg peak at $2\theta = 35.5$ appears, which we attribute to CuO. Note that there is a clear change in its superconducting transition temperature, associated with the structural change (see the insets in Fig. 2).

Resistivity versus temperature data for the unfaulted 2:4:8 sample (curve A) are shown in Fig. 3 along with a 1:2:3 phase (curve B),[8] a faulted 2:4:8 phase (curve C) and a 1:2:3/2:4:8 mixed but unfaulted phase sample (curve D). There are three points to note. (1) The transition temperature of the unfaulted 2:4:8 phase is about 10 K lower than the 91 K normally seen in the 1:2:3 structure. (2) The 2:4:8 phase has a lower resistivity: 150 $\mu\Omega$ cm at 300 K and 30 $\mu\Omega$ cm at 100 K compared with 300 $\mu\Omega$ cm at 300 K and 100 $\mu\Omega$ cm at 100 K for the 1:2:3 phase. (3) The resistivity of the 2:4:8 sample extrapolates to zero around 55 K while the resistivity of the 1:2:3 extrapolates to zero at (or slightly above) 0 K. This intriguing point is discussed below. Some samples with faulted 2:4:8 structure have been observed with onset temperatures as high as 96 K and zero-resistance temperatures as high as 93 K. These values are repeatedly about 3–4 K higher than those of our well-ordered 1:2:3 samples made under the same conditions. Whether this higher T_c is just a sample to sample variation or a special property of this faulted 2:4:8 structure (e.g., due to strain or doping of the 1:2:3 structure produced by the stacking faults or some kind of superstacking) is yet to be clarified. The sample with unfaulted 2:4:8 and 1:2:3 phases (curve D) that are presumably mixed on a macroscopic scale clearly has one transition at 90 K and another transition at 81 K

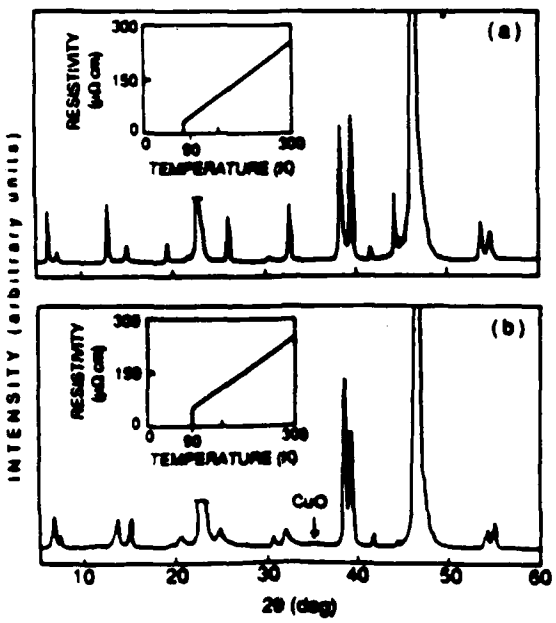

FIG. 2. X-ray diffraction data of a c-axis-oriented 2:4:8/1:2:3 mixed but unfaulted sample (a), and the same sample after high-temperature annealing (b). The shifts of the peaks are consistent with random 2:4:8 stacking faults. Inset shows the resistivity vs temperature data.

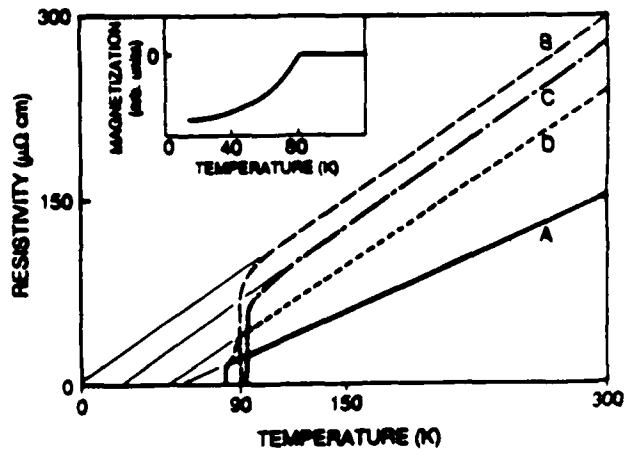

FIG. 3. Resistivity vs temperature data of a c-axis-oriented unfaulted 2:4:8 sample (curve A), a typical c-axis-oriented 1:2:3 sample (curve B), a c-axis-oriented faulted 2:4:8 sample (curve C), and a 1:2:3/2:4:8 mixed but unfaulted sample (curve D). Inset shows magnetization vs temperature data of a c-axis-oriented unfaulted 2:4:8 sample.

corresponding to the 1:2:3 transition and the 2:4:8 transition, respectively.

In order to establish further that the change in T_c is due to the 2:4:8 phase, magnetization versus temperature data taken while heating an unfaulted 2:4:8 sample in a perpendicular field of 100 G are shown in the inset in Fig. 3. The sharp transition temperature at 81 K is in excellent agreement with the resistivity measurement. The critical current density J_c determined from the magnetic hysteresis loop is about 4×10^6 A/cm^2 in 3 kG at 4.2 K and 1×10^6 A/cm^2 in 3 kG at 60 K. These values are comparable to those of good c-axis-oriented epitaxial 1:2:3 films.[5,9]

In Fig. 4, we show that the Hall coefficient data R_H for this unfaulted 2:4:8 sample (curve A) are smaller than those of the 1:2:3 material (curve B),[10] implying higher carrier density, at least within the framework of a simple single-band theory. The 1:2:3/2:4:8 mixed sample (curve C) with stacking faults has the Hall coefficient value in between those of the 1:2:3 sample and the unfaulted 2:4:8 sample. The linear temperature dependence of $1/R_H$ of the unfaulted 1:2:3 phase takes on more curvature as the new stacking sequence appears as seen in Fig. 2. The unfaulted 2:4:8 case displays more complex behavior in this temperature range. It is interesting to note that the temperature at which the inverse Hall coefficient for the unfaulted 2:4:8 phase extrapolates to zero coincides with the temperature at which the resistivity extrapolates to zero. All the samples showed hole-type Hall effects. Finally, we have made preliminary ir reflectance measurements on the unfaulted 2:4:8 material. The results show behavior similar to the 1:2:3 material but with a generally higher reflectance, consistent with the higher carrier density.

We will now interpret these data in terms of the proposed 2:4:8 structure. The fact that the T_c of the unfaulted 2:4:8 sample is only slightly lower than that of a good 1:2:3 sample indicates that high-T_c superconductivity does not depend on the precise ordering of the copper-oxygen layers in the 1:2:3 structure. Furthermore, if 2:4:8 has a different Cu–O chain configuration from 1:2:3, this would imply that the Cu–O chains are not crucial for high T_c, in contrast to models[11] which assign the Cu–O chains a crucial role in the superconducting mechanism of the high T_c. A possible role of these layers is to couple together the two adjacent Cu–O_2 planes; thus, by adding another copper-oxygen layer between the Cu–O_2 planes, the coupling between the Cu–O_2 planes becomes weaker, resulting in a slightly lower T_c. Another possible role of the copper-oxygen layers between the Ba–O layers is to dope the system with carriers.

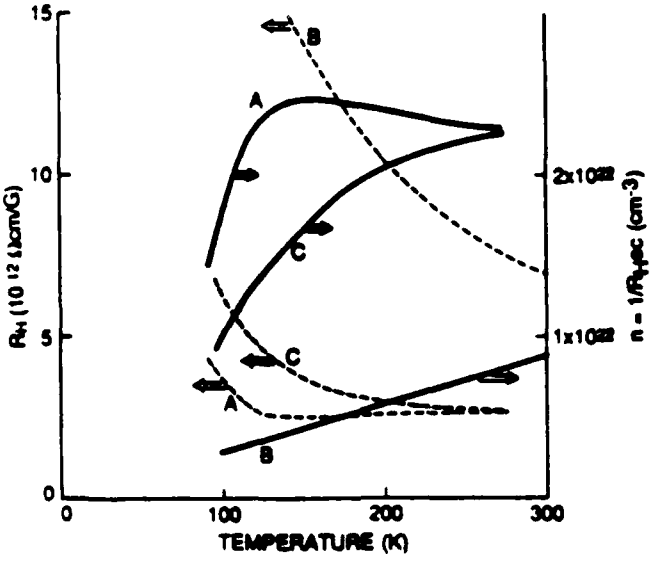

FIG. 4. Hall coefficients R_H and $n=1/R_H ec$ of a c-axis-oriented unfaulted 2:4:8 sample (curve A), a typical c-axis-oriented 1:2:3 sample (curve B), and a c-axis-oriented faulted 2:4:8 sample (curve C).

While the effect of the extra copper-oxygen layer on T_c is relatively small, the effect on the normal-state properties is significant. For example, even though both the 1:2:3 and the 2:4:8 materials show a linear temperature dependence of the resistivity, the absolute value of the resistivity of 2:4:8 is lower than 1:2:3 and its extrapolates to zero at 55 K whereas the 1:2:3 material extrapolates to zero near 0 K. The lower resistivity might originate from the higher carrier density in 2:4:8 material. However, the extrapolation to zero resistivity at 55 K, which we have not seen in any of our other materials, presents a more difficult problem. One possible explanation is that there exists a scattering mechanism in these materials with a characteristic temperature higher than room temperature such that, in the temperature range over which we have been measuring, the temperature dependence of the resistivity is actually a linear approximation to an underlying nonlinear dependence. If this is true, it follows that the apparent linear temperature dependence in these materials is an artifact (similar to the Gruneisen-Bloch formula[12] for pure metals). However, this interpretation requires that the residual resistivity of the 1:2:3 material be much greater than that of the 2:4:8. Finally, the temperature dependence of $1/R_H$ for the 2:4:8 phase is different from that of 1:2:3. The former is not monotonically decreasing and the latter is. Metals that can be described by single-band theory have temperature-independent Hall coefficient. Evidently, a single-band theory is inadequate and two or more bands would be necessary to adequately account for both the anomalous Hall coefficient and resistivity in a single-electron picture.

In summary, we have found additional evidence that stacking faults in the form of extra copper-oxygen layers can be ordered to form a new phase, the 2:4:8 phase. While the unfaulted 2:4:8 phase has T_c of 81 K, faulted 2:4:8 phase can have T_c as high as 96 K, higher than normally seen in good 1:2:3 films. The small change in T_c implies that the precise ordering of copper-oxygen layers in 1:2:3 is not crucial for the high T_c. The normal-state properties of 2:4:8 phase differ significantly from those of the 1:2:3 phase: the 2:4:8 phase has lower resistivity, which extrapolates to zero at temperature of 55 K; its Hall coefficient is smaller and it has a different temperature dependence from that of 1:2:3 phase. The extra copper-oxygen layers seem to play an important role in the normal state.

Part of this work was motivated by some early results on BaF_2 source films made by Dr. O. Asada and Dr. M. Naito. We would also like to thank Professor W. A. Harrison for some useful discussions and S. R. Spielman for help with the evaporation synthesis. Finally, one of us (M.L.) would like to acknowledge financial support from the National Science Foundation (NSF) and A. K. would like to acknowledge support from the Alfred P. Sloan Foundation and the NSF. This work was supported in part by the U.S. Air Force Office of Scientific Research under Grant No. F49620-83-C-0014 and by the Stanford Center for Materials Research under the NSF/MRL program.

[1]A. F. Marshall *et al.*, Phys. Rev. B 37, 9353 (1988).
[2]M. K. Wu *et al.*, Phys. Rev. Lett. 58, 908 (1987).
[3]H. W. Zandbergen *et al.*, Phys. Status Solidi A 105, 207 (1988); H. W. Zandbergen *et al.*, Nature 331, 596 (1988).
[4]M. Naito *et al.*, J. Mater. Res. 27, 713 (1987).
[5]K. Char *et al.*, Appl. Phys. Lett. 51, 1370 (1987).
[6]P. M. Mankiewich *et al.*, Appl. Phys. Lett. 51, 1753 (1987).
[7]S. Hendricks and E. Teller, J. Chem. Phys. 10, 147 (1942); P. J. Mering, Acta Crystallogr. 2, 371 (1949).
[8]S. W. Tozer *et al.*, Phys. Rev. Lett. 59, 1768 (1987); K. Char *et al.* (unpublished). (The 1:2:3 sample was annealed under the same conditions as the 2:4:8 sample.)
[9]P. Chaudhari *et al.*, Phys. Rev. Lett. 58, 2684 (1987); B. Oh *et al.*, Appl. Phys. Lett. 51, 852 (1987).
[10]T. Penney (private communication); K. Char *et al.* (unpublished).
[11]W. W. Warren, Jr. *et al.*, Phys. Rev. Lett. 59, 1860 (1987); J. M. Tarascon *et al.*, Phys. Rev. B 36, 226 (1987); J. D. Jorgensen *et al.*, *ibid.* 36, 3608 (1987).
[12]J. M. Ziman, *Electrons and Phonons* (Oxford Univ. Press, London, 1962), p. 322.

L. Nieto, J. Herranz, M. Rico, J. Santoro, *FEBS Lett.* **221**, 320 (1987).
6. K. R. Shoemaker, P. S. Kim, E. J. York, J. M. Stewart, R. L. Baldwin, *Nature* **326**, 563 (1987).
7. G. E. Schulz and R. H. Schirmer, *Principles of Protein Structure* (Springer, New York, 1979).
8. J. A. Schellman, *Compt. Rend. Trav. Lab. Carlsberg (Ser. Chim.)* **29**, 230 (1955).
9. B. K. Lee and F. M. Richards, *J. Mol. Biol.* **55**, 379 (1971); C. Chothia, *ibid.* **105**, 1 (1976).
10. W. F. DeGrado, F. J. Kezdy, E. T. Kaiser, *J. Am. Chem. Soc.* **103**, 679 (1981); D. Eisenberg, R. M. Weiss, T. C. Terwilliger, *Nature* **299**, 371 (1982).
11. P. Y. Chou and G. D. Fasman, *Biochemistry* **13**, 211 (1974); D. E. Blagdon and M. Goodman, *Biopolymers* **14**, 241 (1975).
12. W. Kabsch and C. Sander, *Proc. Natl. Acad. Sci. U.S.A.* **81**, 1075 (1984).
13. F. C. Bernstein *et al.*, *J. Mol. Biol.* **112**, 535 (1977).
14. E. N. Baker and R. E. Hubbard, *Prog. Biophys. Mol. Biol.* **44**, 97 (1984).
15. R. Taylor and O. Kennard, *Acc. Chem. Res.* **17**, 320 (1984); A. Vedani and J. D. Dunitz, *J. Am. Chem. Soc.* **107**, 7653 (1985).
16. H. A. Scheraga, Quantum Chemistry Program Exchange, Program No. 286, Indiana University Chemistry Department, Bloomington (1975).
17. R. Srinivasan and K. K. Chacko, *Conformation of Biopolymers*, G. N. Ramachandran, Ed. (Academic Press, New York, 1967).
18. G. N. Ramachandran and V. Sasisekharan, *Adv. Prot. Chem.* **23**, 283 (1968).
19. J. Moult and M. N. G. James, *Proteins* **1**, 146 (1986).
20. M. Levitt and C. Chothia, *Nature* **261**, 552 (1976).
21. A. A. Kossiakoff, *Science* **240**, 191 (1988). Kossiakoff suggests that protein deamidation sites involve Asn-Ser sequences in which the Asn makes a hydrogen bond to the backbone at position $i + 2$ while the Ser hydroxyl makes a hydrogen bond to the Asn side chain. It is conceivable that the amino acid at CPA 101 was originally an Asn that became deamidated prior to sequence determination. If so, the one exceptional helix boundary lacking CTB, namely CPA[100], would then have a CTB.
22. C. Schellman, *Protein Folding*, R. Jaenicke, Ed. (Elsevier/North-Holland Biomedical Press, Amsterdam, 1980), p. 53.
23. P. Y. Chou and G. D. Fasman, *Annu. Rev. Biochem.* **47**, 251 (1978).
24. S. Wada, *Adv. Biophys.* **9**, 1 (1976); W. G. J. Hol, *Prog. Biophys. Mol. Biol.* **45**, 149 (1985).
25. L. G. Presta and G. D. Rose, unpublished results.
26. J. S. Richardson and D. C. Richardson, *Science* **240**, 1648 (1988).
27. R. F. Doolittle, *Of Urfs and Orfs* (University Science Books, Mill Valley, CA, 1987).
28. D. Bashford, C. Chothia, A. M. Lesk, *J. Mol. Biol.* **196**, 199 (1987).
29. J. Deisenhofer, O. Epp, K. Miki, R. Huber, H. Michel, *Nature* **318**, 618 (1985).
30. W. A. Hendrickson and M. M. Teeter, *ibid.* **290**, 107 (1981).
31. D. M. Engelman, T. A. Steitz, A. Goldman, *Annu. Rev. Biophys. Biophys. Chem.* **15**, 321 (1986).
32. M. S. Briggs and L. M. Gierasch, *Adv. Prot. Chem.* **38**, 109 (1986).
33. F. A. Quiocho, J. S. Sack, N. K. Vyas, *Nature* **329**, 561 (1987).
34. S. C. Harrison and E. R. Blout, *J. Biol. Chem.* **240**, 299 (1965); J. T. J. Lecomte and G. N. LaMar, *J. Am. Chem. Soc.* **109**, 7219 (1987).
35. D. L. Oxender and C. F. Fox, Eds., *Protein Engineering* (Liss, New York, 1987).
36. P. S. Kim and R. L. Baldwin, *Annu. Rev. Biochem.* **51**, 459 (1982).
37. R. L. Baldwin, *Trends Biochem. Sci.* **11**, 6 (1986).
38. Single letter abbreviations for the amino acid residues are: A, Ala; C, Cys; D, Asp; E, Glu; F, Phe; G, Gly; H, His; I, Ile; K, Lys; L, Leu; M, Met; N, Asn; P, Pro; Q, Gln; R, Arg; S, Ser; T, Thr; V, Val; W, Trp; Y, Tyr.
39. We thank R. Baldwin, P. Kim, S. Taylor, and C. R. Matthews for many useful discussions; B. Zimm and J. Lecomte for their critical reading of the manuscript; an anonymous referee for helpful suggestions, and E. Lattman for insightful comments at every stage of this work. Thirteen years ago, Kensal Van Holde urged that the key question is not which sequences will be found in helices, but rather why all sequences are not found in helices. Good questions, like good teachers, leave a lasting imprint. Supported by NIH grants GM 29458 and AG 06084 and by a Dean's grant from John Burnside.

25 February 1988; accepted 28 April 1988

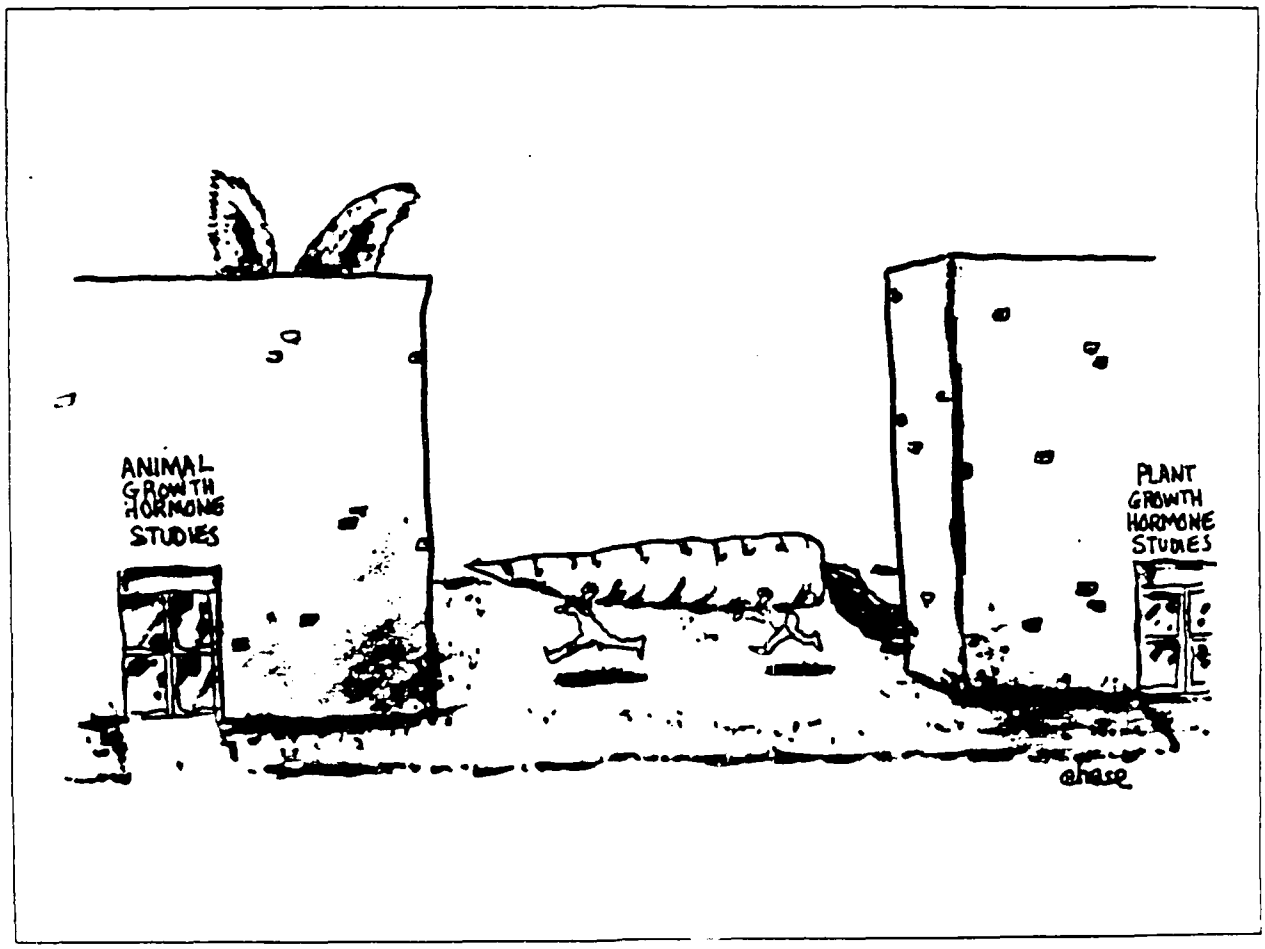

Reports

Superconducting Bi-Ca-Sr-Cu-O Fibers Grown by the Laser-Heated Pedestal Growth Method

R. S. FEIGELSON, D. GAZIT,* D. K. FORK, T. H. GEBALLE

Superconducting fibers of several compositions including the nominal composition $Bi_2CaSrCu_2O_8$ have been grown by means of the laser-heated pedestal growth method. The influence of starting composition and growth conditions on structure and superconducting properties is discussed. The *a-b* planes of the material are parallel to the fiber axis (along the growth direction), providing the ideal condition for conduction along the copper-oxygen planes.

THE LASER-HEATED PEDESTAL GROWTH (LHPG) method has been shown to be a powerful method for rapidly growing small-diameter single crystals, particularly oxides, both for measurements of properties and for fabricating fiber devices (*1*, *2*). It is a containerless technique that does not require a conventional furnace and can be used to grow crystals of very high melting-temperature materials without worry about reactivity with components in the growth system. It characteristically involves steep axial temperature gradients that permit rapid growth rates (typically millimeters per minute) and high quench rates that have made possible the growth of crystals of metastable compounds such as the high-temperature hexagonal form of $BaTiO_3$ (*2*). The sharply focused laser beam permits the formation of narrow molten zones that allow the growth of single-crystal fibers of micrometer diameter.

Following the early work by Burrus and Stone (*3*), an extensive program has been undertaken at Stanford that has produced a large number of different types of single-crystal fibers. Following the discovery of high-temperature superconducting transitions in the copper oxide perovskite systems by Bednorz and Müller (*4*), it seemed worthwhile to attempt to grow single-crystal fibers of the high transition temperature (T_c) materials for a number of reasons. There is evidence that fiber single crystals can be the most perfect crystals that are grown by any means. With the proper choice of seed, fibers of different orientations can be grown, a particularly valuable attribute if it can be done for the highly anisotropic layered copper oxide superconductors. Also, oxide fibers have been grown small enough in cross section to be flexible and thus have the possibility to serve as model systems for making the superconductors in wire form. Finally, the LHPG technique is closely related to the float-zone method, which is known to be the best technique for growing incongruently melting compositions.

Since all the new high T_c superconducting phases exhibit complex incongruent melting behavior, it was suggested (*5*) that the LHPG technique should be ideally suited to the growth of these materials in fiber form. One of the major advantages of this method is that an a priori knowledge of the actual melt composition required to produce the appropriate steady state growth conditions is not needed. The melt automatically adjusts itself to exactly the right composition needed, as demanded by the thermodynamic properties of the system.

Initial attempts with the $(LaSr)_2CuO_4$ and $YBa_2Cu_3O_7$ compounds were not successful owing to decomposition and loss of CuO. Even though some superconductivity was obtained, it was evident that in order to obtain the desired composition and single-crystal structure it would be necessary to enrich the feed stock with CuO. With the discovery of high T_c in the Bi-Ca-Sr-Cu-O system (*6*) and its stability with respect to oxygen (*7*), it became worthwhile to investigate the applicability of the LHPG method to the growth of these new compounds. In this report the preparation, structure, and some of the superconducting properties of dense, oriented, large-grain, polycrystalline fibers grown from $Bi_2CaSr_2Cu_2O_{8-\delta}$ and $Bi_{1.8}Ca_{1.2}Sr_{1.8}Cu_{2.2}O_{8-\delta}$ starting materials will be discussed.

A schematic of the LHPG method is given in Fig. 1, top. The top of the source rod of the material to be grown is melted with a tightly focused laser beam (~50 μm wide) having a circular cross section. A seed crystal is then introduced into the melt and growth is accomplished by withdrawing the seed at a controlled rate. To maintain constant melt volume the source rod is fed into the laser beam at a rate determined by the fiber diameter desired.

The source material in these experiments was prepared from Bi_2O_3, $CaCO_3$, $SrCO_3$, and CuO powders. The appropriate amounts were mixed together, finely ground, pressed into a pellet, and sintered for 15 hours in air at 780°C. The pellet was then ground, pressed again, and sintered under the same conditions. Rectangular rods 1.2 by 1.2 by 20 mm in size were cut out of the polycrystalline pellet and used both as the source material and for seeds.

Four different starting compositions were

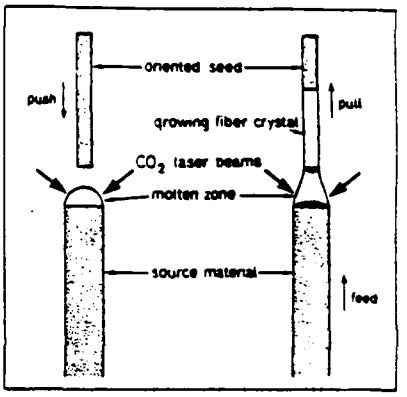

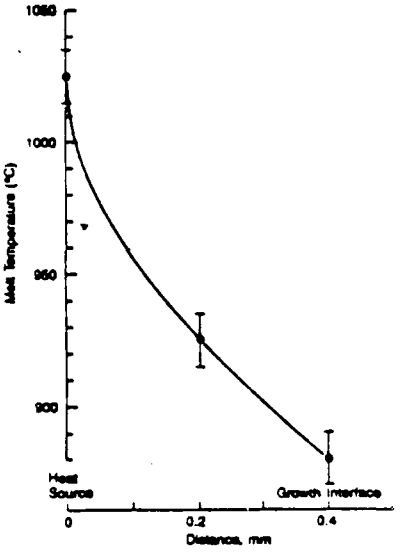

Fig. 1. (**Top**) Schematic diagram of the laser-heated pedestal growth method. (**Bottom**) Variation in surface melt temperature as a function of axial distance from the growth interface to the laser contact point. Error limits represent measurement variations over five experiments.

Center for Materials Research and the Department of Applied Physics, Stanford University, Stanford, CA 94305.

*On leave from the Nuclear Research Center Negev, P.O. Box 9001, Beer Sheva, Israel.

Table 1. Details of the different fiber growth runs. The temperatures are uncorrected optical pyrometer values of the melt temperature at the surface near the growth interface. Fiber 3 exhibited a significantly higher resistivity than fibers grown in air or oxygen.

Fiber type	Starting composition Bi-Ca-Sr-Cu	Growth rate (mm/hour)	Diameter (mm)	Atmosphere	Temperature (°C)
1	2-1-2-2	4.8	1.0	Air	900
2	2-1-2-2	1.5	1.0	Air	900
3	2-1-2-2	4.8	1.0	Argon	800
4	2-1-2-2	4.8	1.0	Oxygen	910
5	1.8-1.2-1.8-2.2	4.8	1.0	Air	900
6	1.8-1.2-1.8-2.2	24.0	0.25–0.35	Air	900
7	1.8-1.2-1.8-2.2	4.8	0.25–0.35	Air	900
8	1-1-1-2	4.8	1.0	Air	900
9	2-1-1-3	4.8	1.0	Air	860

used as listed in Table 1. Two different fiber diameters and lengths were grown from the randomly oriented polycrystalline seeds: 1 mm in diameter, 10 to 12 mm in length and 0.25 to 0.35 mm in diameter and 30 to 40 mm long. Different growth conditions were used for the 1 mm fibers as listed in Table 1. The long thin fibers were grown from melts of the first two compositions in air by means of a two-step procedure. In the first step, 0.7 mm diameter fibers were grown with a manually controlled pull rate that was more rapid than that used later. In the second step, two fibers were grown to their final diameter with pull rates of 24.0 and 4.8 mm/hour, respectively. The two-step procedure was used because the molten zone can become unstable when the ratio of the fiber diameter to the source rod diameter is too small (*3*). The growth rates used for these compounds, as expected, were lower than those required for congruently melting compounds. The approximate liquidus temperatures near the growth interface were measured during growth using a fine-filament optical pyrometer. Measurements were taken once every 20 to 30 minutes. A plot of the axial temperature gradient is given in Fig. 1, bottom. The temperature during growth was observed to remain constant to within the accuracy of the pyrometer reading. The melt temperature at the growth interface decreased dramatically from 900° to 800°C when an argon atmosphere was introduced into the growth chamber, indicating a strong influence of O_2 partial pressure on melt composition. It changed rapidly back to 900°C when air was reintroduced into the system. The fiber grown in argon had a much higher resistivity than the other fibers. Growth in pure oxygen caused the melt to boil. On replacing the oxygen with air, the boiling stopped immediately. All of the fibers were black, with varying degrees of surface smoothness except for the fiber which was grown in argon, which had a blackish-copper color.

The surface structure of the 1-mm diameter fiber grown at 4.8 mm/hour (fiber 1, Table 1) had, as shown in Fig. 2, top, a fibrous appearance owing to numerous facets and growth ridges aligned parallel to the growth direction. Figure 2, bottom, shows a fractured cross section of this fiber that clearly reveals the presence of plate-like crystallites having a highly aligned morphology. All of the plates were elongated along the growth direction. The thinner fiber grown at 24 mm/hour (fiber 6, Table 1) had similar structure but with fewer grains. The surface of the more slowly grown (fiber 7, Table 1) fibers (4.8 mm/hour), however, alternated between highly faceted regions like the previous fibers, and smooth regions. These smooth fiber sections developed gradually, eventually extending to the entire circumference as shown in Fig. 3. These smooth regions always ended abruptly, which suggests that their termination was the result of a dynamical growth instability. Uniform scanning electron microscopy (SEM) backscatter results on the smooth surface of the fiber indicated that the surface composition was homogeneous throughout large areas. The cross section of fiber 1 was composed of oriented platelets (grey), surrounded by a

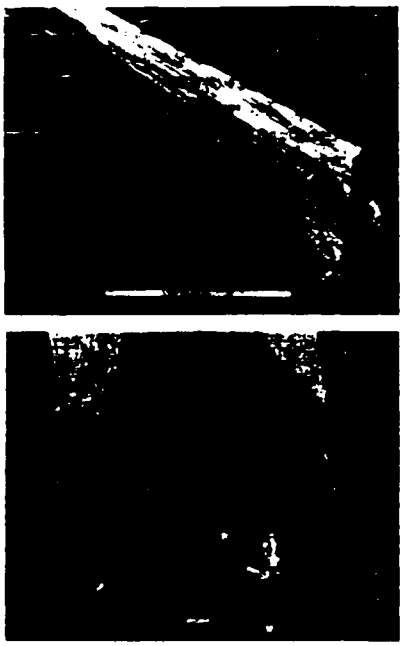

Fig. 2. SEM photographs of 1-mm-diameter $Bi_2CaSr_2Cu_2O_{8-\delta}$ fiber grown at 4.8 mm/hour. (**Top**) Side view. (**Bottom**) Fractured cross section.

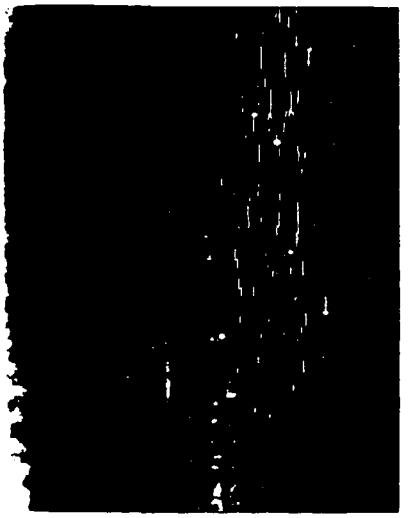

Fig. 3. Optical photograph of a smooth section of $Bi_{1.8}Ca_{1.2}Sr_{1.8}Cu_{2.2}O_{8-\delta}$ fiber.

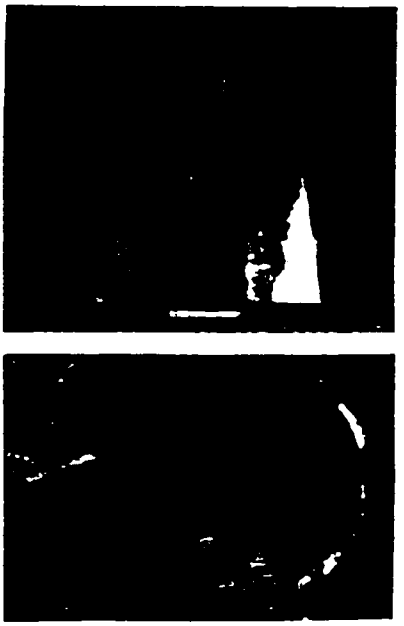

Fig. 4. (**Top**) SEM photograph of a fractured cross section of $Bi_{1.8}Ca_{1.2}Sr_{1.8}Cu_{2.2}O_{8-\delta}$ fiber. (**Bottom**) Optical photomicrograph of a polished cross section of the same fiber. Both pictures reveal a star-shaped second phase in the core region.

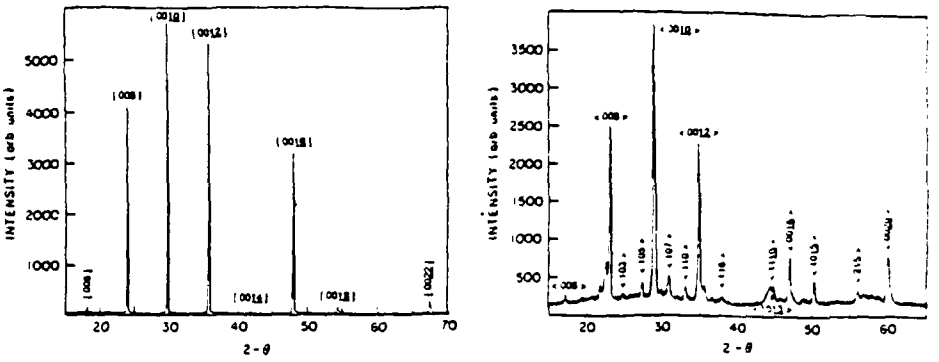

Fig. 5. (**Left**) X-ray diffraction data for a smooth section of fiber 7. The fiber axis is directed normal to the plane of the x-rays. (**Right**) Powder x-ray diffraction data for fiber 1. The predominance of the *c*-axis peaks may be due to a tendency for the crystal to cleave along the *a-b* plane, resulting in small crystals that lie flat with their *c*-axes directed upward. The powder was ground with a mortar and pestle. All of the [00*m*] peaks correspond to a *c*-axis spacing of 30.8 Å.

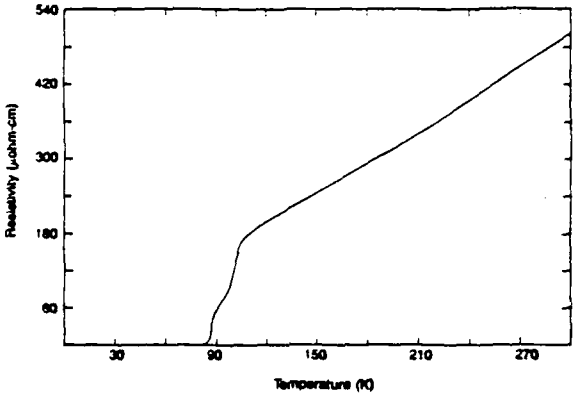

Fig. 6. Resistivity versus temperature for a smooth section of fiber 7.

white matrix phase (~10% by volume). A few tiny dark spots appeared in the microstructure that might be voids or inclusions. Microprobe analysis showed that the grey phase had approximately the 2-1-2-2 composition, whereas the white phase had a variable composition always higher in Bi. The apparent absence of a phase with a circular morphology in the cross section or on the surface led us to the conclusion that the nonsuperconducting needle-like phase usually seen in conventionally melted samples was not formed during the fiber growth experiments. An SEM photograph of the fractured end of a smooth section of fiber is shown in Fig. 4, top. The morphology here is quite different from that seen previously. In these regions several large crystallites cover the entire cross sectional area as can clearly be seen in the photograph of a polished surface given in Fig. 4, bottom. A second phase, in the form of two star-shaped regions near the fiber core, can also be seen. They contain almost pure CaO.

X-ray diffraction measurements were made on a four-circle diffractometer by means of a CuK_α source in the Bragg-Brentano geometry. Five types of x-ray scans were used to verify that the *c*-axis of the crystallites was perpendicular to the fiber's growth axis. The *c*-axis [00*m*] peaks were observed in the smooth fiber section when the plane containing the incident and scattered x-rays was normal to the fiber. Rocking the fiber toward the plane of the x-rays while tuned to the [00$\underline{1}$0] peak indicated that the *c*-axis lies in the cross section to within ~4 degrees. Rotating the fiber about its axis while tuned to the [00$\underline{1}$0] peak revealed several sharp peaks corresponding to individual *c*-axis grains in the cross section of the fiber. This result agrees well with the grain structure observed in the SEM photographs of this fiber (Fig. 2). No *c*-axis–oriented grains were found coaxial with the fiber. Preliminary results indicate that the axial orientation is the [110] direction. The results above were corroborated by placing the fiber axis in the plane of the x-rays and rocking on the *c*-axis peaks. The same series of x-ray measurements was tried on a rough section of a faster grown thin fiber. These data also revealed crystallites with their *c*-axis normal to the fiber axis; however, much weaker scattering (1.5 orders of magnitude) was observed, suggesting that the crystallites were smaller, and perhaps mixed with other phases. Measurements on the thicker fibers (1 and 2) showed the *c*-axis normal to the fiber axis. Grain size seems to be inversely related to growth rate for the growth conditions used in these experiments. It is natural to conclude that the direction of slowest growth is the *c*-direction.

Figure 5, left, shows the 2θ scan on a smooth section of fiber 7 with the axial direction normal to the plane of the x-rays. The [00*m*] peaks are visible against an almost flat background. Figure 5, right, shows a powder diffraction pattern made from one of the thicker fibers (fiber 1). When corrections are made for a misalignment in the diffractionmeter, both sets of diffraction patterns indicate a *c*-axis spacing of 30.8 Å, in agreement with data (*7*) for the 85 K (2-1-2-2) phase of the Bi-Ca-Sr-Cu-O materials. Powder diffraction was used for the thick fiber to increase the signal strength.

The resistivity of the samples was measured with the four-point probe technique. Contacts were made with either silver paint or silver epoxy that was later covered with pressed indium. The contact resistance for these contacts was measured to be as high as 350 mohm/cm^2. The accuracy of the resistivities that we measured was limited by the geometrical factors of cross section and contact spacing. To within orders of unity we could compare the effects of growth and annealing conditions.

The results for the smooth section of fiber 7 show a normal state resistivity which is linear in T and extrapolates to zero at 0 K (Fig. 6). These data were obtained from the same fiber that was photographed in cross section in Fig. 4, bottom, and that produced the diffraction pattern in Fig. 5, left. The two drops in resistivity at 105 K and 85 K as originally observed by Maeda *et al.* (*6*) are believed to correspond to two superconducting phases of the Bi-Ca-Sr-Cu-O system. Also noted is a very shallow resistance tail in the transition between 85 K and 80 K, which we believe is a sign of percolation between crystallites in the smooth section.

It has been established that in the related system $Tl_2Ca_{n-1}Ba_2Cu_nO_{4+2n}$, three different T_c phases with $n = 1,2,3$ exist and correspond to critical temperatures of 80 K, 105 K, and 125 K, respectively (*8*). The 105 K drop in resistivity in Fig. 6 is thus suspected to be the result of a minority phase of

$Bi_2Ca_2Sr_2Cu_3O_{10}$, whose unit cell includes an extra copper-oxygen layer. Tsuchiya *et al.* (9) have presented cross-sectional transmission electron microscopy results of double, triple, and quadruple copper-oxygen layers in the Bi-Ca-Sr-Cu-O systems.

None of the remaining samples, with one exception, had either a linear resistance extrapolating to zero or a pair of two superconducting transitions. To obtain superconducting transitions for the narrow diameter nonsmooth fibers, it was necessary to anneal them in air at 500°C, in contrast to the data in Fig. 6, which were obtained for an unannealed portion of the smooth fiber. This suggests that the process that forms the large oriented crystallites in the smooth fiber sections also accompanies the incorporation of adequate quantities of oxygen. The results thus indicate that an oxygen anneal lowers the resistivity and narrows the superconducting transition of the thick fibers, as well as the rough portions of thin fibers.

It is of great interest to measure the critical currents of the fibers and, following the work by Elkin *et al.* (*10*) on YBCO, improved contacts on the fibers have been made by ion milling the surface and depositing silver or gold contacts on the surface. With a pressed indium overlayer, these contacts had resistivities of 30 to 40 μohm/cm^2, but the critical current measurements are not yet complete.

We have demonstrated a capability for growing, under controlled conditions, superconducting fibers by means of the laser-heated pedestal growth technique. Under the right conditions, the growth process leads to several simultaneously occuring properties which make them ideal for study. The *a-b* planes are directed along the axis of the fiber, which we believe optimizes conduction in the axial direction. A reduced number of larger crystallites takes over during the growth of the smooth sections, which should augment the critical current. The fiber's surface morphology becomes smooth, facilitating the placement of electrical contacts. The superconducting transition consists of two distinct drops which we believe results from a phase with higher T_c.

Note added in proof: Preliminary measurements (*11*) with a pulsed current showed an excess of 60,000 A/cm^2 at 68 K.

REFERENCES AND NOTES

1. R. S. Feigelson, in *Crystal Growth of Electronic Materials*, E. Kaldis, Ed. (North-Holland, Amsterdam, 1985), pp. 127–145; in *Tunable Solid State Lasers*, P. Hammerling, A. B. Budgor, A. Pinto, Eds. (Springer, New York, 1985), pp. 129–141.
2. ———, *J. Crystal Growth* 79, 669 (1986).
3. C. A. Burrus and J. Stone, *Appl. Phys. Lett.* 26, 318 (1974).
4. J. Bednorz and K. A. Müller, *Z. Phys. B* 64, 189 (1986).
5. R. S. Feigelson and Y. X. Fan, paper presented at the Seventh American Conference on Crystal Growth, 12 to 17 July 1987, Monterey, CA.
6. H. Maeda, Y. Tanaka, M. Fukutomi, T. Asano, *Jpn. J. Appl. Phys.* 27, L209 (1988).
7. See, for example: J. M. Tarascon *et al.*, *Phys. Rev. B*, in press; S. A. Sunshine *et al.*, *ibid.*, in press.
8. See, for example: R. M. Hazen *et al.*, *Phys. Rev. Lett.*, 60, 1174 (1988); S. S. Parkin *et al.*, *ibid.*, in press; C. C. Torardi *et al.*, *Science* 240, 631 (1988).
9. J. Tsuchiya *et al.*, in preparation.
10. J. W. Elkin, A. J. Panson, B. A. Blankenship, *Appl. Phys. Lett.* 52, 331 (1988).
11. J. Sun, D. Fork, A. Kapitulnik *et al.*, private communications.
12. We thank R. Ravmakers for making the polycrystalline starting material, C. B. Eom for assistance with the SEM photographs, J. Sun for preliminary resistivity measurements, R. Barton for useful discussions, S. Ladderman for verifying the diffraction techniques, and M. Lee for assistance in making the contacts. This work was supported by the NSF Materials Research Laboratory program through the Center for Materials Research at Stanford University.

27 April 1988; accepted 5 May 1988

Low Lake Stands in Lakes Malawi and Tanganyika, East Africa, Delineated with Multifold Seismic Data

C. A. SCHOLZ AND B. R. ROSENDAHL

Seismic data reveal that water level in Lake Malawi, East Africa, was 250 to 500 meters lower before about 25,000 years ago. Water levels in Lake Tanganyika at that time were more than 600 meters below the current lake level. A drier climate appears to have caused these low stands, but tectonic tilting may also have been a contributing factor in Lake Malawi. High-angle discordances associated with shallow sequence boundaries suggest that these low stands probably lasted many tens of thousands of years. Because of its basement topography, the Lake Tanganyika basin had three separate paleolakes, whereas the Lake Malawi basin had only one. The different geographies of these paleolakes may be responsible in part for the differences in the endemic fish populations in these lakes.

WE HAVE USED 24-FOLD COMMON depth point seismic reflection data (*1*) to delineate the boundaries of the predecessors to Lakes Malawi and Tanganyika, East Africa (Figs. 1 and 2). Mapping of paleoshorelines lying many hundreds of meters below modern lake levels is necessary for examining depositional processes in rifts, the limnology and ichthyology of African rift lakes, and the paleoclimatology of East Africa.

Lake Malawi and Lake Tanganyika occupy the southern and central parts of the western branch of the East African rift system (Fig. 1). They are among the world's deepest lakes, and both lie in a region of savannah and subtropical forest (*2–5*). Structurally, both rifts are composed of a series of linked half-grabens, which tend to have alternating directions of asymmetry along the rift axes (*6*). Modern depocenters coincide with the most subsided parts of these half-grabens. Multifold seismic data (Fig. 2, A and C) indicate that 4 km or more of sediment have accumulated in the northern basins of the Lake Malawi rift (*7*) and over 6 km of sediment fill parts of the Lake Tanganyika rift (*8*, *9*).

Several seismic sequence boundaries (*10*) have been identified in the sediments beneath the main African rift lakes (*7*, *8*, *11*, *12*). These boundaries are major breaks in the lacustrine stratigraphy and represent depositional changes that were caused by climatic, tectonic, and, in the case of the eastern rift (*13*), volcanogenic processes. The stratigraphic record of abrupt changes

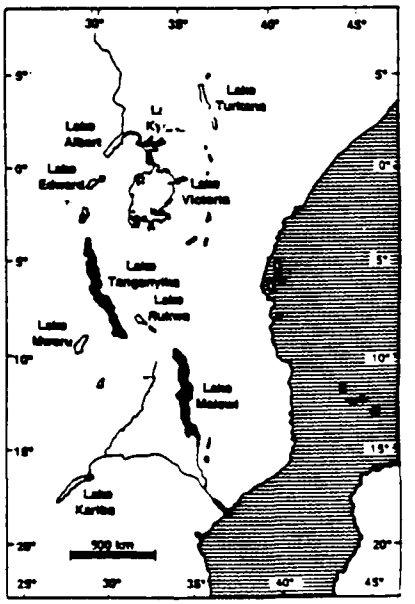

Fig. 1. The lakes of the East African rift system.

Project PROBE, Department of Geology, Duke University, Durham, NC 27706.

may extend back tens of millions of years in Lakes Tanganyika and Malawi (*7*, *8*). Lake levels also were highly variable in East Africa during the late Pleistocene (*12*, *14*–*16*), as well as during historical times (*3*, *5*, *17*).

Lakes, even large ones, are typically subject to more rapid water level changes than oceans. In rift lakes, crustal extension adds a tectonic component to lake level changes. The situation is compounded in warm, arid regions where the primary hydrologic output is by evaporation. Rapid and often large water level variations in small, high-relief drainage basins generate dynamic depositional systems. Sedimentary facies changes are common, both vertically and laterally, across lacustrine rift basins (*18*).

Ancient lacustrine environments and associated paleolake shorelines can be recognized in seismic reflection data by (i) changes in acoustic character, which are diagnostic of shallow- to deep-water facies transitions, (ii) changes in reflection termination geometries along sequence boundaries, and (iii) diagnostic external facies geometries such as wave-cut terraces and barrier systems. For example, a seismic section across the northwest part of Lake Malawi (Fig. 3) shows that a considerable part of the lower, east-dipping sequence has been truncated at the upper (that is, shallowest) sequence boundary. Truncation is a manifestation of subaerial exposure and erosion.

To the east of "b" on Fig. 3A, the reflection configuration along the upper sequence boundary changes to a conformable relation. Along this part of the seismic line, the thin, upper depositional sequence overlies continuous, narrow bandwidth reflections. We interpret the lower reflections as an acoustic facies indicative of continuous, open lacustrine deposits. We interpret the transition area from erosional truncation to conformable reflections as the shoreline of a previous lake level still stand, which on this profile is 400 m below the present level. In regions with steeply dipping sequence boundaries, such as on the shoaling sides of rift half-grabens, this transition is easily identified. Similar stratal relations have been recognized at comparable depths elsewhere in the northern two-thirds of Lake Malawi, as well as in several regions in Lake Tanganyika.

In west-central Lake Malawi, two distinctive acoustic facies are evident beneath the shallowest seismic sequence boundary (Fig. 3B). Toward the center of the lake (from "b" to "c" in Fig. 3B) reflections are indicative of relatively open, deep-water lacustrine sedimentation, as previously discussed. In the region from "a" to "b" the acoustic facies consists of mixed amplitude, variable frequency, wavy, and less continuous reflections. On this profile, this facies occurs at levels that are shallower than 300 m below the modern lake level. We interpret it as lacustrine deposits that were subjected to subaerial erosion and desiccation during the same late Pleistocene low stand of Lake Malawi discussed above.

The acoustic facies and reflection termination geometries that correspond to this low stand have been mapped throughout Lake Malawi (Fig. 4A). About 40 m of lacustrine sediment typically blankets the sequence boundary that is associated with the low stand. The basinward limits of erosional truncation are about 375 to 400 m below the modern lake level in the north-central part of the lake (Fig. 4A). Open lacustrine deposits occur at depths of 400 m in this

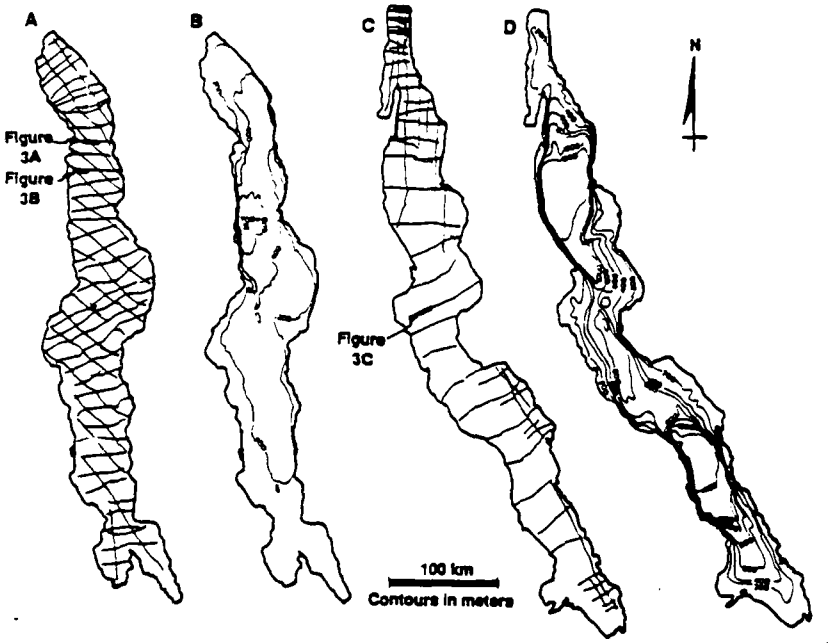

Fig. 2. (**A**) Multifold seismic coverage of Lake Malawi. (**B**) Bathymetry of Lake Malawi. (**C**) Multifold seismic coverage of Lake Tanganyika. (**D**) Bathymetry of Lake Tanganyika. Bold lines indicate locations of seismic lines in Fig. 3.

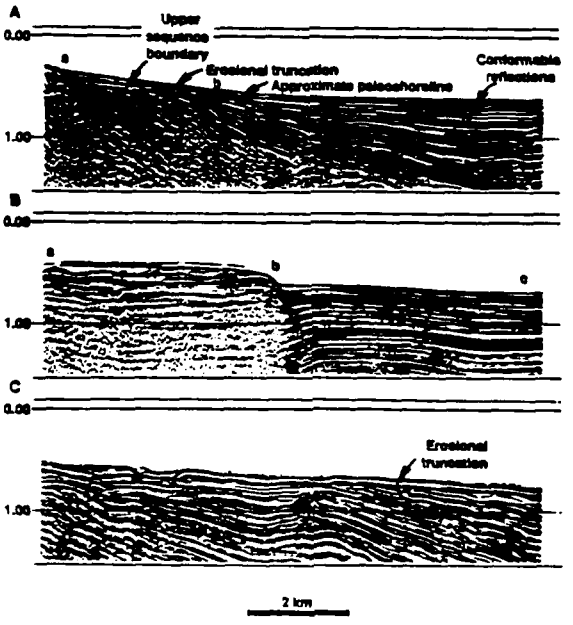

Fig. 3. (**A**) Seismic line 816 from northwestern Lake Malawi. Section from a to b shows zone of erosional truncation beneath the upper sequence boundary. Note change to a conformable relation down dip along the upper sequence boundary. Note the approximate location of the paleoshoreline for the major low lake stage discussed in text. (**B**) Seismic line 820 from west-central Lake Malawi showing continuous "open lacustrine" type acoustic facies (b to c) and wavy, semi-discontinuous "desiccated" facies above shallow basement (a to b). (**C**) Seismic line 214 from central Lake Tanganyika. Note shallow erosional surface at water depths of over 600 m. Lines displayed are 24-fold, stacked time sections with approximately 2.6:1 vertical exaggeration with respect to the water bottom. Line 214 is time-migrated.

Resonance effects in Raman scattering in $YBa_2Cu_3O_7$.

D. Kirillov, Varian Research Center, 611 Hansen Way, Palo Alto, CA 94303;

I. Bozovic, K. Char, and A. Kapitulnik, Department of Applied Physics, Stanford University, Stanford CA 94303-4090.

Abstract.

Raman spectra of $YBa_2Cu_3O_7$ excited by different lines of Ar and Kr lasers have been studied. It was found that significant changes in relative intensity and lineshape of phonon lines occured in the spectra when the excitation frequency was shifted from the red into blue region of the spectrum. The enhancement of high frequency phonons, which involves stretching of Cu-O bonds, and transformation of their asymmetric Fano type lineshape caused by interference with electronic scattering into a symmetric lineshape was attributed to resonance with an interband transition in $YBa_2Cu_3O_7$.

There is strong absorption of light throughout the optical spectrum in the high temperature superconductor $YBa_2Cu_3O_7$ [1,2]. Because the lasers used for Raman measurements in this material have radiation frequencies in the range of strong absorption, anomalies in the scattering due to resonance conditions can be expected [2]. Among these anomalies are breakdown of selection rules, dominant appearance of selected lines and overtone scattering. A clear illustration of the selection rules breakdown due to resonance conditions and, probably, due to distortions in the structure caused by disorder in oxygen distribution is the domination of the

infrared active lines forbidden by electric dipole type selection rules in the Raman spectrum of Cu_2O [4,5]. That spectrum also involves vibrations of copper and oxygen atoms, and phonon frequencies are in the same range as those of $YBa_2Cu_3O_7$. It is important to understand how resonance effects appear in Raman spectra of $YBa_2Cu_3O_7$.

In the present work we studied Raman spectra of $YBa_2Cu_3O_7$ films as a function of laser radiation frequency. We used for excitation of the spectra the following lines of Ar and Kr ion lasers: 647.1, 514.5, 496.5, 488.0, 476.5 and 457.9 nm. The spectra were taken at room temperature with a sample in a He gas environment to exclude the lines in the low energy part of the spectrum due to scattering in the air. We used backscattering configuration, and the scattered light was analyzed by a scanning triple Spex spectrometer. The thin film samples of $YBa_2Cu_3O_7$ studied in the present work were grown epitaxially on $SrTiO_3$ substrates by a magnetron sputtering method [6]. The frequency dependence of the absorption coefficient of $YBa_2Cu_3O_7$ determined from transmittance and reflection measurements [1,2] is presented in Fig.1 for the range covered by available laser lines. In this case the film is oriented along the a axis and the absorption is due to both polarization, $E \parallel c$ and $E \parallel b$. There is anisotropy in optical absorption of $YBa_2Cu_3O_7$ [1,2]. Because our samples consisted of mosaic of alternately oriented grains, we were not able to study the anisotropy in resonance Raman scattering, though we could conclude that resonance effects are present for all polarizations. As can be seen from Fig. 1, the laser frequencies span the range of the absorption edge type structure in the absorption spectrum. Examples of the Raman spectra are shown in Figs. 2-4. The spectra of the film A grown along a axis, with b and c axes oriented alternately along the a and b axes of the $SrTiO_3$ substrate, excited by 647.1 and and 514.5 nm laser lines are compared in Fig. 2. The spectra contain phonon lines and an electronic scattering continuum which are observed in xx, yy and zz polarizations

and formally correspond to A_g irreducible representation. As can be seen from the comparison of the spectra, the intensity of the higher energy phonon line at 499 cm^{-1} grows noticeably in relation to the 148 cm^{-1} line when excitation light frequency moves in the direction of stronger absorption. This intensity increase shows that the line is resonantly enhanced. There are also changes in lineshapes of the lines. Breit-Wigner-Fano type interference between phonons lines and electronic continuum identified earlier for the 112 and 335 cm^{-1} lines [7] is stronger for the spectrum excited by 647.1 nm line, and the asymmetrical lineshape for 499 cm^{-1} line in this spectrum clearly indicates that 499 cm^{-1} phonons also interfere with electronic continuum. Absence, or weakness of interference effects in 514.5 nm and other short wavelength spectra is caused by a frequency dependence of the coupling constant describing the Fano lineshape. Similar effects of frequency dependance of the coupling constant for Fano interference between phonons and electronic continuum was observed earlier in strongly doped p-type Si [8].

One more property of the spectra presented in Fig. 2, which must be considered, is that there are more A_g type modes in the spectra than required by group theory. Group theory predicts 5 A_g modes, while there are 6 A_g modes in the spectra: 112, 148, 335, 442, 499 and 574 cm^{-1}. The line at 574 cm^{-1}, which was not considered as a basic mode in discussion of A_g type phonons [7,9], is always present in $YBa_2Cu_3O_7$ spectra. Also unusual is the fact that only A_g modes are seen in the spectra. Evidently, this problem requires further study.

The spectra of another thin film sample B also predominantly oriented along a-axis are shown in Fig. 3. This sample consists of a mosaic of microcrystals grown alternately along c and a axes, while a, b and c axes in the plane are oriented along a and b axes of the substrate. The spectra of this sample have additional lines at 220, 433, 580 and 640 cm^{-1}. As follows from the polarized spectra, the symmetry types of 220, 433 and 580 cm^{-1} are not consistent with D_{2h} symmetry

group of $YBa_2Cu_3O_7$ because they appear both in parallel and crossed polarization configurations, while the 640 cm^{-1} line behaves similar to A_g modes. Apparently, 433 and 580 cm^{-1}lines, though close in frequency to 444 and 574 cm^{-1} lines of the A sample, correspond to different phonons. These additional lines are often observed in Raman spectra of $YBa_2Cu_3O_7$ and sometime attributed to the presence of $BaCuO_2$ phase in the sample due to the fact that similar lines are present in the spectra of $BaCuO_2$ [10] . Our measurements on many samples with different small content of $BaCuO_2$ determined by X-ray diffraction showed that these lines have no correlation with presence of $BaCuO_2$ impurity phase. They are most probably caused by distortion of the symmetry of $YBa_2Cu_3O_7$ due to variation in the oxygen occupancy in CO_6 octaehdra which distorts the symmetry and makes allowed in the spectra additional lines, most noticeably those involving Cu-O stretching vibrations along the Cu(1)-O(1) chains (640 cm^{-1}). The structure of $BaCuO_2$ contains quite similar CO_6 octaehdra, which explains similarity of the spectral features. As can be seen from Fig. 3, noticeable enhancement of high frequency phonon lines in relation to low frequency lines is also observed in the B sample for higher energy excitation. Breit-Wigner-Fano type interference between phonons and electronic continuum again appears for line 499 cm^{-1} in addition to well pronounced interferences for 112 and 335 cm^{-1} lines, see Fig. 3(c).

Additional feature of resonance scattering is the appearance of the overtone scattering. As can be seen from Fig.4, which shows the spectrum excited by a 4880 A line in conditions of strong resonance, the second overtones of 499 and 640 cm^{-1} lines are observed at 1000 and 1280 cm^{-1}, correspondingly, and even a trace of the third overtone of the 640 cm^{-1} line is noticeable at 1920 cm^{-1}.

The data on resonance Raman scattering in $YBa_2Cu_3O_7$ are summarized in Fig. 1. Peak intensities, measured from the level of the electronic continuum, of the resonantly enhanced lines at 499 cm^{-1} (A sample) and 640 cm^{-1} (B sample)

in relation to the line at 148 cm^{-1}, which is not enhanced, are shown in this figure together with the absorption spectrum. The lines at 442 and 574 cm^{-1} of the A sample and 433 and 580 cm^{-1} of the B sample were also enhanced, but not so strongly. As can be seen from Fig.1, the functional form of the frequency dependence of relative scattering intensity is similar to that of the absorption coefficient. This can be expected because both dependences reflect the number of oscillators participating in the resonance absorption and scattering. Due to the fact that mostly high frequency phonon lines which involve stretching of Cu-O bonds are enhanced at resonance, the resonant electronic transitions in the studied spectral range most likely correspond to interband transitions between the occupied states close to the Fermi level, and an unoccuppied band at 2-3 eV above E_F formed by oxygen and copper states.

In conclusion, resonance effects in the Raman scattering in YBa_2Cu3O_7 have been observed. These effects included change of lineshape and increase of intensity of high frequency phonon modes, dominance of scattering without change of the polarization of light, and appearance of overtone scattering. Variations in resonance scattering were pronounced in the spectral region having an absorption edge like feature at 2-3 eV in the absorption spectrum.

Figure captions.

Fig. 1. Absorption spectrum of $YBa_2Cu_3O_7$ ($E \parallel c$, $E \parallel b$) in the range of laser frequencies used for excitation of Raman spectra. Peak intensities of the 499 cm^{-1} Raman line, sample A, and 640 cm^{-1} line, sample B, in relation to the intensity of 148 cm^{-1} line at different excitation wavelengths are shown in the same figure. Lines drawn through experimental points are guide lines only.

Fig. 2. Raman spectra of the A film. The spectra appear only in yy and zz polarizations.

(a) The spectrum excited by a 514.5 nm laser line.

(b) The spectrum excited by a 647.1 nm line.

Fig. 3. Raman spectra of the B film.

(a) The spectrum excited by a 514.5 nm laser line.

(b) The spectrum excited by a 647.1 nm line.

(c) The spectrum excited by a 647.1 nm line in the aged part of the sample with reduced intensity of the 640 cm^{-1} phonon line. The spectrum show clearly the interference of three phonon lines at 112, 335 and 499 cm^{-1} with an electronic continuum component.

Fig. 4. Higher order Raman scattering, film B, 488.0 nm excitation. Overtones at 1000, 1280 and 1920 cm^{-1} are indicated.

References.

1. I. Bozovic, D. Kirillov, A. Kapitulnik, K. Char, M.R. Beasley, T.H. Geballe, Y.H. Kim, and A.J. Heeger, Phys. Rev. Lett. 59, 2219 (1987).

2. I. Bozovic, K. Char, S.J.B. Yoo, A. Kapitulnik, M.R. Beasley, T.H. Geballe, Z.Z. Wang, S. Hagen, N.P. Ong, D.E. Aspnes, and M.K. Kelly, Phys. Rev. B (1988). In print.

3. R.M. Martin and L.M. Falicov, Resonant Raman Scattering, in Light Scattering in Solids I, ed. M. Cardona, Springer Verlag, Berlin, Heidelberg, New York, 1983.

4. P. Dawson, M.M. Hargreave and G.R. Wilkinson, J. Phys. Chem. Solids, 34, 2201 (1973).

5. P.Y. Yu and Y.R. Shen, Phys. Rev. B12, 1377 (1975).

6. K. Char et al., Appl. Phys. Lett. 51, 1370 (1987).

7. S.L. Cooper, M.V. Klein, B.G. Pazol, J.P. Rice, and D.M. Ginsberg, Phys. Rev. B37, 5920, (1988).

8. F. Cerdeira, T.A. Fjeldly, and M. Cardona, Phys. Rev. B8, 4734 (1973).

9. R. Liu, C. Thonsen, W. Kress, M. Cardona, B. Gegenheimer, F.W. de Wette, A.D. Kulkarni, and H. Schroder, Phys. Rev. B37, 7971 (1988).

10. H. Rosen, E.M. Engler, T.C. Strand, V.E. Lee, and D. Bethune, Phys. Rev. B36, 726 (1987).

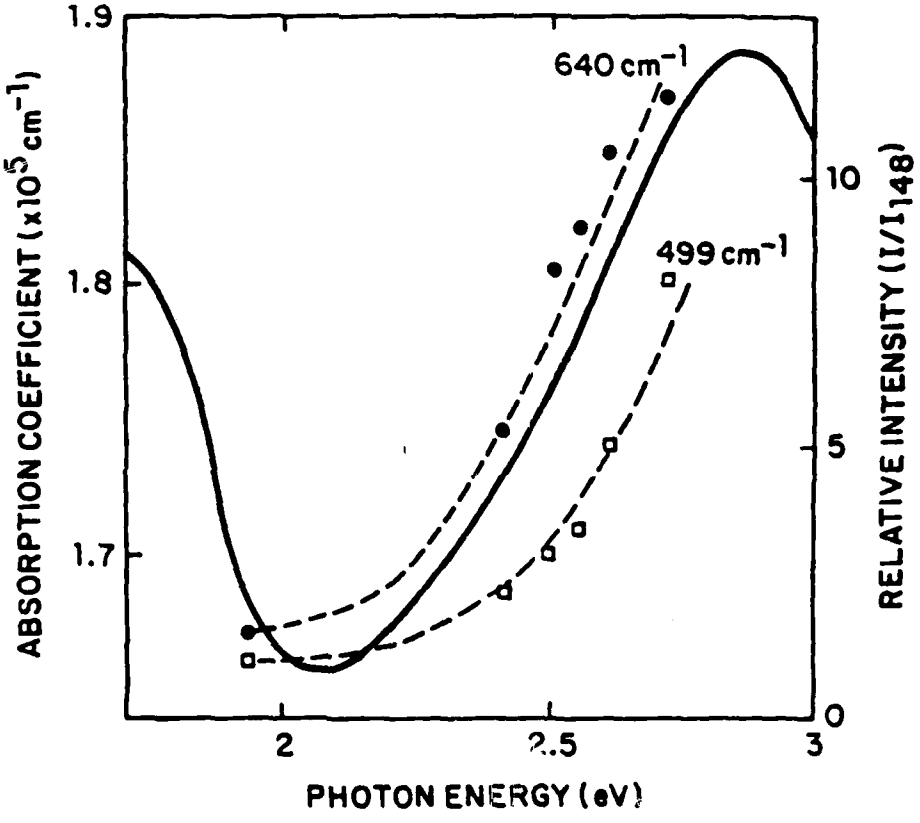
1.9
1.8
1.7
ABSORPTION COEFFICIENT (x10^5 cm^{-1})
640 cm^{-1}
499 cm^{-1}
10
5
0
RELATIVE INTENSITY (I/I$_{148}$)
2
2.5
3
PHOTON ENERGY (eV)

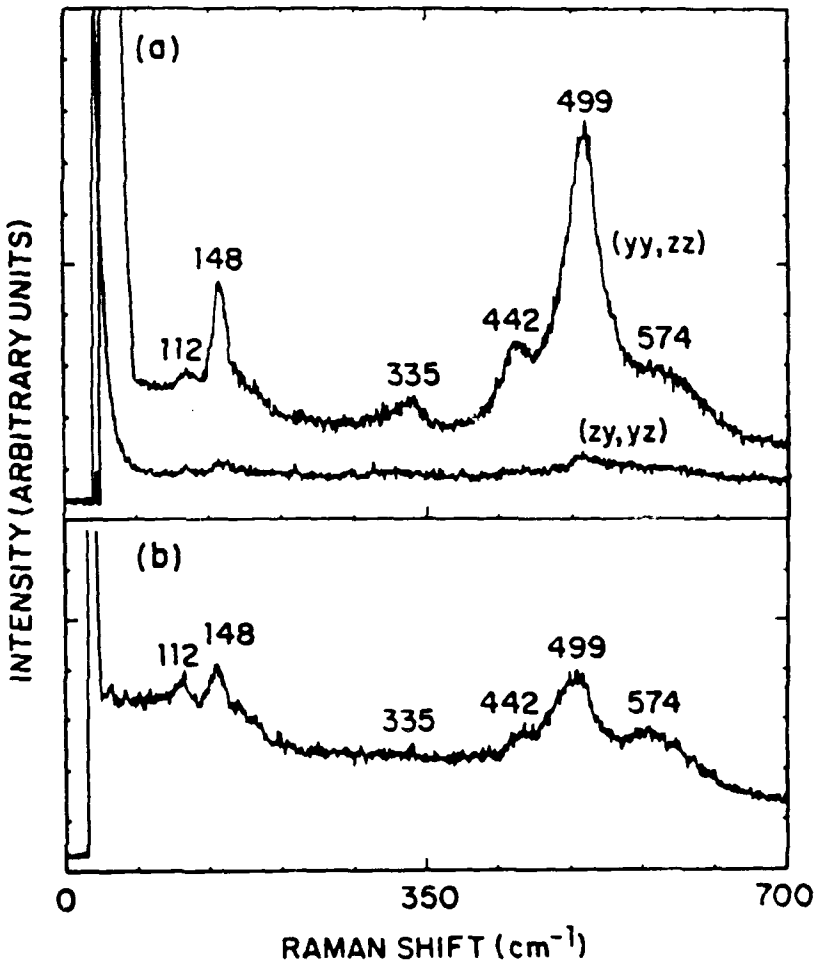
(a)
499
148
(yy,zz)
442
574
112
335
(zy,yz)
(b)
112
148
499
335
442
574
0
350
700
INTENSITY (ARBITRARY UNITS)
RAMAN SHIFT (cm^{-1})

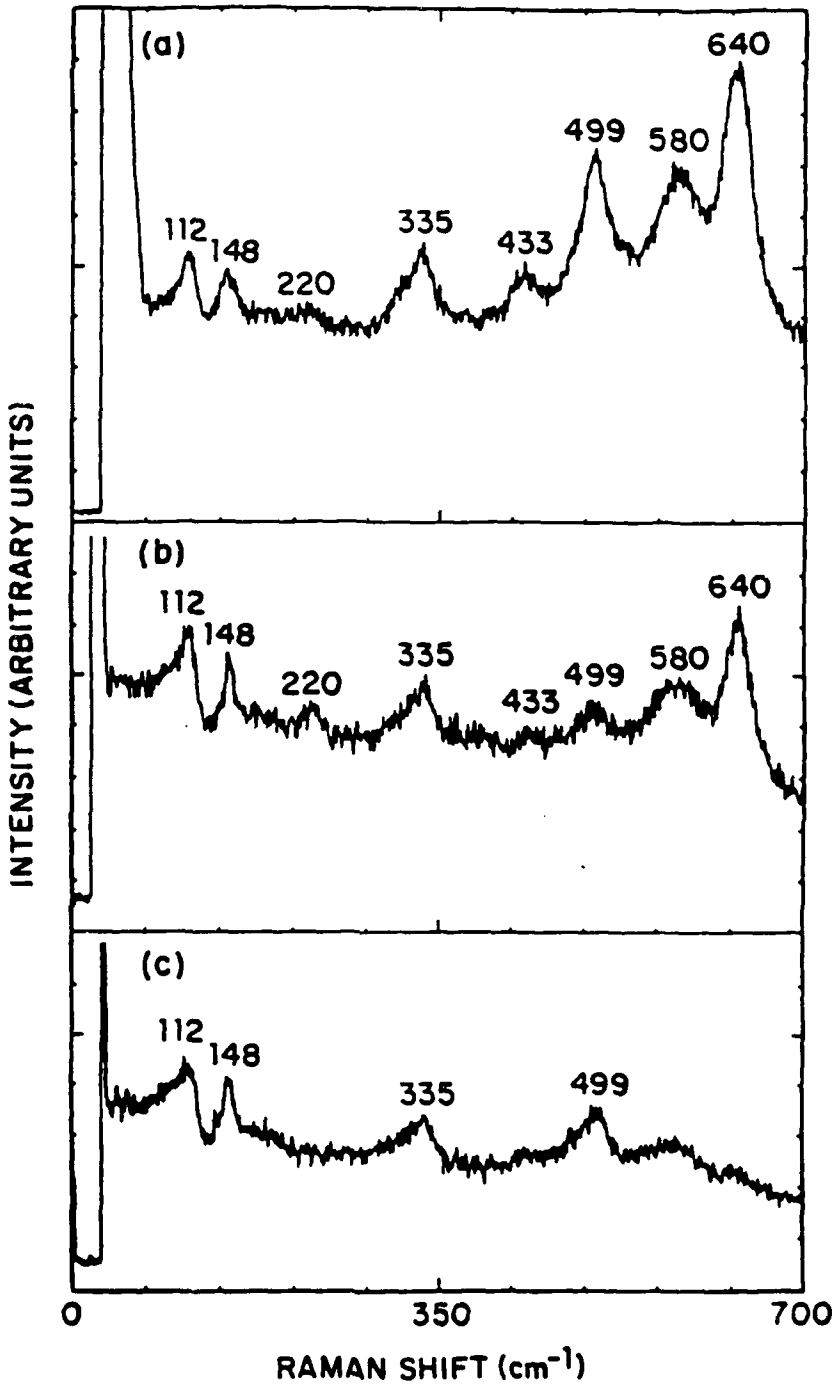
(a)
640
499
580
112
148
220
335
433
(b)
112
148
220
335
433
499
580
640
(c)
112
148
335
499
INTENSITY (ARBITRARY UNITS)
0
350
700
RAMAN SHIFT (cm^{-1})

Optical anisotropy of $YBa_2Cu_3O_{7-x}$

I. Bozovic, K. Char, S. J. B. Yoo, A. Kapitulnik, M. R. Beasley, and T. H. Geballe
Department of Applied Physics, Stanford University, Stanford, California 94305-4090

Z. Z. Wang, S. Hagen, and N. P. Ong
Department of Physics, Princeton University, Princeton, New Jersey 08544

D. E. Aspnes and M. K. Kelly
Bellcore, Red Bank, New Jersey 07701-7020

(Received 11 May 1988)

The optical anisotropy of $YBa_2Cu_3O_{7-x}$ in the 0.08–5.6 eV region is investigated by polarized reflectance measurements on single crystals, and by transmittance, reflectance, and ellipsometric measurements on oriented thin films. In the visible–near-uv spectral region the anisotropy is relatively mild, but a huge anisotropy is observed in the infrared. Here, the reflectance increases with decreasing frequency for *both* polarizations, consistent with metallic conductance both parallel and perpendicular to the *ab* plane. The *c*-axis plasma frequency is strikingly low, but there is strong damping which could originate from a continuum of low-energy interband transitions.

LS3721BR 1988 PACS numbers 74.70.Jm 78.30.Er

$YBa_2Cu_3O_{7-x}$ (Y-Ba-Cu-O) and related high-T_c cuprates are currently the subject of intensive research worldwide.[1,2] One of the major issues is the effective dimensionality of these materials, which can be addressed in principle from the anisotropy of their electronic properties. With this objective, the conductance anisotropy of Y-Ba-Cu-O single crystals has been studied by several groups,[3,4] who reported values of $\rho_\perp/\rho_\parallel$ between 30 and 200. However, extrinsic effects such as planar stacking faults, microcracks, inhomogeneous oxygen concentration, etc., may be a serious problem in single crystals and could well affect the dc results. In principle, high-frequency ac conductance and optical measurements are less subject to ambiguities of these sorts, because charge displacements are rather small in such experiments. However, no conclusive results have been reported yet. Some indirect information has been inferred from apparent discrepancies between single-crystal[5,6] and bulk-ceramic[7] reflectance data, which have been resolved,[6,8] based on analogy with La_2NiO_4, by *postulating* Y-Ba-Cu-O (as well as $La_{2-x}Sr_xCuO_4$) to be highly anisotropic—in fact, metallic in the *ab* plane and insulating in the *c*-axis direction.

Here, we present optical data which show that, although Y-Ba-Cu-O is indeed highly anisotropic in the infrared region, the *c*-axis polarized reflectance is not characteristic of insulating material but rather shows a metalliclike rise with decreasing photon energy.

Single crystals of Y-Ba-Cu-O were grown at Princeton University by the flux method in an oxygen flow. The average size of the crystals was $0.5\times0.5\times0.1$ mm^3 and they had shiny faces of high optical quality and sharply defined edges. Typical T_c's were between 91 and 93 K, with 0.5-K wide transitions. To measure the resistivity by the Montgomery technique, 25-μm Au wires were indium-soldered onto the largest crystal faces near the corners.

Thin Y-Ba-Cu-O films were deposited on $SrTiO_3$ substrates by reactive magnetron sputtering[9,10] at Stanford University. Thicknesses ranged from 500 Å to 1 μm. The quality of the films can be judged from their low normal-state resistivities, sharp (1–2 K wide) superconducting transitions, and high critical current densities of up to 1.2×10^7 A/cm^2 at 4.2 K. X-ray diffractograms of these films showed a high degree of epitaxial orientation. Some of the films were grown with the *c* axis and others with the *a* axis (predominantly) perpendicular to the (001) face of the substrate.

Mid-ir reflectance spectra of the single crystals were obtained with a Digilab FTS-40 Fourier-transform infrared spectroscopy (FTIR) spectrometer coupled to a Spectratech ir-PLAN microscope that provided spatial resolution of 50 μm. This allowed us to record polarized ir reflectance spectra not only from the large platelet faces which are parallel to the *ab* plane, but also from the platelet sides which are perpendicular to the *ab* plane. We changed the polarization by rotating the Zn-Se polarizer or by rotating the sample; the results were consistent in both cases as can be seen from spectra D and E in Fig. 1.

As no instrumentation available to us could achieve sufficient spatial resolution to measure the optical spectra of the platelet sides at higher photon energies, we supplemented these results with near-ir, visible, and near-uv data obtained from transmittance, reflectance, and ellipsometric measurements on oriented thin films. In addition to the FTIR spectrometer, we used a near-ir–visible–near-uv Perkin-Elmer Lambda-9 double-monochromator double-beam spectrophotometer and a near-ir–visible–near-uv spectroellipsometer.[11]

For a normal-incidence measurement on a film with a typical grain orientation of ~80%, one has $E\perp c$ in ~60% of the grains in *a*-axis-oriented films, as compared to ~90% in *c*-axis-oriented ones, for either polarized or unpolarized light. Although ellipsometry is a non-normal-incidence technique, the pseudodielectric response $\langle\epsilon\rangle$ (that calculated from the ellipsometric data in the two-phase model without regard to anisotropy or surface

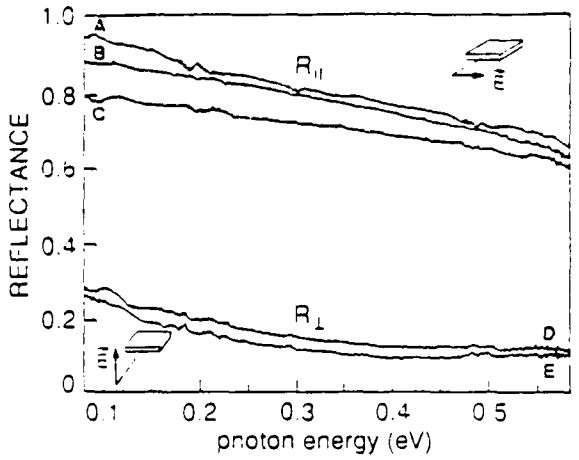

FIG. 1. Polarized infrared reflectance of Y-Ba-Cu-O, at normal incidence, from A, single crystal, *ab* face; B, D, E, single crystal, side perpendicular to *ab* face; C, *c*-axis-oriented film (pristine surface). The $R_{\perp}(\omega)$ spectra were obtained by rotating for 90° the polarizer (D) or the crystal (E). The reflectance of films can be raised to that of A when the surface was cleaned by ion milling the top 500–1000 Å.

effects) can give a fairly accurate measure, under certain conditions and for properly aligned samples, of the individual principal components of the dielectric tensor of a uniaxial medium.[12] Using the orientation statistics of these films, we estimate that Fig. 2(a) (in the whole energy range) and Fig. 2(b) (above 2.5 eV) yield $|\epsilon_{\parallel}|$ and $|\epsilon_{\perp}|$, respectively, to within 20%.

Since many physical parameters of Y-Ba-Cu-O depend very sensitively on preparation, impurities, defects, etc. (which accounts for many conflicting reports), at this stage we prefer to use large sample sets. Hence, we recorded altogether about 50 reflectance spectra from various faces of four single crystals, ellipsometric spectra from about two dozen thin films, and transmittance and reflectance spectra from a few hundred films.

Typical normal-incidence ir reflectance spectra from a "side"—i.e., a face perpendicular to the *ab* plane—of a Y-Ba-Cu-O single crystal are shown in Fig. 1 for light polarized parallel and perpendicular to the CuO_2 layers. A large anisotropy is apparent. The actual anisotropy may be even larger because of possible artifacts due to surface imperfections, sample misalignment, incomplete light polarization, etc. However, the high metallic $R_{\parallel}(\omega)$ shown in curve B does not differ by more than a few percent from the reflectance spectra of the large platelet faces which are parallel to the *ab* plane (curve A) or from those of our other single crystals and our best *c*-axis oriented films (curve C).

The real and the imaginary parts of the pseudodielectric function $\langle\epsilon(\omega)\rangle = \epsilon_1(\omega) + i\epsilon_2(\omega)$, determined from ellipsometric measurements, are shown in Figs. 2(a) and 2(b) for a *c*-axis- and an *a*-axis-oriented thin Y-Ba-Cu-O film, respectively. (Note that these films are not as dense as Y-Ba-Cu-O single crystals, which indeed show[13] somewhat larger ϵ_1 and ϵ_2.) The overall similarity of the two sets of spectra is clearly apparent, with the major differences being in the occurrence and position of spectral features above 3 eV and in the appearance of a free-electronlike component in the *c*-axis data below about 2.5 eV. This low-energy feature is also seen in data taken on the *ab* faces of single crystals.

To cast these data in the form more directly suitable for comparison to the reflectance data of Fig. 1, we have used them to calculate the corresponding reflectance spectra and have also plotted the results in Fig. 3. The measured reflectance of a *c*-axis-oriented film (the dashed curve)

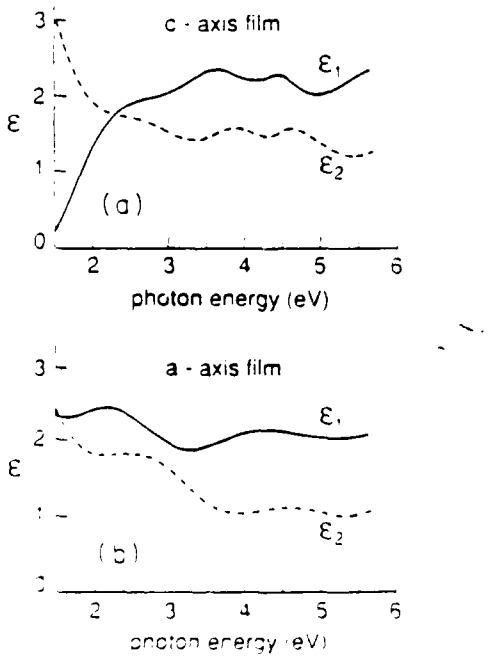

FIG. 2. The complex pseudodielectric functions $\epsilon(\omega) = \epsilon_1(\omega) + i\epsilon_2(\omega)$ of (a) *c*-axis oriented thin Y-Ba-Cu-O film, and (b) *a*-axis-oriented film, of comparable density.

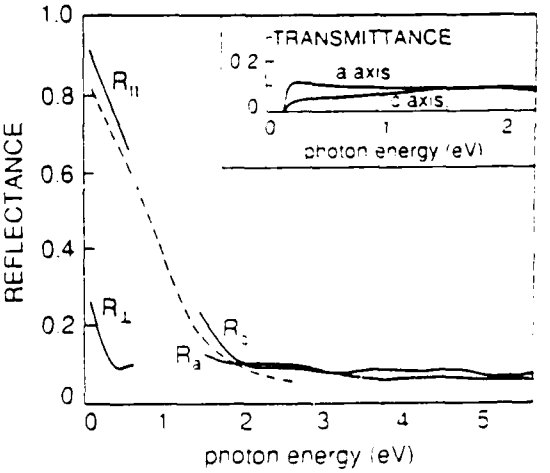

FIG. 3. Reflectance (from Fig. 1) of Y-Ba-Cu-O single crystal, $R_{\parallel}$ and $R_{\perp}$, compared to that of thin films, R_c and R_a (broken curves: measured; solid curves: calculated from Fig. 2). Note that R_a has a component of $R_{\parallel}$. Inset: Transmittance of ~2000-Å-thick Y-Ba-Cu-O films on $SrTiO_3$ substrates, oriented with *c* axis and *a* axis perpendicular to the substrate. The cutoff is due to the substrate absorption.

and the transmitances of both c-axis- and a-axis-oriented films (the inset) are shown in Fig. 3. Consistency among the three experimental techniques utilized is apparent and, in fact, is further improved when the differences in the degree of orientation are taken into account. The anisotropy is seen to be very large in the ir region and to decrease with increasing photon energy, diminishing to relatively small values in the visible and near-uv regions. These spectra, and hence the anisotropy, do not change much[14] with temperature down to 77 K, i.e., well below the superconducting transition, in the $0.15 < \hbar\omega < 3$-eV spectral range.

Let us turn now to the question of effective dimensionality. Of principal interest here are the low-frequency single-crystal polarized-reflectance data of Fig. 1. Notice first that $R_\perp(\omega)$ actually also shows a metalliclike upturn at frequencies below ~ 0.4 eV or so; this is even more apparent in Fig. 3. It does not appear insulatinglike in any event, in contrast to tetrathiafulvalene tetracyanoquinodimethane (TTF-TCNQ), hocamethyltetravelenafulvalene tetracyanoquinodimethane (HMTSF-TCNQ), or $K_2Pt(CN)_4Br_{0.3}\cdot 3H_2O$ and similar low-dimensional materials where $R_\perp(\omega)$ remains low and nearly constant down to the phonon-frequency region. Hence Y-Ba-Cu-O, although certainly strongly anisotropic, does not look like a quasi-two-dimensional metal on the basis of its optical properties. Furthermore, some consistency among different experimental data can be achieved within the present description.

We use the least-squares fit to the simple Drude model, $\epsilon(\omega) = \epsilon(\infty) - \omega_p^2/\omega(\omega + i\Gamma)$, and get $\hbar\omega_p^\perp \approx 0.7$ eV, $\hbar\Gamma_\perp \approx 0.9$ eV, $\epsilon_\perp(\infty) \approx 4$ eV. From these parameters and utilizing the relation $\rho = 4\pi\Gamma/\omega_p^2$, one gets $\rho_\perp \approx 10$ mΩ cm. Since $\rho_\parallel = 250$–400 $\mu\Omega$ cm, this amounts to $\rho_\perp/\rho_\parallel = 25$–$40$, in reasonable agreement with dc conductance experiments.[15] Notice, however, that the above values of $\omega_p^\perp$ and $\Gamma_\perp$ are quite uncommon to ordinary metals: The plasma frequency is more than order-of-magnitude too low while the damping is anomalously strong. Another important parameter is the optical effective mass, $m_\perp^*$. From $\omega_p^2 = 4\pi ne^2/m^*$ and assuming the carrier density $n \approx 6\times 10^{21}$ cm^{-3} (which has been suggested from the Hall effect measurements[3,10]) one gets $m_\perp^* \approx 15 m_e$, which certainly is uncommon.

As for the low-frequency "heavy-axis" plasmons —which play the central role in some theoretical models of high-T_c superconductivity—it seems that in Y-Ba-Cu-O they are too strongly damped to be well-defined excitations of the system. In fact, we expect two or more bands to cross the Fermi level[16] in Y-Ba-Cu-O. In that case, there should be a continuum of optically allowed (i.e., "vertical") low-energy interband transitions. That could well be related to the observed "strong damping of free carriers." A continuum of electronic transitions, featureless and nearly flat (at room temperature) should show up also in Raman scattering, and indeed it was observed[14] in dozens of good superconducting Y-Ba-Cu-O thin films (from the lowest Raman shifts detectable all the way up to 1 eV), as well as in single crystals.[17] It would be interesting to see what is happening in other high-T_c superconductors not isostructural with Y-Ba-Cu-O, i.e., the cuprates containing La, Bi, and Tl.

Finally, our $R_\perp(\omega)$ does come with an error bar, as pointed out above; also, it would be desirable to extend the single-crystal reflectance anisotropy data further into far infrared. From the present reflectance data, we cannot rule out the existence of a very small gap, of ~ 50 meV or so, for the conduction in the c-axis direction. If that were the case, one would expect $R_\perp(\omega)$ to show a strong temperature dependence.[18]

In conclusion, we have presented optical data (polarized reflectance spectra from different faces of single crystals, and transmittance, reflectance, and ellipsometric spectra of oriented thin films), which show that Y-Ba-Cu-O is not very anisotropic in the visible/near-uv region, but that it is rather anisotropic in the midinfrared and below. However, the reflectance with light polarization perpendicular to the CuO_2 layers rises at low frequencies, as expected from metallic rather than insulating behavior. In the range of frequencies investigated here, no evidence is found for the qualitatively distinct in-plane and out-of-plane transport mechanisms. The data are consistent with existence of a continuum of low-energy interband transitions. Given the important theoretical implications of this issue, extension of the spectroscopical measurements to the lower frequencies and to other related cuprate materials is important and is underway.

This research was supported in part by the Air Force Office of Scientific Research (Contract No. F49620-88-K0002), the Stanford Center for Materials Research under the National Science Foundation/Materials Research Laboratory program, and by the Physics Department, Princeton University.

[1] *Novel Superconductivity*, edited by S. A. Wolf and V. Z. Kresin (Plenum, New York, 1987); *High Temperature Superconductors*, edited by S. Lundquist, E. Tosati, M. P. Tosi, and Y. Lu (World Scientific, Singapore, 1987).

[2] J. Miller and J. L. Olson, in *Proceedings of the International Conference on High-Temperature Superconductors: Materials and Mechanisms of Superconductivity, Interlaken, Switzerland, 1988*, edited by J. Muller and J. L. Olsen [Physica C (to be published)].

[3] S. W. Tozer *et al.*, Phys. Rev. Lett. **59**, 1768 (1987); S. J. Hagen *et al.*, Phys. Rev. B **37**, 7929 (1988).

[4] Y. Iye *et al.*, in Ref. 2, and (unpublished).

[5] Z. Schlesinger *et al.*, Phys. Rev. Lett. **59**, 1958 (1987).

[6] S. Uchida, Physica B **148**, 185 (1987); S. Tajima *et al.* (unpublished).

[7] S. L. Herr *et al.*, Phys. Rev. B **36**, 733 (1987); K. Kamaras *et al.*, Phys. Rev. Lett. **59**, 919 (1987); S. Etemad *et al.*, Phys. Rev. B **37**, 3396 (1988).

[8] G. L. Doll *et al.*, Phys. Rev. B **36**, 8884 (1987); J. Orenstein and D. H. Rapkine, Phys. Rev. Lett. **60**, 968 (1988).

[9] K. Char *et al.*, Appl. Phys. Lett. **51**, 1370 (1987); and (unpublished).

[10] A. Kapitulnik, in Ref. 2.

[11] D. E. Aspnes and A. A. Studna, Appl. Opt. **14**, 220 (1975);

Rev. Sci. Instrum. 43, 291 (1978).
[12]D. Aspnes, J. Opt. Soc. Am. 70, 1275 (1980).
[13]M. K. Kelly *et al.*, Phys. Rev. B 38, 870 (1988).
[14]I. Bozovic *et al.*, Phys. Rev. Lett. 59, 2219 (1987).
[15]Actually, $\rho_\perp$ was observed to increase with decreasing temperature in Refs. 3. However, Iye *et al.* (Ref. 4) found that both $\rho_\parallel$ and $\rho_\perp$ show metallic behavior in some Y-Ba-Cu-O single crystals—reportedly those which showed sharper superconducting transitions. A similar finding was reported also by S. Hagen *et al.*, at the American Physical Society Meeting, New Orleans, 1988 (unpublished).
[16]Indeed, in Y-Ba-Cu-O two CuO_2 layers traverse the unit cell and one expects that a pair of $3d_{x^2-y^2}/2p_x(2p_y)$ bands should be close and nearly parallel to one another throughout the Brillouin zone.
[17]S. L. Cooper *et al.*, Phys. Rev. B 37, 5290 (1988).
[18]None of the (over a dozen) optical studies on polycrystalline samples published so far by several groups showed more than a few percent change in reflectance, for $0.03 < \hbar\omega < 3$ eV, when the temperature was lowered from 300 down to 10 K. However, a recent study on Y-Ba-Cu-O single crystals [A. G. Thomas *et al.* (unpublished)] reports a substantial decrease of $R_\parallel(\omega)$, for $\hbar\omega < 0.15$ eV, at low temperatures.